



저작자표시-비영리-변경금지 2.0 대한민국

이용자는 아래의 조건을 따르는 경우에 한하여 자유롭게

- 이 저작물을 복제, 배포, 전송, 전시, 공연 및 방송할 수 있습니다.

다음과 같은 조건을 따라야 합니다:



저작자표시. 귀하는 원저작자를 표시하여야 합니다.



비영리. 귀하는 이 저작물을 영리 목적으로 이용할 수 없습니다.



변경금지. 귀하는 이 저작물을 개작, 변형 또는 가공할 수 없습니다.

- 귀하는, 이 저작물의 재이용이나 배포의 경우, 이 저작물에 적용된 이용허락조건을 명확하게 나타내어야 합니다.
- 저작권자로부터 별도의 허가를 받으면 이러한 조건들은 적용되지 않습니다.

저작권법에 따른 이용자의 권리는 위의 내용에 의하여 영향을 받지 않습니다.

이것은 [이용허락규약\(Legal Code\)](#)을 이해하기 쉽게 요약한 것입니다.

[Disclaimer](#)

Complex network analysis  
and topology-based data analysis  
for identifying risk factors of delirium



Sunghyon Kyeong

Department of Medical Science

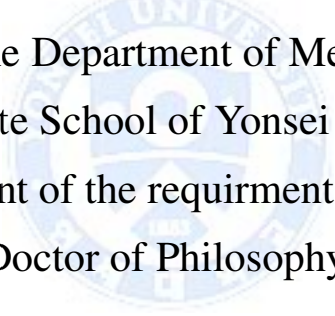
The Graduate School, Yonsei University



Complex network analysis  
and topology-based data analysis  
for identifying risk factors of delirium

Directed by Professor Jae-Jin Kim

The Doctoral Dissertation  
submitted to the Department of Medical Science,  
the Graduate School of Yonsei University  
in partial fulfillment of the requirements for the degree of  
Doctor of Philosophy



Sunghyon Kyeong

December 2015

This certifies that the Doctoral Dissertation  
of Sunghyon Kyeong is approved.



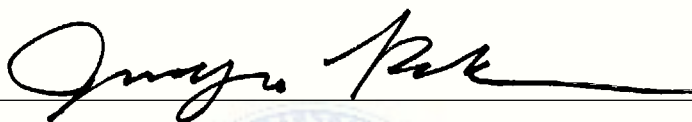
---

Thesis Supervisor: Jae-Jin Kim



---

Thesis Committee Member #1: Hae-Jeong Park



---

Thesis Committee Member #2: Jin Young Park



---

Thesis Committee Member #3: Soo-Hee Choi



---

Thesis Committee Member #4: Hosung Jung

The Graduate School  
Yonsei University

December 2015

## ACKNOWLEDGEMENTS

There was once a time when I was an undergraduate student. I was badgered by the question, “*how far would dirt on a car’s wheel fly?*” I remember myself pondering the question for weeks. In retrospect, I could have simply found the answer on the answer sheet. I just giggle at my somewhat nerdy youthful years. Consistently satiating my curiosities and learning the answers, I finally followed through my degree dissertation to completion. Lots of people have provided me with support and advice during this long and arduous process. I ask for everyone’s gracious understanding in not being able to visit everyone in person and instead extending my gratitude in writing.

First and foremost, I would like to send the most sincere gratitude to Professor Jae-Jin Kim, who has guided me through every step of the way and fostered me to grow as a true scholar. Professor, you have waited for me with patience and trust during the times I had struggled. You have encouraged and motivated me to stand again and move forward. I was able to grow and mature, as well as deepen the extent of my studies, only with your support. Even a hundred words could not fully express my gratitude for you. I will commit to my studies more and repay your support with steady outcomes.

I would also like to thank the professors of the thesis committee. Professor Hae-Jeong Park, thank you. You have taught me when I was

merely beginning my studies in neuroscience. I have learned an enormous amount of knowledge and research skills during the two years I had spent in the MoNeT Laboratory under your supervision. Your guidance has helped me to reach further in my studies. Professor Jin Young Park, thank you. Because you had allowed me to accompany you during ICU rounds for almost a year since September of 2014, I was able to examine the symptoms of delirium up close. Professor Soo-Hee Choi at Seoul National University, thank you. Thanks to the questions you have posed, I was able to extend my knowledge on delirium in more depth. Finally, Professor Hosung Jung, thank you. Your advice has allowed me to review my background knowledge in delirium and neuroimaging analysis, strengthening the academic foundation of my dissertation.

I would like to send special regards to Doctor Jung Eun Shin. Jung Eun, thank you for conducting MRI experiments and acquiring relevant datasets to this study for a full year. If it wasn't for your efforts, I could not have completed my dissertation. Furthermore, you have also been my mental counselor, always listening to and empathizing with my frustrations and hardships. Words cannot describe how much I appreciate your support.

In addition, I would like to thank my colleagues, who have invigorated somewhat mundane times spent at the laboratory and have always laughed at my stale jokes. Yu-Bin Shin, I wish the best for your

career and hope that you will become a valuable asset in the field of Neuropsychology. Yeon-Ju Hong, I wish the best for your new challenge of making a foray into the new academic field of Neuroaesthetics. I am confident that you will become an outstanding cognitive scientist with exceptional expertise in both arts and neuroscience. Erin Kim, I have always been impressed by your enterprising and enthusiastic attitude. I am confident that these qualities will drive you forward in your studies and life. Also, thank you for keeping me company next to my seat and always listening to my petty talks. Young Hoon Jung, I believe that you will become a great medical scientist. I ask that you support your seniors at all times. Eun Seong Kim, I hope you can complete your doctoral degree soon. Doctor Ji-Won Chun, thank you always for being there for all of us, as the super senior (haha) of our laboratory. I would also like to thank many colleagues in the Department of Psychiatry at the Gangnam Severance Hospital. Thank you, Professor Jeong Ho Seok, Professor Eunjoo Kim, Doctor Jung Suk Lee, Dr. Sunyoung Park, Dr. Seung Taek Oh, Dr. Min-Kyeong Kim, and Dr. Byung-Hoon Kim. Your remarkable presentations at the research club have helped me considerably in studying a broad range of mental disorders.

I would also like to thank several colleagues at the National Institute of Mathematical Sciences. In particular, thank you, Doctor Dong-Uk Hwang, Doctor Jung Min Lee, Doctor Tae-Wook Ko, Doctor Hyuk

Kang, and Doctor Woosik Son. I was able to advance my knowledge about complex network by watching your work closely in the computational neuroscience team. Doctor Eun-Youn Kim, thank you so much. You have been so kind to me and helped me accommodate to the Daejeon life when I had difficulties. Doctor Seonjeong Park, thank you. Your tips on the mathematical backgrounds of topological data analysis have helped me greatly.

Finally, I would like to thank my beloved wife, Eunha Lim. Eunha, you have been my inspiration for the past ten years we have spent together. Your motivating and warm smile and loving advice have driven me through my twenties. Without your encouragement, it would have been difficult to continue my studies when my family had financial troubles. You have motivated me to persevere and hold onto the joy of studying even during difficult times. Thank you, endlessly, for your support.

Sincerely,  
December 2015  
Sunghyon Kyeong

# TABLE OF CONTENTS

<b>ABSTRACT</b> . . . . .	<b>1</b>
<b>ABBREVIATIONS</b> . . . . .	<b>3</b>
<b>I. INTRODUCTION</b> . . . . .	<b>5</b>
1. Overview of Delirium . . . . .	5
2. Related Researches . . . . .	7
A. Human Connectome . . . . .	8
B. Modular Organizations of the Human Brain . . . . .	10
C. Brain Network During an Episode of Delirium . . . . .	11
D. Topological Data Analysis . . . . .	11
3. Research Goals and Approaches . . . . .	11
<b>II. MATERIALS AND METHODS</b> . . . . .	<b>13</b>
1. Preoperative and Postoperative Dataset . . . . .	13
2. Preoperative Demographic and Clinical Information . . . . .	15
3. Assessments of Severity of Postoperative Delirium . . . . .	15
4. Neuroimaging Data Acquisition . . . . .	15
A. Diffusion Tensor Imaging . . . . .	16
B. Resting State Functional MRI . . . . .	16
C. Imaging Parameters . . . . .	17
5. Preprocessing of Structural Neuroimaging . . . . .	17
A. Cortical Parcellation . . . . .	18

B.	Structural Network Construction . . . . .	19
C.	Group Representing Structural Network . . . . .	20
6.	Preprocessing of Resting State Functional Neuroimaging . . . . .	21
A.	Functional Network Construction . . . . .	21
B.	Group Representing Functional Network . . . . .	21
7.	Neural Substrates of Preoperative Delirium . . . . .	22
A.	Sparse and Dense Graph . . . . .	22
B.	Graph Theoretical Measures . . . . .	23
C.	Thresholding on Functional Network . . . . .	25
D.	Modular Organizations . . . . .	26
E.	Connectivity Density . . . . .	27
8.	Prediction Model for Preoperative Delirium . . . . .	28
A.	Logistic Regression . . . . .	29
B.	Model Selection . . . . .	31
9.	Brain Network Alteration during an Episode of Delirium . . . . .	32
A.	SN–FN Coupling – Old Approach . . . . .	32
B.	SN–FN Coupling – New Approach . . . . .	33
C.	Multi-sliced Functional Modular Organizations . . . . .	34
10.	Topology-based Subgroups Identification in Delirium . . . . .	35
A.	Filter function . . . . .	36
B.	Distance function . . . . .	38
C.	Clustering method . . . . .	38
D.	Visualization . . . . .	38
11.	Statistical Analysis . . . . .	39



A. Multiple Comparison Correction . . . . .	39
B. Correlation with Clinical Variables . . . . .	39
C. Mixed Design Analysis of Variance . . . . .	40
<b>III. RESULTS . . . . .</b>	<b>41</b>
1. Demographic and Clinical Variables . . . . .	41
2. Neural Substrates of Preoperative Delirium . . . . .	44
A. Structural Network Properties . . . . .	44
B. Functional Network Properties . . . . .	44
C. Structural Modular Organizations . . . . .	44
D. Connectivity Density Analysis . . . . .	49
E. Relationships with Clinical Variables . . . . .	53
3. Prediction Model for Preoperative Delirium . . . . .	54
A. Bivariate Logistic Regression . . . . .	55
B. Model Selection . . . . .	55
4. Brain Network and Motor Subtypes of Delirium . . . . .	58
5. Delirium with Hallucination . . . . .	60
6. Brain Network Alteration during an Episode of Delirium . . . . .	62
A. Preserved Graph Measures . . . . .	62
B. Altered Functional Connectivity . . . . .	63
C. Altered SN-FN Coupling Strength . . . . .	65
D. Multi-sliced Functional Modular Organization . . . . .	66
7. Topology-based Subgroups Identification in Delirium . . . . .	70
A. Variable Selection . . . . .	70
B. Distribution for Image of Filter Function . . . . .	71

C. Graphical Illustration of the Output Topology . . . . .	72
D. Post-hoc Analysis among Subgroups of Delirium . . . . .	73
<b>IV. DISCUSSION . . . . .</b>	<b>75</b>
1. Neural Substrates of Preoperative Delirium . . . . .	75
A. Structural Modular Organization . . . . .	77
B. Neuroimaging-based Delirium Prediction Model . . . . .	77
C. Brain Network and Motor Subtypes of Delirium . . . . .	79
D. Delirium and Hallucination . . . . .	80
2. Brain Network Alteration during an Episode of Delirium . . . . .	81
A. Alteration of Functional Network Properties . . . . .	81
B. Altered Structural-Functional Coupling Strength . . . . .	82
C. Multi-sliced Functional Modular Organization . . . . .	83
3. Topology-based Subgroups Identification in Delirium . . . . .	84
4. Limitations . . . . .	84
<b>V. CONCLUSION . . . . .</b>	<b>86</b>
<b>REFERENCES . . . . .</b>	<b>95</b>
<b>APPENDICES . . . . .</b>	<b>96</b>
<b>ABSTRACT (IN KOREAN) . . . . .</b>	<b>100</b>
<b>PUBLICATION LIST . . . . .</b>	<b>102</b>

## LIST OF FIGURES

Figure 1.	Distribution of the number of publications related to the human connectome . . . . .	8
Figure 2.	Summary of clinical and neuroimaging datasets and description of how datasets were used in three separate research topics . . . . .	14
Figure 3.	A schematic diagram for structural network construction . . . . .	20
Figure 4.	Illustration of sparse and dense graph . . . . .	22
Figure 5.	Description of <i>Dijkstra</i> algorithm to find geodesic shortest path length . . . . .	24
Figure 6.	Graphical illustrations for a measure of coupling strength between structural network and functional network . . . . .	33
Figure 7.	Shape encodes structure and meaning of complex data . . . . .	35
Figure 8.	Schematic diagram of topological data analysis using <i>Mapper</i> . . . . .	37
Figure 9.	Visualization of structural network modular organizations for each weighting method . . . . .	47
Figure 10.	Connectivity density analysis for the best partitions obtained from NOS-ROI weighted and FA weighted structural network . . . . .	49
Figure 11.	Comparisons of functional network properties among three motor subtypes of delirium . . . . .	58
Figure 12.	Significant group by time interactions for functional connectivity density . . . . .	64

Figure 13. Significant group by time interactions for the coupling strength . . . . .	66
Figure 14. Multi-layered modularity optimization for (A) delirium and (B) non-delirium using pre- and post-operative functional network data . . . . .	67
Figure 15. Significant group by time interactions for functional connectivity density of the multi-layered modular organizations . . . . .	68
Figure 16. Distribution of the filter function and its correlation with the prediction probability for post-operative delirium . . . . .	71
Figure 17. Output of topological data analysis . . . . .	72
Figure 18. Summary of methods and key results . . . . .	76



## LIST OF TABLES

Table 1.	Prevalence of delirium for various populations obtained from DSM-5 . . . . .	6
Table 2.	Summary of streamline statistics after structural network construction for each group . . . . .	18
Table 3.	Demographic and clinical characteristics of the preoperative delirium and non-delirium patients with the hip fracture . . . . .	42
Table 4.	Summary of preoperative patients characteristics and operation-related information . . . . .	43
Table 5.	Group averaged values of structural network properties and statistical comparisons between preoperative delirium and non-delirium . . . . .	45
Table 6.	Group averaged values of functional network properties and statistical comparisons between preoperative delirium and non-delirium . . . . .	46
Table 7.	Similarity of the structural modular organizations between the preoperative delirium and non-delirium comparison groups . . . . .	48
Table 8.	Structural path length density and functional connectivity density for NOS-ROI weighted structural modular organizations . . . . .	51
Table 9.	Structural path length density and functional connectivity density for FA weighted structural modular organizations . . . . .	52
Table 10.	Correlations between the clinical variables and the characteristic path length of the preoperative structural network . . . . .	53

Table 11.	Preoperative risk factors for postoperative delirium using logistic regression . . . . .	54
Table 12.	Delirium prediction models using multivariate logistic regression . . . . .	56
Table 13.	Differences of preoperative structural and functional network properties as a function of motor subtypes . . . . .	59
Table 14.	Statistical comparison of network properties between hallucination and non-hallucination groups within preoperative delirium . . . . .	61
Table 15.	A repeated-measures analysis of variance to test for group and time effects and group by time interactions in functional network properties . . .	62
Table 16.	A repeated-measures analysis of variance to test for group, time, and group by time interaction effects in functional connectivity density for structural modular organization . . . . .	63
Table 17.	A repeated-measures analysis of variance to test for group and time effects and group by time interactions in the SN–FN coupling strength . . .	65
Table 18.	A repeated-measures analysis of variance to test for group and time effects and group by time interactions in functional connectivity for multi-sliced functional modules . . . . .	69
Table 19.	Statistical comparisons of graph metrics among three phenotypic subgroups of delirium . . . . .	74
Table A1.	NOS-ROI weighted structural modular organizations using preoperative structural network data of patients with delirium . . . . .	97

Table A2. FA weighted structural modular organizations using preoperative structural network data of patients with delirium . . . . .	98
Table A3. Multi-sliced functional modular organizations using pre- and postoperative functional network data of patients with delirium . . . . .	99



## ABSTRACT

Complex network analysis and topology-based data analysis  
for identifying risk factors of delirium

**Sunghyon Kyeong**

*Department of Medical Science  
The Graduate School, Yonsei University*

(Directed by Professor Jae-Jin Kim)

**Objective:** The human brain is a complex network of interlinked regions and composed of the structural (or backbone) network and dynamic functional networks. Studies revealed that the abnormal brain network has associated with the emergence of brain diseases. Delirium is one of brain diseases, and its etiologies are multifactorial. To identify risk factors of delirium, this study aimed to investigate neural substrates of delirium using complex network analysis and investigate phenotypic subgroups of delirium using topology-based data analysis.

**Materials and Methods:** A total of fifty-eight hip fracture patients were recruited in this study. Structural and functional neuroimaging data from all participants were acquired before hip fracture surgery. Among the participants, only thirty-two patients were scanned for postoperative MRI data acquisition. Neural substrates in preoperative delirium, and functional connectivity re-organization during an episode of delirium were studied using a framework of complex network analysis. In topological data analysis, cognitive impairment, personality scales such as neuroticism and conscientiousness, and delirium rating scale were considered to identify phenotypic subgroups of delirium.



**Results:** Among fifty-eight patients, twenty-five patients were identified as delirium after hip fracture surgery. In the study of neural substrates of delirium, the significant increase of characteristic path length in structural network was observed in preoperative delirium ( $P < 0.05$ ). Also, increased structural path length densities connecting frontal to subcortical and visual sensory regions were played a pivotal role in characterizing delirious patients (corrected  $P < 0.05$ ). Furthermore, functional connectivity density between the prefrontal cortex and audiovisual sensory areas were significantly increased in preoperative delirium (corrected  $P < 0.05$ ). Interestingly, functional connectivity density between the visual cortex and the frontal and auditory areas were strongly suppressed in during-delirium patients ( $P < 0.05$ ). Finally, topology-based data analysis identified three subgroups of delirium in dimensions of cognitive function and personality.

**Conclusion:** This study investigated neuroimaging-based neural risk factors for delirium. The increased path length of structural network in preoperative delirium implies that there existed disruptions of the connection weights such as a fractional anisotropy and the number of streamlines in the backbone network. The significantly suppressed functional connectivity from the visual cortex to the auditory cortex and frontal regions may play a pivotal role in characterizing the delirious phenomena such as dysfunction in perception, a deficit in sustaining the conscious mental state, and hallucination. Lastly, topological data analysis suggests that neural substrates of delirium could be different for phenotypic subgroups of delirium.

---

**Key words:** Complex network analysis, topology-based data analysis, human connectome, delirium, hip fracture surgery

## ABBREVIATIONS

- **AAL**: Automated anatomical labeling
- **ANOVA**: Analysis of variance
- **BFI**: Big five inventory
- **BFI-C**: Conscientiousness item score of BFI
- **BFI-N**: Neuroticism item score of BFI
- **BOLD**: Blood Oxygen-Level Dependent
- **DSM-5**: Diagnostic and Statistical Manual of Mental Disorders, Fifth Edition
- **DTI**: Diffusion tensor imaging
- **FA**: Fractional anisotropy
- **FCD**: Fractional connectivity density
- **fMRI**: Functional magnetic resonance imaging
- **FN**: Functional network
- $S(\text{FN})$ : Sparse adjacency matrix of the functional network, which are the counterparts of the corresponding structural network
- $\mathcal{F}(\text{FN})$ : Full adjacency matrix of the functional network
- **HAS**: Hamilton Anxiety Scale
- **HRSD**: Hamilton Rating Scale for Depression
- **IQCODE**: Informant Questionnaire on Cognitive Decline in the Elderly
- **K-DRS**: Korean version of Delirium Rating Scale
- **MMSE**: Mini Mental State Examination
- **MRI**: Magnetic resonance imaging
- **NMI**: Normalized mutual information
- **NOS-ROI**: Number of streamlines corrected for volume of each region of interest
- **Post-Op**: Postoperative
- **Pre-Op**: Preoperative

- **ROC**: Receiver operating characteristic
- **ROI**: Region of interest
- **SN**: Structural network
- **SPLD**: Structural path length density
- $\mathcal{D}(\text{SN})$ : A distance matrix obtained using *Dijkstra* shortest path length algorithm
- **TDA**: Topological data analysis



Complex network analysis and topology-based data analysis  
for identifying risk factors of delirium

Sunghyon Kyeong

*Department of Medical Science*  
*The Graduate School, Yonsei University*

(Directed by Professor Jae-Jin Kim)

## **I. INTRODUCTION**

Delirium is categorized into neurocognitive disorder according to the Diagnostic and Statistical Manual of Mental Disorders, Fifth Edition (DSM-5).<sup>1</sup> Also, delirium is accompanying the dysfunctions in domains of cognition, attention and orientation to the environment, and language. The prevalence of delirium is highest among hospitalized elderly patients and varies depending on the individuals' characteristics, setting of care, and sensitivity of the detection method (Table 1). In this section, characteristics of postoperative delirium, previous neuroimaging studies, and analysis methodologies will be reviewed. Also, the research goals and outline of this thesis will be presented.

### **1. Overview of Delirium**

Postoperative delirium is a common medical complication after various surgery. Postoperative delirium is associated with various adverse outcomes including a longer intensive care unit stay, longer hospital stays, increased mortality, higher hospital costs, and a greater need for nursing-home care afterwards.<sup>1</sup> In general, symptoms of postoperative

Table 1. Prevalence of delirium for various populations obtained from DSM-5

Population	Prevalence	Note
People in the overall community	1 – 2 %	This number ideally should be 0 %
Individuals older than 85 years	14 %	
General hospital people	6 – 56 %	
People who just had surgery	15 – 53 %	Increased in older individuals
People in intensive care unit	70 – 87 %	Increased in older individuals
People in nursing homes	60 %	or people in post-acute care settings
People who are at “end of life”	83 %	

delirium arise shortly after surgery and usually persist for a few days. In some cases, however, they can last up to several weeks.<sup>2</sup>

The probability of postoperative delirium increases if a patient is an older adult, already has dementia or a physical disability, abuses alcohol, or has very abnormal blood tests. Also, certain types of surgeries are more frequently associated with delirium. For example, delirium is much more common after hip fracture<sup>3-7</sup> and cardiac surgery.<sup>7-10</sup>

According to previous studies, the incidence of postoperative delirium after surgery varies from 15 % to 53 % (Table 1), with the highest incidences among elderly patients.<sup>11-15</sup> With an aging population, the number of elderly patients undergoing surgery is growing, and this will continue to increase over time.<sup>16</sup>

Typical symptoms of delirium are characterized as following: Sudden onset over hours to days; Disturbance in sleep-wake patterns; Audio and visual hallucinations; Slurred speech and language difficulties; Dysfunctions in perception and environmental awareness; Usually more alert in the morning than at night; Slow moving or very restless.

## **2. Related Researches**

Over the last decades, various studies focusing on postoperative delirium found many risk factors because the early detection and intervention of delirious patients related to reducing the adverse outcome of delirium. Most studies used the clinically available information. A few studies focused on finding preoperative delirium risk factors in the neural basis.

Most of the literature, related to the neural correlates of delirium, has been summarized by a systematic review.<sup>17</sup> This review included 12 articles, mostly with small sample sizes (a total of 127 cases). However, there was substantial heterogeneity in populations and neuroimaging modalities such that conclusions remained to unclear.

In general, structural brain abnormalities such as atrophy and leukoaraiosis (or white matter hyperintensities) might be associated with delirium.<sup>18</sup> After publication of the systematic review by Soiza, five further studies have been published.<sup>17</sup> The largest-scale report was VISIONS.<sup>19,20</sup> This prospectively examined the neural correlates of delirium in 47 participants after critical illness. A duration of delirium was related to measures of white matter tract integrity and this in turn was related to poorer cognitive outcomes at 3 and 12 months. Also, brain volumes were also assessed and related to cognitive outcomes in the same manner. Overall, the study found that longer duration of delirium was associated with smaller brain volume and a white matter disruption, and both these correlated with worse cognitive scores 12 months later.

Two studies examined delirium risk as a postoperative complication after elective cardiac surgery. These both showed that white matter damage predicted postoperative delirium.<sup>21,22</sup> So far, only one study investigated an alteration of the functional connectivity

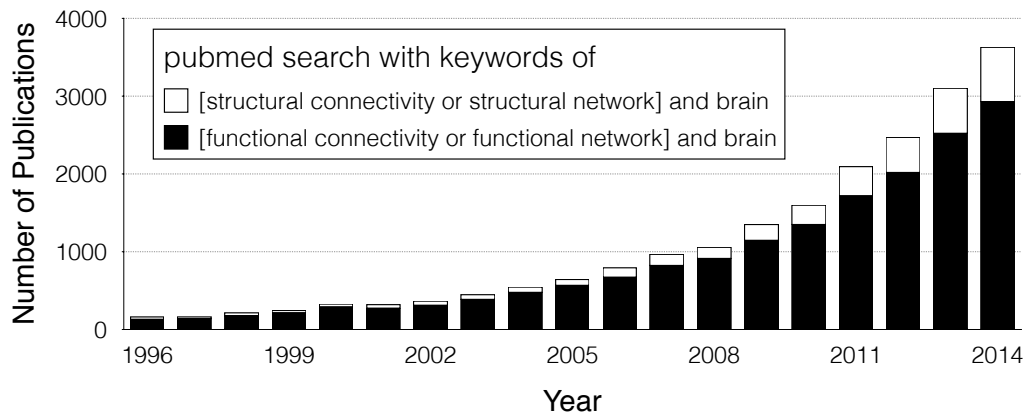


Figure 1. Distribution of the number of publications related to the human connectome.

during an episode of delirium. Choi revealed the decreased functional connectivity between the dorsolateral prefrontal cortex and posterior cingulate cortex during an episode of delirium and its reversibility after recovery of delirium.<sup>23</sup> A reversible reduction of the functional connectivity has been revealed by using the follow-up MRI scanning after recovering from delirium. However, there were no graph theoretical approaches focusing on the functional network alteration in a comparison of preoperative and postoperative measurements.

### A. Human Connectome

With advancing neuroimaging technologies such as magnetic resonance imaging (MRI) together with analysis methodologies, mysteries of the human brain are uncovered. Over the two past decades, the study of structural and functional networks has enormously grown as shown in Figure 1. However, studies were mostly focused in analyzing the functional network.

There have been a lot of advances in the analysis of resting state functional connectivity.

A correlation analysis between a single seed region of interest to the whole-brain regions was the first attempt to investigate the functional connectivity developed by Biswal.<sup>24</sup> Later on, at the beginning of the 21st centuries, Calhoun applied the independent component analysis to the resting state functional network data to unmix the independent sources of functional connections in the human brain.<sup>25</sup> After that, a graph theoretical analysis was introduced in the connectome studies and currently it is widely used for studying the resting state functional connectivity.<sup>26</sup>

Also, using the graph theoretical approach, researchers attempted to reveal the modular organization of the whole-brain. Detecting modules (or communities) is based on the analysis of the interactions or connections between elements of systems, and thus partitioning modules has become an important approach in the various network study.<sup>27-30</sup> Specifically, Davis revealed the different patterns of the whole-brain modular organizations for the low, intermediate, high impulsivity groups.<sup>31</sup> Meunier found the age-related changes in modular organization of human brain functional networks.<sup>32</sup> Kyeong found the significantly different patterns of the functional connectivity between two contrasting temperament groups.<sup>33</sup> In brain networks, densely connected brain regions, which are sparsely connected to other regions, are considered to form the modules.

The study of the structural connectivity, in contrast to the functional connectivity, has been rarely investigated. The history of the methodological advancement is very short. The structural network is the set of nerve fibers linking neuronal units at a given time. Therefore, the structural connectivity is the network backbone in the brain and rarely changed over short time, whereas the functional network is the state dependent brain networks.



Before the advent of graph theoretical approaches in the human connectome, voxel- or tract-based statistical comparisons of fractional anisotropy were the only structural properties that can be measured from the diffusion tensor imaging data. Recently, researchers could construct a connection matrix using the streamlines that connect two brain regions. The structural network is a sparse matrix (see Figure 4 in materials and methods section) and thus we could easily apply the graph theoretical analysis without additional thresholding steps.<sup>34</sup>

In this study, we fully analyze the structural and functional network properties in the preoperative delirium and comparison groups. Then, overlapping the functional network properties on the structural network.

## **B. Modular Organizations of the Human Brain**

A graph theory (or complex network in Physics) is a methodological background of this dissertation. The major methodological framework used in this study is the community detection in the structural network of the human brain. There have been a few studies related to the community detection of the functional brain network: intrinsic modular organizations in the normal controls;<sup>35</sup> impulsivity related modular organizations;<sup>31</sup> age-related functional modular organizations;<sup>32</sup> functional modular organization of two contrasting temperament groups.<sup>33</sup> In the study of structural community detection, the cortical thickness network was widely used in many literatures.<sup>36,37</sup> However, detecting the structural modular organizations using the structural network from a streamline tractography was rarely studied. Here, by extending the community detection method and connectivity density analysis used in Kyeong, the development of community detection

procedures from the structural network were achieved.<sup>33</sup>

### **C. Brain Network During an Episode of Delirium**

Increasingly, the study of complex networks has expanded across diverse scientific fields. The network science is concerned with the network of the network (*i.e.*, coupled network) because an interdependency of two networks could cause a catastrophic failure in the coupled network system.<sup>38</sup> Study of group differences between two preoperative patients' is important to identify neural risk factors for delirium. However, since delirium is accompanying an altered state of consciousness, investigating the functional connectivity during an episode of delirium would enable us to gain a deeper understanding of how the functional network reorganizes during an episode of delirium.

### **D. Topological Data Analysis**

In the era of big data, finding the new insight from the huge amount of dataset is one of the most fascinating research areas. Especially, in the medical data analytics, detecting subtypes or hidden phenotypic subgroups within the heterogeneous patient group is essential for the personalized treatment. Recently, the advanced unsupervised machine learning technique to identify subgroups using a mathematical framework called as "topological data analysis" was developed and applied for detecting subtypes of breast cancer<sup>39</sup> and diabetes subtypes.<sup>40</sup> Also, the topology-based data analysis was applied in analyzing neuroimaging data.<sup>41,42</sup>

## **3. Research Goals and Approaches**

There are three hypotheses in this dissertation. First, there existed a structural network alteration in preoperative delirium (*i.e.*, alteration of brain network backbone). Also,

delirium prediction model would be established using preoperative neuroimaging data. Second, although hip fracture surgery has no direct connection to brain function, it would change the patterns of functional connectivity, and cause delirious phenomena. Third, among preoperative delirium patients, there existed phenotypic subgroups in dimensions of individual's personality and levels of cognitive function.

The methodological approaches of each research goal are summarized as following. First, to achieve an invention of a neuroimaging-based delirium prediction model, comprehensive analysis of structural and functional connectivity properties using preoperative neuroimaging datasets was conducted. Second, to understand how the normally working conscious brain becomes an acute confusion state after hip fracture surgery, a new approach to computing the synchrony of structural and functional network was developed. Also, since preoperative and postoperative functional networks are interdependent to each other, modularity optimization of a multi-sliced network was introduced to find the functional modules in delirium and non-delirium groups. Third, topological data analysis method was used for identifying phenotypic subgroups of delirium.

## **II. MATERIALS AND METHODS**

This dissertation is a study about investigating the preoperative neural risk factor for delirium, and functional network changes before and after hip fracture surgery. For this, the multimodal neuroimaging data, demographic information, and various clinical scales were obtained from fifty-eight hip fracture patients.

The functional and structural brain networks were constructed from the resting state functional magnetic resonance imaging (MRI) and diffusion MRI, respectively. There are many steps should be conducted to get the noise-free standardized brain network connection matrix from the raw neuroimaging data. In this section, parameters for MRI data acquisitions, steps in preprocessing of neuroimaging data, brain network construction, and analysis methods will be described.

### **1. Preoperative and Postoperative Dataset**

A total of eighty-four hip fracture patients were enrolled from the inpatients unit of Gangnam Severance Hospital at Yonsei University in Seoul, Korea from September 2013 to July 2014. All hip fracture patients were participated in the preoperative MRI scanning. After hip fracture surgery, postoperative MRI scanning was conducted for the thirty-two patients. Based on clinical interviews with trained psychiatrists, a diagnosis of delirium was made according to DSM-IV criteria. In the preoperative dataset, twenty-five patients were identified as postoperative delirium, and thirty-three patients were identified as non-delirium according to the follow-up assessment of delirium. Also, in the postoperative follow-up dataset, fourteen patients identified as postoperative delirium, and eighteen patients were identified as non-delirium comparison patients. We obtained

## Preoperative Datasets

Delirium (n=25) and Non-delirium (n=33)

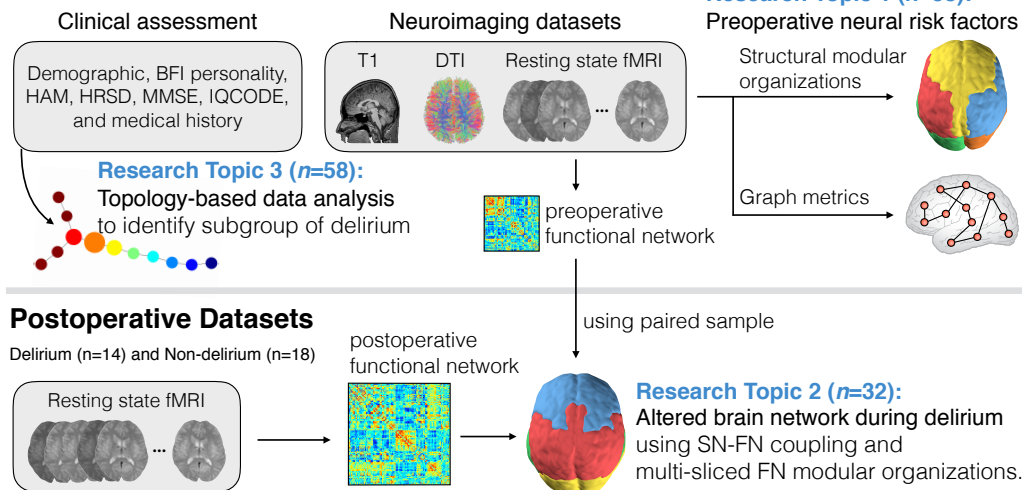


Figure 2. Summary of clinical and neuroimaging datasets and description of how datasets were used in three separate research topics. In the first research topic, structural modular organizations were obtained by using DTI and various graph metrics were obtained from structural and functional networks. In the second research topic, paired samples of pre- and postoperative functional networks were used to obtain the multi-sliced functional network modular organizations. Also, preoperative and postoperative SN-FN coupling strengths were computed. In the third research topic, MMSE, IQCODE, and BFI were used for topology-based data analysis. Abbreviations: BFI, big five inventory; DTI, diffusion tensor imaging; IQCODE, informant questionnaire on cognitive decline in the elderly; MMSE, mini mental state examination; SN-FN, structural network and functional network.

written informed consent from the participants or their surrogates after giving them a complete description of the study. The Institutional Review Board at Gangnam Severance Hospital approved this study. The summary of clinical and neuroimaging datasets and description of how datasets were used in three separate research topics were illustrated in Figure 2.

## **2. Preoperative Demographic and Clinical Information**

Demographic variables such as age and sex were collected before hip fracture surgery. The participant's cognitive level, prior to the hospitalization, was measured using short Korean version of informant questionnaire on cognitive decline in the elderly (IQCODE). Also, to assess comorbidity of dementia, a total of 30-points mini-mental state examination (MMSE) was acquired. The MMSE can detect cognitive impairment by evaluating orientation, attention, recall, language and ability to follow commands. A score higher than 23 is considered as normal, although individual performance varies with the patient's age and education.<sup>43</sup> Furthermore, anxiety and depression level were assessed by Hamilton's anxiety scale and Hamilton's rating scale for depression, respectively. Finally, individual's personality was assessed by Big Five Inventory.

## **3. Assessments of Severity of Postoperative Delirium**

The presence and severity of delirium after hip fracture surgery were assessed using the Confusion Assessment Method and Delirium Rating Scale-Revised-98,<sup>44</sup> which includes three diagnostic items and 13 severity items (scores range from 0 to 46). The motor subtypes, such as hyperactive, hypoactive, and mixed were classified based on the Delirium Motor Subtype Scale ("decreased or increased psychomotor activity"). Patients' clinical status was assessed every other day. A MRI scan was obtained from patients during an episode of delirium, and a follow-up was obtained after resolution.

## **4. Neuroimaging Data Acquisition**

The participants underwent resting state functional MRI, diffusion tensor imaging, and high-resolution structural image scanning. For each neuroimaging modality, the underlying

ing principles and scanning parameters will be described in the following subsections. A total of thirty-two patients with and without delirium were scanned before and after hip fracture surgery. For the delirious patients, the postoperative follow-up functional images were acquired on the next day of diagnosing delirium at the moment when they were in the best cooperative time of the day. Whereas, the postoperative follow-up functional images were acquired at 5-th day after surgery if they were not diagnosed as delirium.

### **A. Diffusion Tensor Imaging**

Diffusion tensor imaging (DTI), also referred to as diffusion MRI, allows the mapping of the diffusion process of molecules in the white matter tissues. Molecular diffusion reflects interactions with cell membranes, axonal fibers and myelin in white matter tissues. Tractography technique allows to represent neural tracts using DTI data. Fiber bundles extracted through the tractography can be used to model a structural brain network. The steps for the preprocessing and structural network construction were described in this section.

### **B. Resting State Functional MRI**

Resting state fMRI reflects the low-frequency fluctuation by the Blood-Oxygen-Level Dependent (BOLD) contrast imaging during eyes closed resting state. The resting state neural fluctuation is present even in the absence of an externally applied task, and thus any brain region will have spontaneous fluctuations. Also, it influenced to the BOLD signal. The resting state functional connectivity is the connection between brain regions that share the fluctuation patterns of the BOLD signal. Specifically, it can be defined as the temporal correlation between two time-series. There are various ways to access the

functional connectivity using the resting state fMRI data: A seed region based correlation analysis; independent component analysis; and graph theoretical approaches. Before looking at the functional connectivity, the preprocessing in the spatial and temporal domains should be conducted.

### **C. Imaging Parameters**

Functional images were obtained over 5 minutes using gradient-echo echo-planar imaging sequence in a Signa EXCITE 3.0 Tesla MR system (GE, Milwaukee) with the following parameters: matrix size,  $64 \times 64$ ; echo time (TE), 17.6 msec; repetition time (TR), 2,000 msec; field of view, 240 mm; slice thickness, 3 mm; flip angle,  $90^\circ$ ; number of slices, 50. All participants were instructed to rest with their eyes closed during the scan. High-resolution anatomical images were obtained using a spoiled gradient-echo sequence (matrix= $512 \times 512$ , TE=3.2 msec, TR=8.2 msec, field of view=240 mm, slice thickness=1.2 mm, flip angle= $20^\circ$ , number of slices=116) to serve as an anatomical underlay. Sixteen diffusion tensor imaging volumes were obtained for each participant, including 15 volumes with diffusion gradients applied along 15 non-collinear directions ( $b = 1000 \text{ s/mm}^2$ ) and one volume without diffusion weighting ( $b = 0$ ). A total of 64 continuous axial slices (slice thickness=2.6 mm) were acquired using a single shot spin-echo echo planar imaging sequence with the following parameters: TR, 8000 msec; field of view, 240 mm; matrix size,  $128 \times 128$ .

## **5. Preprocessing of Structural Neuroimaging**

The preprocessing of diffusion tensor imaging (DTI) included the following steps. First, DTI images were corrected for eddy-current distortions<sup>45</sup> and realigned to the  $b = 0$  im-



Table 2. Summary of streamline statistics after structural network construction for each group

Variable	Pre-Op Delirium	Comparison patients	<i>T</i> statistic	<i>P</i> value
Total number of tracts [ $\times 10^3$ ]	314 (41)	313 (35)	0.096	0.924
Usable tracts [ $\times 10^3$ ]	130 (23)	129 (19)	0.142	0.888
Usable tracts, %	41.3 (3.9)	41.3 (3.2)	0.039	0.969
Mean length, mm	19.2 (1.8)	19.3 (1.7)	-0.197	0.844

The numbers represent mean (standard deviation) value.

age through FSL's 'eddy\_correct' function. Second, the tractography program (Diffusion Toolkit, Version 0.6.3)\* and the diffusion-weighted images were used for the fiber tract extraction. The white matter tracts of the brain structural networks were reconstructed by using the deterministic fiber tracking method, based on a fiber assignment by continuous tracking (FACT) algorithm.<sup>46</sup> Within each voxel in the brain mask (*i.e.*, the total of gray and white matter), one seed was started, evenly distributed over the volume of the voxel. A streamline was started from each seed following the principal diffusion direction from voxel to voxel, thus reconstructing white matter fibers. Stopping criteria were used as following: an angular threshold of  $60^\circ$ , fractional anisotropy (FA) threshold of 0.1, and the track length of 5 mm. Table 2 shows the summary of streamline statistics for each group.

### A. Cortical Parcellation

After the preprocessing steps, the cortical and sub-cortical brain areas were parcellated into 90 regions of interest (ROIs) using the automated anatomical labeling (AAL) atlas.<sup>47</sup> A total of 90 anatomically defined ROIs covered the whole-brain except for the

\*<http://www.trackvis.org>

cerebellum. In this study, we included the subcortical regions such as the thalamus, caudate, putamen, and pallidum<sup>48-50</sup> even though some other studies ignores these parts of the brain.<sup>34,51</sup> Since the thalamus or the amygdales has keep vital connections with cortical areas, subcortical structures were included in this study.<sup>48</sup>

## **B. Structural Network Construction**

Figure 3 illustrates the procedures for individual structural network construction. The structural networks were constructed through the following steps: (i) To obtain the transformation matrix ( $\mathcal{T}$ ), coregistration of the T1-weighted image to  $b = 0$  image. (ii) normalization of the coregistered T1-weighted image to the standard MNI template image. (iii) The non-linear inverse transformation matrix was applied to the parcellation atlas such as AAL to generate corresponding parcellation volumes in each individual's diffusion-weighted image native space. (iv) Then, individually fitted parcellation map divides the whole-brain into 90 cortical regions in the individual space. (v) Finally, we constructed the structural network using two weighting methods:  $W^{NOS-ROI}$ , Weighted by streamline counts, corrected for ROI volume.<sup>34,49</sup> The number streamlines between region  $i$  and  $j$  was normalized by the sum of the volumes of ROI  $i$  and  $j$  was computed for all pairs of ROIs;  $W^{FA}$ , Weighted by FA values.<sup>34,50</sup> The voxel-wise FA values for the existing streamlines were extracted and averaged for each edge connecting region  $i$  and  $j$ . Edges having fewer than three streamlines were considered potentially spurious and were deleted from the connection matrix.<sup>50,51</sup>

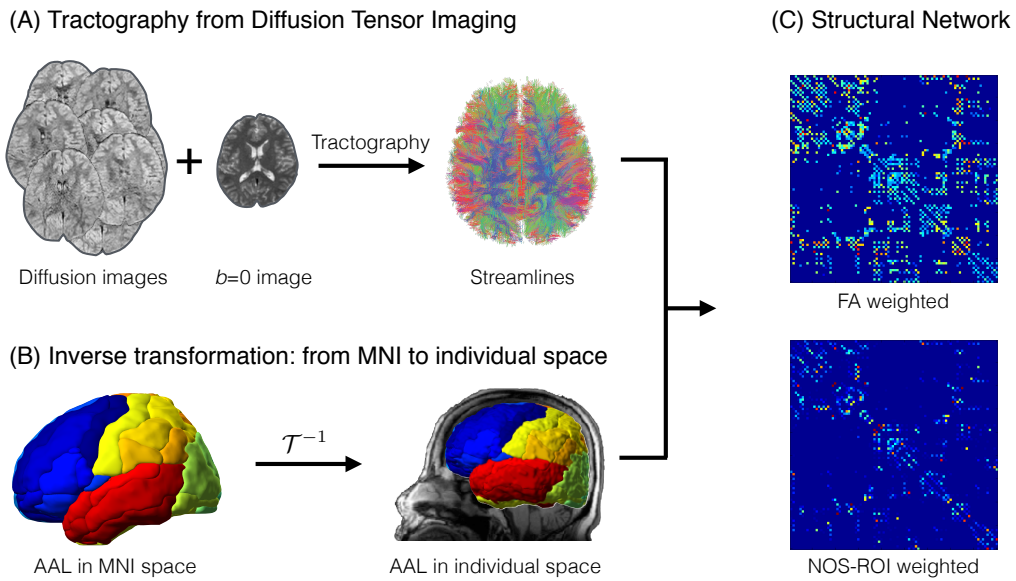


Figure 3. A schematic diagram for structural network construction. (A) Fifty directional diffusion images were registered to non-diffusion weighted ( $b = 0$ ) image using non-linear affine transformation. Then, the whole-brain tractography were obtained using the FACT algorithm. (B) The inverse transformation matrix  $\mathcal{T}^{-1}$  was applied to AAL atlas to create corresponding AAL volume in individual's diffusion-weighted image native space. (C) Structural network constructions by determining the white matter connection for each pair of AAL volume. The connection weights for each pair of nodes were obtained from two methods: Fractional Anisotropy (FA) and Number of Streamlines corrected for volume of each ROI (NOS-ROI). Abbreviations: AAL, automated anatomical labeling; FACT, fiber assignment by continuous tracking; MNI, montreal neurological institute.

### C. Group Representing Structural Network

For each preoperative group, a group representing structural network was obtained by averaging the connection weights from the individual matrices that were present in at least 75% of the group of subjects.<sup>34</sup> These group representing brain networks will be used for investigating the structural modular organizations.

## 6. Preprocessing of Resting State Functional Neuroimaging

All acquired neuroimaging data were preprocessed using Statistical Parametric Mapping (SPM12)<sup>†</sup> Matlab toolbox. Realignment to correct head motion artefacts were performed for all volumes within a subject. The realigned fMRI data were normalized through bilinear interpolation at a  $2 \times 2 \times 2$  mm<sup>3</sup> resolution using the parameters from a spatial normalization of T1-weighted images. The spatial smoothing was performed with a Gaussian kernel of 6 mm full-width at half-maximum. Then, a linear detrending and band-pass filtering (0.009~0.08 Hz) were applied to time series at each voxel. The effects of head motions, global signal activity, and the physiological noise from white matter and ventricle regions were also removed to eliminate sources of spurious variances.

### A. Functional Network Construction

The mean time series within each Region of Interest (ROI) were obtained from cortical parcellation method. The adjacency matrix ( $A_{ij}$ ) for each subject was computed with Pearson's correlation coefficients between the  $i$ -th and  $j$ -th mean time series for each parcellation, respectively.

### B. Group Representing Functional Network

The average adjacency matrix, computed as the mean functional network (FN) for each group, showed the representative group FN.

$$FN_{ij}^l = \frac{1}{n_l} \sum_{k \in G_l} A_{ij}^k \quad (1)$$

---

<sup>†</sup><http://www.fil.ion.ucl.ac.uk/spm/>

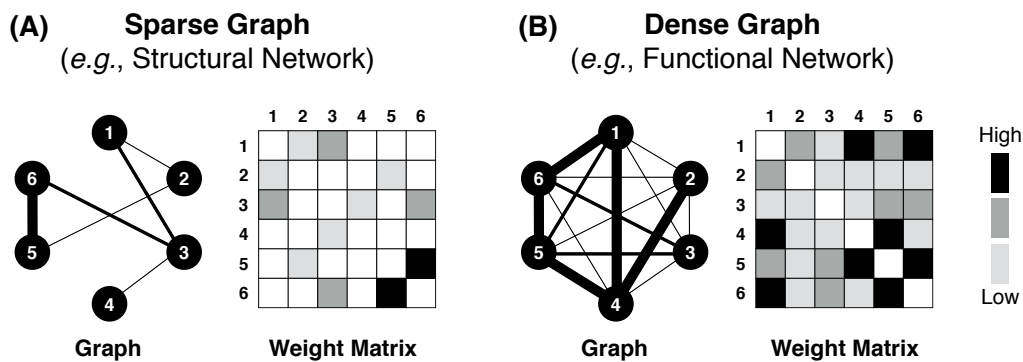


Figure 4. Illustration of (A) sparse and (B) dense graph. The structural network is the example of sparse graph and the functional network is the example of dense graph.

where  $l$  is the group index;  $G_l$  is a set of subjects within group  $l$ ; and  $n_l$  is the number of subjects in group  $l$ .

## 7. Neural Substrates of Preoperative Delirium

The applications of graph theory to the functional and structural brain networks are growing rapidly to reveal the global or local features of the brain connectome. Global and local properties of the brain networks were measured by graph theory and they were considered to investigate the neurobiological substrates for preoperative delirium. To begin with graph theoretical analysis, characteristics of sparse and dense graph will be introduced in the following subsection because a structural and functional network can be represented by a sparse and dense graph, respectively. Also, definitions of various graph metrics, modular organization of the human brain, and connectivity density will be described.

### A. Sparse and Dense Graph

When we were dealing a complex network, which has a huge amount of nodes and

edges, there are several ways to extract informative features from them. The characteristic path length and average clustering coefficients of the network usually explain the integration and segregation of the network. These graph metrics are very useful when we want to get comprehensive insight from a graph. However, before analyzing graphs, an appropriate threshold on edge weights is necessary for the densely connected graph (Figure 4). Because the functional connectivity matrix was computed by Pearson's correlations between time series, all nodes are interconnected with different connection weights. Therefore, we have to apply a threshold on connection weights to yield a sparse adjacency matrix when we extract graph metrics from the functional network. Figure 4B illustrates the dense graph. In contrast, the connection matrix of the structural network is intrinsically sparse since a single streamline does not connect all pairs of nodes.

## B. Graph Theoretical Measures

Several graph metrics are frequently used in analyzing the brain network, such as the degree, efficiency, characteristic path lengths, clustering coefficients, and modularity. The characteristic path length and global efficiency are a measure of functional integration. The clustering coefficient and the local efficiency are a measure of functional segregation. Modularity characterizes the segregation of a network.<sup>26,52</sup>

**Clustering Coefficient:** The conceptual meaning of the clustering coefficients of each node ( $C_i$ ) is known as a fraction of triangles around an individual node. The average clustering coefficient is defined as following:

$$C = \frac{1}{n} \sum C_i, \quad C_i = \frac{1}{k_i(k_i - 1)} \sum_{j,h \in N} (w_{ij}w_{ih}w_{jh})^{1/3},$$

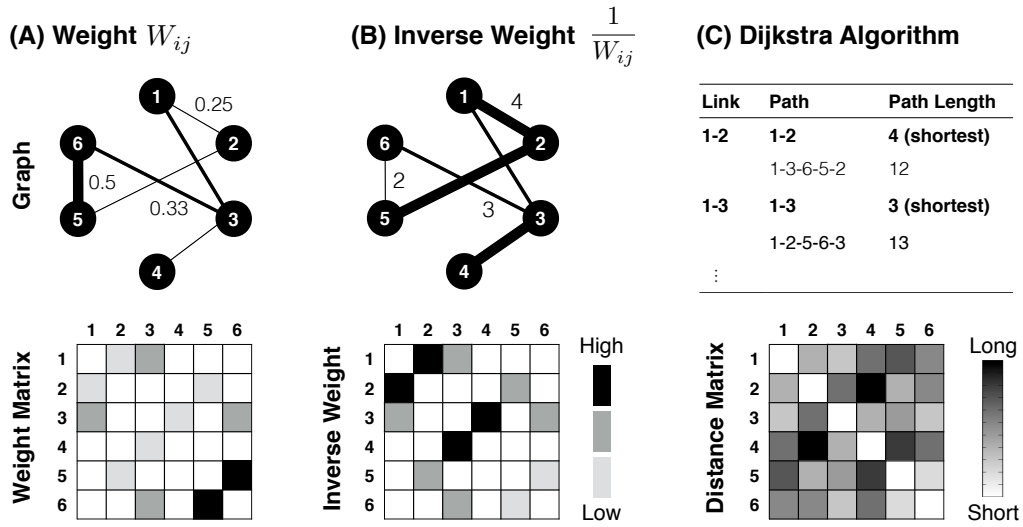


Figure 5. Description of *Dijkstra* algorithm to find geodesic shortest path length. Computing (B) the inverse matrix from (A) connection weight matrix. Then, searching the shortest path between links using *Dijkstra* algorithm.

where  $k_i$  is the degree of node  $i$ .

**Characteristic Path Length:** Although there was no direct link between a pair of nodes in a sparse graph, there existed some geodesic path between that nodes. The characteristic path length of the network is the average of all geodesic shortest path length ( $d_{ij}$ ) as following:

$$L = \sum_{i \in N} \sum_{j \in N, i \neq j} \frac{d_{ij}}{n(n-1)},$$

where  $d_{ij}$  is the geodesic distance between nodes  $i$  and  $j$  obtained by *Dijkstra* algorithm. In the evaluation of  $d_{ij}$ , the inverse of the similarity weight  $1/w_{ij}$  is used for a distance metric as illustrated in Figure 5. Basically, the higher similarity values implies the shorter the distance.

**Global Efficiency:** The global efficiency of the network can be defined as the harmonic mean of the shortest path as following:

$$E = \frac{1}{n(n-1)} \sum_{i \in N} \sum_{j \in N, j \neq i} d_{ij}^{-1}$$

where  $N$  is the set of all nodes in the graph,  $n$  is the number of nodes in the graph.

**Local Efficiency:** The local efficiency of node  $i$  is an efficiency of a subgraph including all neighbor nodes of  $i$ .

$$E_{loc} = \frac{1}{n} \sum_{i \in N} E_{loc,i} = \frac{1}{n} \sum_{i \in N} \frac{\sum_{j,h \in N, j \neq i} w_{ij} w_{ih} [d_{jh}(N_i)]^{-1}}{k_i(k_i - 1)}$$

where  $E_{loc,i}$  is the local efficiency of node  $i$ ,  $k_i = \sum_{j \in N} a_{ij}$  is the degree, and  $d_{jh}(N_i)$  is the length of the shortest path between node  $j$  and  $h$ , that contains only neighbors of node  $i$ .

**Small-world Network Property:** Small-world network shows a ratio  $\gamma$  defined as  $C/C^{\text{random}}$  of  $\gg 1$  and a ratio  $\lambda$  defined as  $L/L^{\text{random}}$  of  $\approx 1$ , with the clustering coefficient  $C^{\text{random}}$  and characteristic path length  $L^{\text{random}}$  of a random organized network of similar size.<sup>53,54</sup>  $C^{\text{random}}$  and  $L^{\text{random}}$  were computed as the average clustering coefficient and characteristic path length of a set of 100 random networks with a comparable total degree and degree distribution as that of the corresponding networks.

### C. Thresholding on Functional Network

In contrast to the (sparse) structural network, which was constructed by an existence of the streamlines between two nodes, the functional network has a dense connection matrix. Thus, thresholding the weakly connected links should be conducted before computing the graph metrics. For the functional network analysis, sparsity threshold ( $0.08 \leq$



$S \leq 0.48$ ) was used to compute network properties for each thresholding value.<sup>55,56</sup> Then the area under the curve for each graph metric was calculated for statistical comparison.

#### **D. Modular Organizations**

In addition to the graph metric, the modular organizations of the brain network are different between controls and patients group or between two contrasting personality groups. In the previous studies, impulsivity groups have the different modular characteristics.<sup>31</sup> Also, in the normal controls, a functional modular organization of the two contrasting temperament groups have different patterns of functional connectivity among the pre-frontal cortex, basal ganglia, and limbic system.<sup>57</sup>

**Modularity:** Modularity was computed from the weighted networks using a Louvain community detection algorithm.<sup>58</sup>

$$Q = \frac{1}{2m} \sum_{i,j} \left( W_{ij} - \frac{s_i s_j}{2m} \right) \delta(C_i, C_j),$$

where  $W_{ij}$  represents the connection weights between  $i$  and  $j$ ;  $s_i = \sum_j W_{ij}$  is the sum of the connection weights attached to node  $i$ ;  $C_i$  is the modular (community) structure to which node  $i$  is assigned; the delta function  $\delta(u, v)$  is 1 if  $u = v$  and 0 otherwise; and  $m = \frac{1}{2} \sum_{i,j} W_{ij}$ .

The group representative structural modular organizations were obtained from 1000 independent modularity optimization runs for the group averaged NOS-ROI and FA weighted structural networks, respectively. All reported modular organizations represent optimal solutions, which have the maximum modularity  $Q$  for each optimization process. Since Louvain method uses a heuristic strategy to maximize network modularity for a given

initial condition, every independent optimization run produces a different modular organization.<sup>59</sup> Normalized mutual information (NMI) was used to determine which community had the most similar structure to the other.<sup>33,60</sup> The community structure having the largest average value of NMI over all other optimization results was called *best partition* of the network.

**Jaccard index:** Jaccard similarity coefficient ( $J$ ) is a statistic used for comparing the similarity and diversity of modular structures. The Jaccard coefficient is defined as the size of the intersection divided by the size of the union of the modules (*i.e.*, sets of nodes).

$$J(A, B) = \frac{|A \cap B|}{|A \cup B|}$$

To compute the statistical significance of the Jaccard indices, we performed the 1000 independent permutation tests to get the null distribution. Finally, we identified the similar modules between groups by using the permutation test results ( $P < 0.05$ ).

### **E. Connectivity Density**

The between-group comparison of structural and functional connectivity density was performed as a post-hoc analysis. This analysis is necessary because the individual variations in the group-averaged brain network were ignored in the group averaged network. Thus, to support the different patterns of modular organizations between groups and to provide a quantitative statistics, the structural and functional connectivity density within- and between-modules should be further investigated.

**Functional Connectivity Density:** The functional connectivity density (FCD) was computed by averaging all within-module and between-modules connection weights as following:

$$\text{FCD}_{\alpha\beta} = \frac{1}{N} \sum_{i \in \text{CI}_{\alpha}} \sum_{j \in \text{CI}_{\beta}} A_{ij},$$

**Structural Path Length Density:** The structural path length density (SPLD) was computed from the distance matrix  $d_{ij}$  for each weighting method.

$$\text{SPLD}_{\alpha\beta} = \frac{1}{N} \sum_{i \in \text{CI}_{\alpha}} \sum_{j \in \text{CI}_{\beta}} d_{ij},$$

where the distance matrix between nodes  $i$  and  $j$  ( $d_{ij}$ ) is a set of the geodesic shortest path length computed by *Dijkstra* algorithm (Figure 5).

## 8. Prediction Model for Preoperative Delirium

The prediction of delirium is important because early intervention of delirium reduces the duration of delirium, length of hospitalization, and mortality in delirious patients.<sup>61</sup> Therefore, there have been a lot of studies in investigating risk factors for delirium in the domain of a demographic characteristic, cognitive deficit, medication status, and comorbidity.<sup>62,63</sup> Despite many studies, delirium remains frequently unrecognized and poorly understood.<sup>7,64</sup>

The clinical presentation of delirium is varying but can be classified into three subtypes, such as hypoactive, hyperactive and mixed, on the basis of psychomotor behavior.<sup>1</sup> Among the three motor subtypes, the hypoactive subtypes most frequently occurs in elderly patients, and these patients are frequently overlooked or misdiagnosed as having depression or a form of dementia.<sup>65</sup> Although there has been a guideline for diagno-

sis of delirium for the elderly patients, the clinical assessment for those patients with hypoactive delirium is limited.<sup>64</sup>

For non-communicative patients with hypoactive delirium, the neuroimaging methods without task stimulus would be useful for assessing a diagnosis and severity of delirium. In this study, a prediction model for postoperative delirium will be introduced using the preoperative neuroimaging data. The preoperative risk factors were computed for predicting postoperative delirium using the structural and functional network properties.

### **A. Logistic Regression**

The central statistical concept that underlies logistic regression is the logit, which is the natural logarithm of an odds ratio. For the binary output variable  $Y$ , what is the best way to model the conditional probability  $P(Y = 1|X = x)$  as a function of  $x$ ? The most obvious idea is to let  $\pi$  be a linear function of  $x$ . Every increment of a component of  $x$  would add or subtract so much to the probability. The conceptual problem here is that  $\pi$  must be between 0 and 1, and linear functions are unbounded. The next most obvious idea is to let  $\ln \pi$  be a linear function of  $x$ , so that changing an input variable multiplies the probability by a fixed amount. The problem is that logarithms are unbounded in only one direction, and linear functions are not. Finally, the easiest modification of  $\ln \pi$  which has an unbounded range is the logistic (or logit) transformation,  $\ln \frac{\pi}{1-\pi}$ . This transformation makes a linear function of  $x$ . Formally, the logistic regression model is can be written as following:

$$\text{logit}(Y) = \ln(\text{odds}) = \ln\left(\frac{\pi}{1-\pi}\right) = \alpha + \beta X.$$

If we solve the logit ( $Y$ ) for  $\pi$  - Probability( $Y = 1|X = x$ , a specific value of  $X$ ), we have

$$\pi = \frac{e^{\alpha+\beta x}}{1 + e^{\alpha+\beta x}} = \frac{1}{1 + e^{-(\alpha+\beta x)}}.$$

For the prediction of the disease,  $Y = 1$  when  $\pi \geq 0.5$  and  $Y = 0$  when  $\pi < 0.5$ . This means guessing 1 wherever  $\alpha + \beta x$  is non-negative, and 0 otherwise.

Extending the logic of the simple logistic regression to multiple predictors (say  $X_1 = \text{age}$  and  $X_2 = \text{gender}$ ), a complex logistic regression for  $Y$  as following:

$$\text{logit}(Y) = \ln\left(\frac{\pi}{1 - \pi}\right) = \alpha + \beta_1 X_1 + \beta_2 X_2.$$

Therefore,  $\pi$ -Probability( $Y = 1|X_1 = x_1, X_2 = x_2$ ) becomes

$$\pi = \frac{e^{\alpha+\beta_1 x_1+\beta_2 x_2}}{1 + e^{\alpha+\beta_1 x_1+\beta_2 x_2}},$$

where  $\pi$  is once again the probability of the event,  $\alpha$  and  $\beta$ s are regression coefficients, and  $X$ s are a set of predictors. Parameters  $\alpha$  and  $\beta$ s are typically estimated by the maximum likelihood methods.

The target dataset of the prediction modeling includes 58 preoperative hip fracture patients. In the prediction model, the outcome variable was the incidence of postoperative delirium and independent predictors are structural and functional connectivity densities. As a first step towards establishing the association between the incidence of postoperative delirium and the graph metrics obtained from the preoperative neuroimaging data. Before conducting the multivariate logistic regression analysis, bivariate logistic regression analysis was conducted to produce unadjusted odds ratios and corresponding 95 % confidence intervals. Then, multivariate logistic regression was performed to evaluate

the outcome of postoperative delirium with the main explanatory variables measured in the bivariate logistic regression.

## **B. Model Selection**

To select a best prediction model for delirium, several measures of a goodness of prediction models were considered. Classification tables using the predicted probabilities that provide sensitivity and specificity, and area under the receiver operating characteristics (ROC) curves. The area under ROC curve provides an overall measure of fit of the model. In particular, the area under curve provides the probability that a randomly selected pair of subjects, one truly positive, and one truly negative, will be correctly ordered by the test. In this study, we used analysis of ROC to measure a goodness of fit. The overall classification accuracy and area under ROC curve provides an overall measure of fit of the model.

As explained earlier, logistic regression predicts the logit of an event outcome from a set of predictors. Because the logit is the natural log of the odds (or  $\frac{\pi}{1-\pi}$ ), it can be transformed back to the probability scale. The resultant predicted probabilities can then be revalidated with the actual outcome to determine if high probabilities are indeed associated with events and low probabilities with non-events. The degree to which predicted probabilities agree with actual outcomes is expressed as either a measure of area under ROC curve or a classification table.

## 9. Brain Network Alteration during an Episode of Delirium

In this section, a new approach to the structural network and functional network (SN-FN) coupling and multi-sliced functional network modularity optimization methods will be introduced. A total of thirty-two the preoperative and postoperative paired samples (Delirium=14, Non-delirium=18) was used to investigate brain network alteration during an episode of delirium.

### A. SN–FN Coupling – Old Approach

In the structural network, a thresholding process was not necessary because the weighted connection matrix is intrinsically sparse since most node pairs are not interconnected by even a single streamline. In contrast, function network driven by resting state fMRI data albeit a possibly small functional correlation is found between all network nodes, hence necessitating the use of a thresholding procedure to yield a sparse adjacency matrix.

For pre- and postoperative brain imaging data, a pair of structural and functional network used to compute a structure network and function network (SN-FN) coupling strength to test the synchrony or desynchrony of FN from structural network. To evaluate a coupling strength between the FN and SN for each subject a correlation analysis between the weights of the SN connection matrix and their functional counterparts (*i.e.*,  $\mathcal{S}(\text{FN})$ , a sparse FN), was conducted as illustrated in Figure 6A. All nonzero elements of the SN connection matrix were selected, rescaled to a Gaussian distribution, and correlated with their counterparts selected from the FN matrix as described elsewhere.<sup>49,66</sup> This implies a single SN– $\mathcal{S}(\text{FN})$  coupling metric for individual's the brain networks.

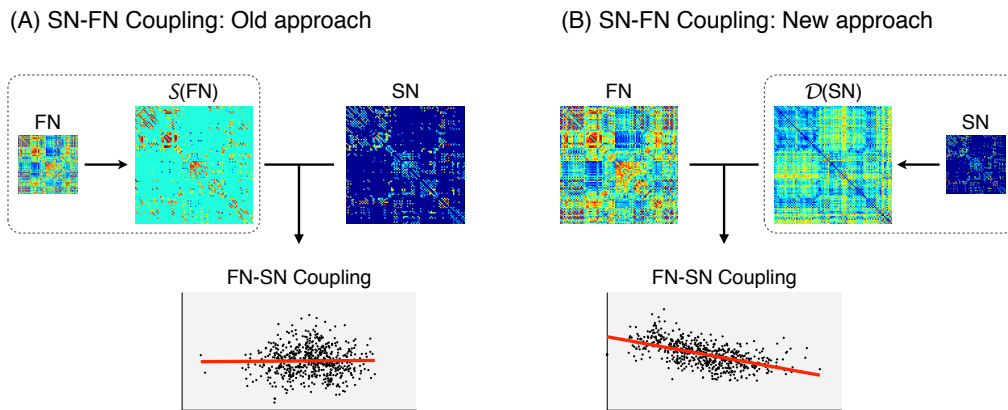


Figure 6. Graphical illustrations for a measure of coupling strength between structural network (SN) and functional network (FN). SN-FN coupling strength was computed by two different methods: (A) An old approach for SN-FN coupling analysis. In old approach of SN-FN coupling analysis, sparse functional network connection matrix was obtained from the counterparts of nonzero SN elements. (B) A proposed approach for SN-FN coupling analysis. Full functional network elements and distance matrix from SN was used for the new approach of SN-FN coupling analysis.

## B. SN-FN Coupling – New Approach

The idea of the old approach for SN-FN coupling is to select a sparse FN from fully connected FN in evaluation of a synchrony between sparse SN and all-to-all connected FN. Here, a new approach for SN-FN coupling is proposed. The essential part of the proposed SN-FN coupling method is to convert sparse SN to a densely connected distance network,  $\mathcal{D}(SN)$ , by *Dijkstra* shortest path length algorithm (Figure 5). Then, a functional connectivity synchrony with structural backbone network was computed by using fully connected FN,  $\mathcal{F}(FN)$ , and densely connected distance matrix of SN,  $\mathcal{D}(SN)$ .



### C. Multi-sliced Functional Modular Organizations

In this subsection, multi-slice (or time-dependent) modularity optimization network will be introduced. The previously introduced modularity optimization method was not suitable for the multi-sliced network system. So, to identify the modular organizations of delirium and non-delirium functional networks before and after a hip fracture surgery, the generalized modularity optimization algorithm will be used. The generalized form of modularity optimization algorithm was recently introduced and it could be applied to multislice and multiplex network.<sup>67</sup> The generalized modularity function is defined as

$$Q_{\text{multi}} = \frac{1}{2\mu} = \sum_{i,j,s,r} \left[ \left( A_{ijs} - \gamma_s \frac{k_{is}k_{js}}{2m_s} \right) \delta_{sr} + \delta_{ij} \omega_{jsr} \right] \delta(C_{is}, C_{jr})$$

where  $C_{is}$  indicates that community assignment of node  $i$  from slice  $s$ , the intraslice edge strength of node  $j$  in slide  $s$  is  $k_{js} = \sum_i A_{ijs}$ , the corresponding interslice edge strength is  $c_{js} = \sum_r \omega_{jsr}$ , and  $2\mu = \sum_{jr} k_{jr} + c_{jr}$ . In the multi-sliced modularity ( $Q_{\text{multi}}$ ), one can use a different resolution parameter  $\gamma_s$  in each slice. For a given slice  $s$ , the quantity  $A_{ijs}$  gives the edge weight between node  $i$  and  $j$ . For a given node  $j$ , the quantity  $\omega_{jsr}$  give the interslice coupling between the  $r$ th and  $s$ th slices.

The interslice edge strength (or coupling strength) between pre- and postoperative functional networks was obtained by Pearson's correlations for delirium and non-delirium groups, respectively.

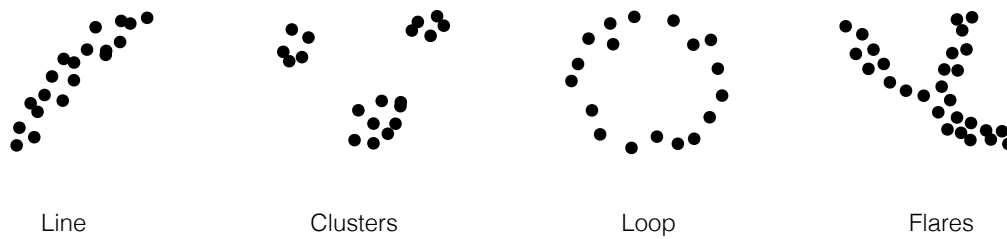


Figure 7. Shape encodes structure and meaning of complex data: Line or linear shape, clustered data, loop, and flares.

## 10. Topology-based Subgroups Identification in Delirium

*Topology* is a field of mathematics and a sort of geometry concerning the shape. Topological data analysis refers to the adaptation of this discipline to analyzing high dimensional and complex data.<sup>40,68</sup> One of the key messages around topological data analysis is that the data has a shape, and the shape matters (Figure 8). For understanding and interpreting the data, the different statistical or mathematical methods should be applied to the different shapes of data. Figure 8 showed four different shapes of data. A linear regression is the best way to fit the data in the linearly distributed points cloud (see line-shaped point clouds in Figure 8). Unfortunately, the data does not always cooperate and fit along a line. For example, point clouds can be distributed in the shapes of clusters, loop, or flares as shown in Figure 8. It is easy to see that no straight line represents these data. Thus, some clustering algorithm should be used to describe the clustered points cloud. Also, loopy or flare shaped data can not be explained by a straight line. For describing flares, researchers might separate data for each flare and analyze them independently. The modern technology called as machine intelligence combines topological data analysis and unsupervised machine learning methods to find patterns in data by various sta-

tistical or mathematical approaches. Topology-based data analysis produces a compact representation of the data that shows us all of those shapes at once. Whatever shape data has, without having to know it in advance, topological data analysis can map that out for us in a way that we can use as a foundation for further analysis.

In this section, topological data analysis will be introduced to get more insights about delirium. The essence of topological data analysis is to extract a geometric shape from the relationships among patients by using *partial clustering* method. *Mapper* is a tool for topological data analysis that was introduced in bioinformatics<sup>39</sup> and neuroimaging data analytics.<sup>42</sup>

Figure 8 showed analysis procedures of topological data analysis. The first and second steps toward for using topological data analysis is to define filter and distance functions. There are various ways to define filter and distance functions.<sup>40</sup> However, in this particular study, clinical variables such as IQCODE, MMSE, and K-DRS scales were used for topological data analysis. The filter function is used to measure of overall magnitude of delirium in combination of three clinical scales, and distance function is used to measure the relationships between patients. The step by step procedures of topological data analysis are introduced in the following subsection.

### **A. Filter function**

The first step for topological data analysis is to define the filter function. For five-dimensional clinical variables of the patient  $i$ , dataset  $T$  become a matrix with dimensions of  $58 \times 5$  (*i.e.*, number of patients  $\times$  number of clinical variables).

$$T = \{\text{IQCODE, MMSE, K - DRS, BFI - C, BFI - N}\}.$$

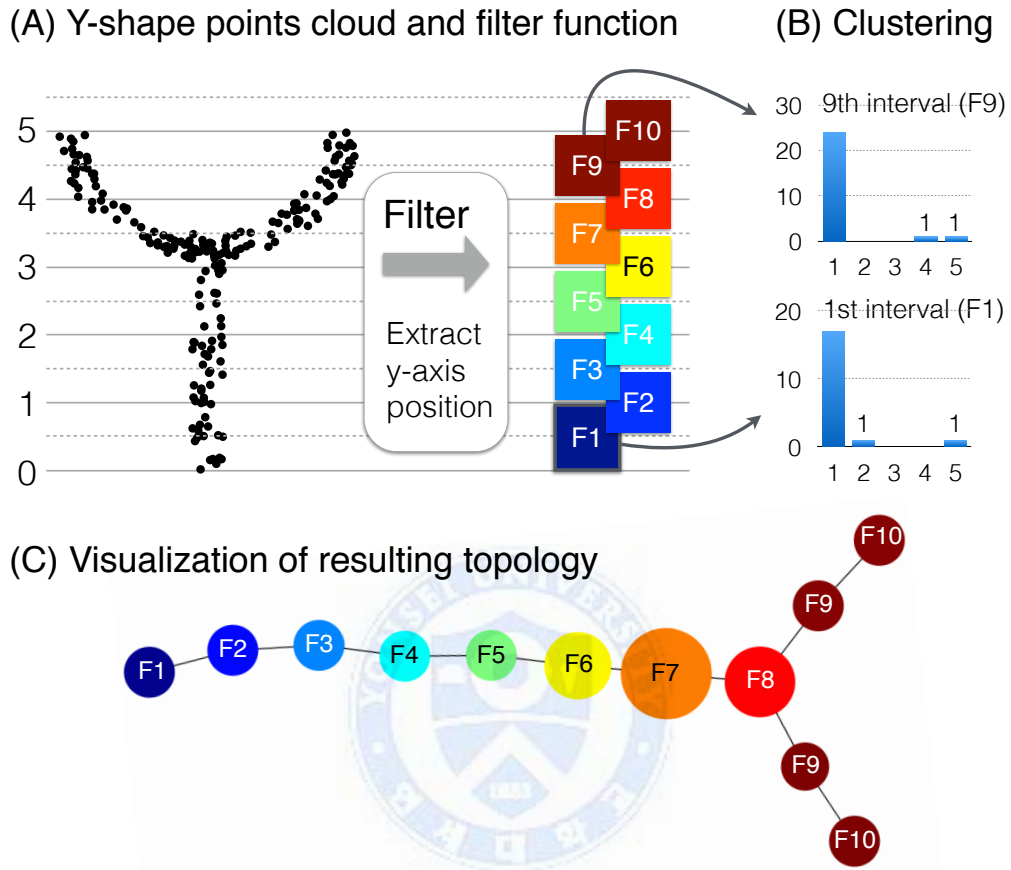


Figure 8. Schematic diagram of topological data analysis using *Mapper*. Steps for topological data analysis are as following: (A) The data is sampled from a noisy Y-shape points cloud in the two-dimensional space, and the filter function is  $f(x,y) = y$ . The range of filter was divided into five intervals with a 50 % overlap. (B) For each interval, the partial clustering of the points lying within the domain of filter restriction to the intervals was performed. Distributions of the distances from single linkage dendrogram in each filter bin. For example, distance distributions for 1st and 9th filter bin were presented. The summation of frequencies appeared after zero bins is the number of clusters. (C) The graphical illustration of the simplicial complex by connecting the clusters whenever they have non-empty intersection. The color of vertices represents the average filter value.

Now, to project multidimensional dataset to a linear space, principal component analysis was applied and first eigen variate was selected for the value of the filter function.

### **B. Distance function**

The second step to define the distance function. In this study and most other studies, Euclidean distance was used to obtain dissimilarity matrix from all pairs of data points:

$$d(\mathbf{x}, \mathbf{y}) = \sqrt{(x_1 - y_1)^2 + (x_2 - y_2)^2 + \cdots + (x_n - y_n)^2},$$

where  $x$  and  $y$  indicate a vector  $T_i$  for each patient.

### **C. Clustering method**

The third step is to define the clustering method. The single-linkage method was chosen for clustering method that showed good performances in various topological data analysis studies.<sup>39,69</sup> A detailed description of these particular clustering procedures can be found in literatures.<sup>69</sup>

### **D. Visualization**

The last step is to visualize the resulting topology using a graph as shown in Figure 8C. For visualization, the two resolution parameters were required to zoom in and out the hidden patterns in the dataset. In the visualization, each node in the graph is a subset of patients and edges connect similar nodes. A color of each node encodes the value of the filter function averaged across all the data points to the node, with blue representing a low value and red denoting a large value.

## **11. Statistical Analysis**

Delirium and non-delirium group differences in various graph metrics, structural path length density, and functional connectivity density were tested by an independent sample *T*-test with a significance level of corrected  $P < 0.05$ . In general, demographic variables such as age and sex were known to be related functional and structural connectivity. However, in a case of group comparisons for graph metrics, covariates were not considered if two independent groups have no differences in demographic characteristics.<sup>70–72</sup>

### **A. Multiple Comparison Correction**

In general, the modularity optimization of the whole-brain network produces five to seven modules. This implies that a total of ten to twenty-one univariate comparisons of the intra- and inter-module connectivity density would be conducted to find group differences in functional connectivity density and structural path length density. Therefore, a controlling the family-wise error rate is necessary. The network-based statistic (NBS) is a method to control the family-wise error rate when mass-univariate testing is performed at every connection comprising the graph.<sup>73</sup> In the current study, the NBS was applied and 10,000 permutation tests were performed to estimate the null distribution of maximal component size.

### **B. Correlation with Clinical Variables**

The graph metrics and connectivity densities, which show the significant group differences, were further investigated. A Spearman's correlation analysis was performed to unfold the relationships between the network variables and clinical variables. The statistical significance level was set to a *P* value less than 0.05.

### **C. Mixed Design Analysis of Variance**

Mixed design analysis of variance (ANOVA) was used to examine brain network alterations. Mixed design ANOVA tested the differences in between-subjects effect (delirium and non-delirium), within-subject effect (preoperative and postoperative), and interaction effects between them. In mixed ANOVA, one repeated-measures independent variable and one between-group independent variable were included. In this study, mixed design ANOVA was used to investigate changes in mean values of the functional network characteristics over two-time points (preoperative and postoperative) for delirium and non-delirium groups. A within-subject effect (pre- and postoperative), a between-subjects effect (delirium and non-delirium), and a group by time interactions were tested with a significance level of  $P < 0.05$ .



### III. RESULTS

Various graph metrics and connectivity densities, which introduced in the materials and methods, are summarized in this section. First, group differences in demographic and clinical variables and medical history will be presented. Second, structural and functional neural substrates of preoperative delirium will be shown through a between-group comparison. This includes the statistical comparison of graph metrics between preoperative delirium and non-delirium patients, qualitative descriptions of the structural modular organization, and delirium prediction model obtained from a logistic regression approach. Third, results from a study of brain network alteration during an episode of delirium will be described. The mixed design analysis of variance was chosen for comparing the paired sample of pre- and postoperative neuroimaging dataset. Lastly, a topology-based delirium subgroups identification will be presented.

#### 1. Demographic and Clinical Variables

Table 3 showed the summary of demographic variable and clinical scales. Age, sex, educational year, and IQCODE showed no significant differences between groups. However, the significantly decreased MMSE was found in preoperative delirium compared to preoperative non-delirium ( $P = 0.048$ ). Medical history such as dementia, brain injury, hypertension, and diabetes showed no significant group differences (Table 4). However, the number of major mental disorder history found to be twice in delirium ( $n = 8$  and 32 %) compared to non-delirium ( $n = 4$  and 12 %). In the comparison of psychological scales, Hamilton anxiety scale was marginally increased in preoperative delirium ( $P = 0.065$ ). Whereas, Hamilton Rating Scale for Depression was showed no differences



Table 3. Demographic and clinical characteristics of the preoperative delirium and non-delirium patients with the hip fracture

Characteristic	Preoperative dataset			Postoperative dataset			
	Delirium (n = 25)	Non-delirium (n = 33)	Statistic	Delirium (n = 14)	Non-delirium (n = 18)	Statistic	P value
<b>Preoperative assessment</b> ( <i>i.e.</i> , before the hip fracture surgery)							
Age, year <sup>d</sup>	83.5 (6.2)	80.6 (6.8)	1.7	83.9 (6.7)	81.1 (7.5)	1.1	0.271
Sex, M/F <sup>b</sup>	7/18	4/29	2.3	5/9	3/15	1.5	0.217
Education, year <sup>d</sup>	9.0 (4.2)	7.9 (5.0)	0.8	9.6 (4.4)	8.2 (3.8)	0.9	0.361
IQCODE <sup>a</sup>	91.5 (14.2)	85.6 (10.6)	1.8	94.7 (16.2)	86.4 (11.7)	1.6	0.113
MMSE <sup>a</sup>	17.2 (6.4)	20.5 (6.1)	-2.0	16.8 (7.1)	21.2 (6.4)	-1.8	0.079
<b>Postoperative assessment</b> ( <i>i.e.</i> , during the episode of Delirium)							
Delirium Assessment							
Delirium duration, days	5.6 (6.3)			5.4 (3.0)			
K-DRS score <sup>c</sup>	19.8 (4.3)			20.2 (4.3)			
Motor subtype, No. (%) <sup>d</sup>							
Mixed	13 (52 %)			8 (32 %)			
Hypoactive	9 (36 %)			5 (20 %)			
Hyperactive	3 (12 %)			1 (4 %)			

The numbers in the table represent mean (standard deviation) value.

Abbreviations: IQCODE, Informant Questionnaire on Cognitive Decline in the Elderly; K-DRS, Korean version of Delirium Rating Scale;

MMSE, Mini Mental State Examination; M/F, male/female.

<sup>a</sup>Independent sample *T*-Test.

<sup>b</sup> $\chi^2$  Test.

<sup>c</sup>The number of missing values in IQCODE are 1 in the preoperative delirium patients and 2 in the non-delirium patients.

<sup>d</sup>K-DRS scores were assessed at the first day of the patients were identified as Delirium after the hip fracture surgery.

<sup>e</sup>Motor subtypes of delirium were made based on the Delirium Motor Subtype Scale (DMSS)

Table 4. Summary of preoperative patients characteristics and operation-related information

Medical history	Delirium (n = 25)	Non-delirium (n = 33)	T or $\chi^2$	P value
<b>Medical history, No. (%)</b>				
Major mental disorder history	8 (32.0)	4 (12.1)	3.43	0.064
Dementia history	7 (28.0)	6 (18.2)	0.79	0.375
Delirium history	4 (16.0)	2 (6.1)	1.32	0.251
Brain injury history	3 (12.0)	6 (18.2)	0.42	0.520
Hypertension	19 (76.0)	22 (66.7)	0.60	0.439
Diabetes	8 (32.0)	10 (30.3)	0.02	0.890
<b>Preoperative psychological scales, mean (SD)</b>				
Hamilton Anxiety Scale	10.1 (8.1)	6.1 (7.5)	1.89	0.065
Hamilton Rating Scale for Depression	6.0 (5.3)	4.0 (4.7)	1.49	0.141
<b>Operation-related data</b>				
Regional anesthesia, No. (%)	13 (52.0)	14 (42.4)	0.52	0.469
Anesthesia duration, mean (SD), min.	132.0 (40.4)	114.4 (26.5)	2.00	0.050

between delirium and non-delirium (Table 4). Finally, in the comparison of operation-related variables, the significant increase of anesthesia duration was found in delirium ( $P = 0.05$ ).

## **2. Neural Substrates of Preoperative Delirium**

The independent samples *T*-test compares the mean values of graph metrics between delirium and non-delirium groups. The significant differences between two groups will be presented in the following subsections.

### **A. Structural Network Properties**

The mean values of various graph metrics between the preoperative delirium and non-delirium comparison patients were compared. Table 5 shows the statistical comparisons of all graph metrics for two different weighting methods. Among the various network properties, the characteristic path length was significantly increased in the preoperative delirium compared to non-delirium comparison patients ( $P < 0.05$ ).

### **B. Functional Network Properties**

For functional networks, we measured graph metrics for various thresholding value and computed the area under a curve for each graph metric. The statistical comparisons were conducted for the area under a curve of each graph metric. As summarized in Table 6, no significant differences between two groups in graph metrics were found.

### **C. Structural Modular Organizations**

The modularity is a measure of how the community structure of a graph is different from the random graph. Also, a quantitative value representing the modularity ( $Q$ ) would not provide the geometric topology of the brain connectivity. Therefore, the investigation of brain network patterns was performed to understand the topological alteration of the brain network in preoperative delirium. The best modular organizations of the struc-

Table 5. Group averaged values of structural network properties and statistical comparisons between preoperative delirium and non-delirium

Graph measures	Delirium ( <i>n</i> = 25)	Non-delirium ( <i>n</i> = 33)	<i>T</i> statistic	<i>P</i> value
<b>NOS-ROI weighted</b>				
Global Efficiency	7.10 (1.07)	7.48 (0.65)	-1.69	0.097
Local Efficiency	11.65 (1.47)	11.93 (0.91)	-0.90	0.373
Characteristic Path Length	0.21 (0.07)	0.18 (0.02)	2.01	0.049
Clustering Coefficient	2.01 (0.22)	2.04 (0.15)	-0.64	0.522
$\lambda$	1.49 (0.31)	1.37 (0.11)	2.01	0.049
$\gamma$	4.51 (0.31)	4.45 (0.25)	0.84	0.406
Modularity, <i>Q</i>	0.58 (0.02)	0.58 (0.02)	-0.11	0.913
<b>FA weighted</b>				
Global Efficiency	0.25 (0.04)	0.27 (0.02)	-1.436	0.157
Local Efficiency	0.35 (0.05)	0.37 (0.03)	-1.576	0.121
Characteristic Path Length	4.61 (0.60)	4.33 (0.37)	2.157	0.035
Clustering Coefficient	0.12 (0.01)	0.12 (0.01)	-0.947	0.348
$\lambda$	1.16 (0.03)	1.16 (0.03)	0.368	0.714
$\gamma$	3.44 (0.29)	3.35 (0.18)	1.33	0.189
Modularity, <i>Q</i>	0.43 (0.03)	0.43 (0.03)	0.11	0.913

The numbers represent mean (standard deviation) value.

Abbreviations: FA, fractional anisotropy; NOS-ROI, number of streamlines corrected for volume of each region of interest,  $\gamma$ , normalized clustering coefficient;  $\lambda$ , normalized characteristic path length.

tural network were obtained by maximizing the average normalized mutual information (NMI) value over all optimization results. The best partition is the representative structural network modular organization for each group and each weighting method. The structural modular architectures obtained from both weighting methods showed almost symmetrical clustering except for the left visual and temporal regions. The detailed descriptions of structural modular organizations are described in the below.

Table 6. Group averaged values of functional network properties and statistical comparisons between preoperative delirium and non-delirium

Graph measures	Delirium ( <i>n</i> = 25)	Non-delirium ( <i>n</i> = 33)	<i>T</i> statistic	<i>P</i> value
Global Efficiency	0.24 (0.01)	0.24 (0.01)	0.27	0.792
Local Efficiency	0.31 (0.01)	0.32 (0.01)	-0.21	0.833
Characteristic Path Length	0.85 (0.07)	0.85 (0.04)	0.31	0.755
Clustering Coefficient	0.24 (0.02)	0.24 (0.02)	-0.38	0.708
$\lambda$	0.47 (0.04)	0.47 (0.02)	0.32	0.748
$\gamma$	1.04 (0.09)	1.05 (0.08)	-0.44	0.664
Modularity, <i>Q</i>	0.35 (0.03)	0.35 (0.04)	-0.37	0.710

The numbers represent mean (standard deviation) value.

Abbreviations:  $\gamma$ , normalized clustering coefficient;  $\lambda$ , normalized characteristic path length.

**Modular organizations - NOS-ROI weighted:** As shown in Figure 9A-B, seven distinct structural communities were found. The overall patterns of the structural network modular organizations showed almost indistinguishable between preoperative delirium and non-delirium (NMI = 0.78).

Among seven distinct partitions, the modular organization of the right frontal-parietal regions were the exactly the same between two groups ( $J = 1$  and  $P < 0.05$ ). Also, the similarity of a module between two groups were significant ( $P < 0.05$ ) in the left frontal-parietal regions ( $J = 0.81$ ), medial frontal-parietal regions ( $J = 0.72$ ), orbitofrontal cortex and basal ganglia regions ( $J = 0.76$ ). However, there showed significant differences in the temporal and visual regions. In the preoperative delirium, the left and right visual cortex regions were divided into two separate modules. Whereas, in the non-delirium comparison patients, visual-temporal regions were divided into three parts: The left temporal lobe and left visual cortex, right temporal lobe and right lateral visual cortex, and

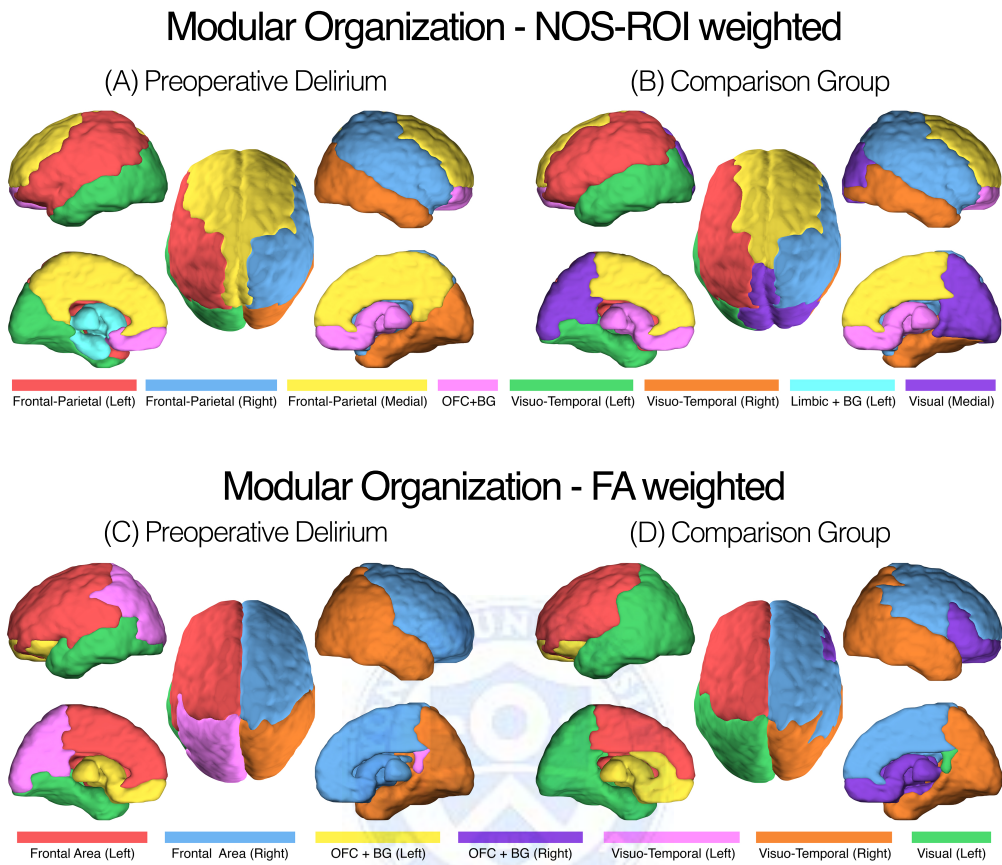


Figure 9. Visualization of structural network modular organizations for each weighting method. See Tables A1–A2 for a detailed description of brain areas for each module.

the medial part of the visual cortex. The Jaccard indices for all modules in the preoperative delirium and non-delirium comparison patients were summarized in Table 7.

**Modular organizations - FA weighted:** Figure 9C-D showed the FA weighted structural network modular organizations. The overall patterns of the structural network modular organizations were almost similar across two groups (NMI = 0.75). Unlike the modular architectures obtained from the NOS-ROI weighted structural network, clear

Table 7. Similarity of the structural modular organizations between the preoperative delirium and non-delirium comparison groups

Module in preoperative delirium	Modules in non-delirium comparison patients
<b>NOS-ROI weighted</b>	
Lt. Frontal-Parietal (FP)	Lt. FP (0.81*), Lt. Temporal (0.08)
Rt. Frontal-Parietal	Rt. FP (1.0*)
Med. Frontal-Parietal	Med. FP (0.72*), Med. Visual (0.15), Lt. FP (0.03)
OFC plus BG	OFC plus BG (0.76*)
Lt. Visual-Temporal (VT)	Lt. Temporal (0.47*), Med. Visual (0.16)
Rt. Visual-Temporal	Rt. Temporal (0.62*), Med. Visual (0.25)
Lt. Limbic	OFC plus BG (0.2), Lt. Temporal (0.19)
<b>FA weighted</b>	
Lt. Frontal Lobe (FL)	Lt. FL (0.82*), Lt. VT (0.05), Lt. OFC plus BG (0.04)
Rt. Frontal Lobe + BG (FL+BG)	Rt. OFC plus BG (0.5*), Rt. FL (0.4*)
Lt. OFC plus BG	Lt. OFC plus BG (0.9*)
Lt. Visual	Lt. visuotemporal (0.45*)
Lt. Temporal	Lt. visuotemporal (0.45*)
Rt. visuotemporal	Rt. VT (0.76*), Rt. OFC plus BG (0.09), Rt. FL (0.06)

The number in the parenthesis indicate the Jaccard similarity statistic.

Abbreviations: BG, basal-ganglia; Lt, left; Med, medial; OFC, Orbitofrontal cortex; Rt, right.

\*Values represent the significantly similar modular structures between the preoperative Delirium and non-delirium comparison patients ( $P < 0.05$ ).

hemispheric separations of the modules were observed.

Among them, the modular organizations of the left frontal lobe ( $J = 0.82$ ), left orbitofrontal cortex plus basal ganglia ( $J = 0.9$ ), and right visual-temporal modules ( $J = 0.76$ ) were almost the same between two groups ( $P < 0.05$ ). However, there showed significantly different patterns of modules in the left temporal and visual regions. In the preoperative delirium, the left visual and temporal areas were divided into two separate modules. Whereas, in non-delirium comparison patients, the left visual-temporal regions were clustered into a single module. Also, the brain regions covering the right frontal

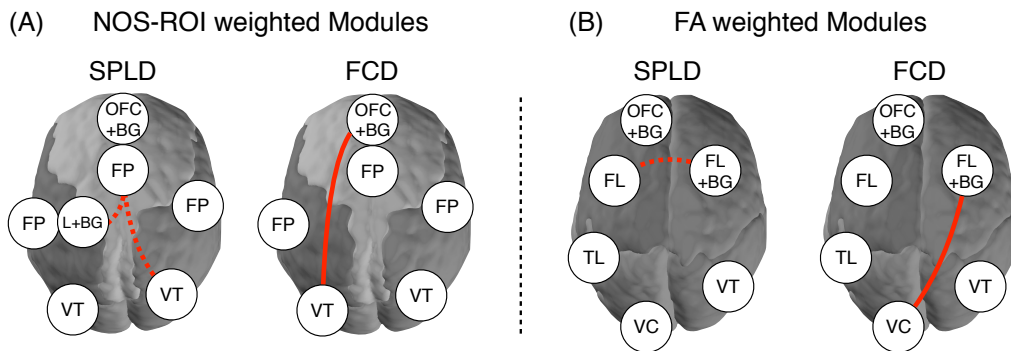


Figure 10. Connectivity density analysis for the best partitions obtained from (A) NOS-ROI weighted and (B) FA weighted structural network. The dotted red curves represent increased structural path length density (SPLD) and the solid red curves represent functional connectivity density (FCD) in preoperative delirium compared to the non-delirium comparison patients. Abbreviations: BG, basal ganglia; FL, frontal lobe; FP, frontal-parietal; L+BG, limbic areas plus basal ganglia; OFC, orbitofrontal cortex; TL, temporal lobe; VT, visual-temporal; VC, visual cortex

lobe, orbital cortex, and the basal ganglia regions showed different patterns of the modular organizations. In preoperative delirium, all those brain regions were clustered into a single module. Whereas, in non-delirium comparison patients, the right orbitofrontal cortex plus basal ganglia regions were clustered into a single module, and the rest of the brain regions in the right frontal lobe formed a separate module. The Jaccard indices for all modules in the preoperative delirium and non-delirium comparison patients were summarized in Table 7.

#### D. Connectivity Density Analysis

The statistical comparisons of the connectivity densities for the best partitions were conducted for NOS-ROI and FA weighted structural networks, respectively. The statistical comparisons of the connectivity densities for structural and functional networks were



summarized in Tables 8–9. Where, structural path length density, which was calculated from the distance matrix, was used for the alternative measures of structural connectivity density instead of computing averaging connection weights itself. During the statistical comparisons, functional connectivity density was computed for the corresponding modules obtained from the NOS-ROI and FA weighted structural network, respectively.

**Connectivity Density in NOS-ROI weighted structural module:** Figure 10A shows the significant differences in the connectivity density between preoperative delirium and non-delirium groups. Structural path length density connecting the medial frontal-parietal regions to the right visual-temporal module and the left frontal-parietal modules was significantly increased in preoperative delirium compared to non-delirium comparison patients (corrected  $P < 0.05$ ). Also, functional connectivity density between the left visual-temporal and orbitofrontal cortex plus basal ganglia modules was significantly increased in the preoperative delirium (corrected  $P < 0.05$ ). The rest of the statistical comparisons are summarized in Table 8.

**Connectivity Density in FA weighted structural module:** Figure 10B shows the significant differences in the connectivity density between preoperative delirium and non-delirium groups. Structural path length density connecting the left frontal lobe to the right frontal lobe plus basal ganglia was significantly increased in preoperative delirium compared to non-delirium (corrected  $P < 0.05$ ). In the analysis of functional connectivity density, the right frontal lobe plus basal ganglia and the left visual cortex have significantly increased in the preoperative delirium (corrected  $P < 0.05$ ). The rest of the statistical comparisons are summarized in Table 9.

Table 8. Structural path length density (SPLD) and functional connectivity density for NOS-ROI weighted structural modular organizations

Module	SPLD (NOS-ROI weighted)		Functional connectivity density	
	Delirium ( <i>n</i> = 25)	Non-delirium ( <i>n</i> = 33)	Delirium ( <i>n</i> = 25)	Non-delirium ( <i>n</i> = 33)
<b>Intra-Module Connectivity Density</b>				
Left Frontal-Parietal (Lt. FP)	0.105 (0.036)	0.102 (0.027)	0.22 (0.10)	0.24 (0.12)
Right FP (Rt. FP)	0.237 (0.445)	0.137 (0.073)	0.22 (0.11)	0.24 (0.11)
Medial FP (Med. FP)	0.100 (0.017)	0.093 (0.013)	0.15 (0.10)	0.17 (0.08)
OFC and BG	0.102 (0.074)	0.107 (0.113)	0.30 (0.11)	0.30 (0.12)
Left Visuotemporal (Lt. VT)	0.099 (0.032)	0.094 (0.027)	0.25 (0.12)	0.27 (0.12)
Right Visuotemporal (Rt. VT)	0.123 (0.077)	0.098 (0.029)	0.22 (0.12)	0.20 (0.10)
Left Limbic+BG (Lt. L+BG)	0.076 (0.022)	0.066 (0.016)	0.30 (0.12)	0.32 (0.12)
<b>inter-module Connectivity Density</b>				
Lt. FP ↔ Rt. FP	0.328 (0.268)	0.258 (0.040)	-0.05 (0.11)	-0.09 (0.15)
Lt. FP ↔ Med. FP	0.175 (0.031)	0.169 (0.028)	-0.02 (0.07)	-0.03 (0.07)
Lt. FP ↔ OFC plus BG	0.200 (0.039)	0.198 (0.069)	0.00 (0.09)	-0.02 (0.09)
Lt. FP ↔ Lt. VT	0.165 (0.036)	0.159 (0.034)	-0.02 (0.09)	0.00 (0.13)
Lt. FP ↔ Rt. VT	0.268 (0.054)	0.242 (0.039)	-0.10 (0.07)	-0.08 (0.10)
Lt. FP ↔ Lt. L+BG	0.157 (0.027)	0.149 (0.024)	0.06 (0.09)	0.08 (0.12)
Rt. FP ↔ Med. FP	0.251 (0.266)	0.181 (0.039)	-0.05 (0.08)	-0.04 (0.06)
Rt. FP ↔ OFC plus BG	0.261 (0.286)	0.194 (0.087)	0.02 (0.09)	0.04 (0.09)
Rt. FP ↔ Lt. VT	0.330 (0.266)	0.254 (0.048)	-0.11 (0.09)	-0.12 (0.11)
Rt. FP ↔ Rt. VT	0.248 (0.284)	0.170 (0.055)	0.01 (0.06)	0.02 (0.09)
Rt. FP ↔ Lt. L+BG	0.324 (0.276)	0.245 (0.046)	-0.05 (0.08)	-0.06 (0.10)
Med. FP ↔ OFC plus BG	0.169 (0.035)	0.166 (0.064)	0.03 (0.09)	0.02 (0.09)
Med. FP ↔ Lt. VT	0.213 (0.030)	0.203 (0.028)	-0.01 (0.18)	0.01 (0.18)
Med. FP ↔ Rt. VT <sup>a</sup>	0.217 (0.049)	0.190 (0.022)	-0.06 (0.15)	-0.02 (0.12)
Med. FP ↔ Lt. L+BG <sup>a</sup>	0.204 (0.029)	0.186 (0.023)	-0.13 (0.17)	-0.14 (0.17)
OFC plus BG ↔ Lt. VT <sup>b</sup>	0.237 (0.042)	0.223 (0.065)	-0.10 (0.13)	-0.17 (0.11)
OFC plus BG ↔ Rt. VT	0.207 (0.088)	0.183 (0.069)	0.01 (0.12)	-0.02 (0.10)
OFC plus BG ↔ Lt. L+BG	0.163 (0.053)	0.162 (0.078)	0.21 (0.12)	0.21 (0.10)
Lt. VT ↔ Rt. VT	0.225 (0.053)	0.198 (0.042)	0.04 (0.13)	0.03 (0.10)
Lt. VT ↔ Lt. L+BG	0.160 (0.035)	0.145 (0.031)	0.12 (0.14)	0.10 (0.13)
Rt. VT ↔ Lt. L+BG	0.248 (0.064)	0.215 (0.035)	0.04 (0.16)	0.01 (0.09)

The numbers represent mean (standard deviation) value.

Abbreviations: BG, basal ganglia; FP, frontal-parietal; Lt, left; L+BG, limbic areas plus basal ganglia; Med, medial; OFC, orbitofrontal cortex; Rt, right.

<sup>a</sup>Significantly different structural path length density (NOS-ROI weighted) between groups (corrected  $P < 0.05$ ).

<sup>b</sup>Significantly different functional connectivity density between groups (corrected  $P < 0.05$ ).

Table 9. Structural path length density (SPLD) and functional connectivity density for FA weighted structural modular organizations

Module	SPLD (FA weighted)		Functional connectivity density	
	Delirium ( <i>n</i> = 25)	Non-delirium ( <i>n</i> = 33)	Delirium ( <i>n</i> = 25)	Non-delirium ( <i>n</i> = 33)
<b>Intra-Module Connectivity Density</b>				
Left Frontal lobe (Lt. FL)	3.28 (0.36)	3.11 (0.25)	0.20 (0.11)	0.20 (0.10)
Right FL and BG (Rt. FL+BG)	3.31 (0.50)	3.11 (0.44)	0.16 (0.08)	0.19 (0.09)
Left OFC and BG (Lt. OFC plus BG)	2.29 (0.30)	2.35 (0.48)	0.31 (0.12)	0.29 (0.11)
Left Visual Cortexl (Lt. VC)	2.46 (0.45)	2.33 (0.33)	0.21 (0.09)	0.23 (0.13)
Left Temporal Lobe (Lt. TL)	3.01 (0.44)	2.89 (0.40)	0.24 (0.17)	0.21 (0.11)
Right visuotemporal (Rt. VT)	3.53 (0.53)	3.36 (0.34)	0.12 (0.06)	0.11 (0.08)
<b>inter-module Connectivity Density</b>				
Lt. FL ↔ Rt. FL+BG <sup>a</sup>	4.87 (0.70)	4.46 (0.42)	-0.02 (0.09)	-0.03 (0.11)
Lt. FL ↔ Lt. OFC plus BG	3.79 (0.41)	3.59 (0.42)	0.09 (0.12)	0.08 (0.10)
Lt. FL ↔ Lt. VC	4.09 (0.64)	3.79 (0.45)	-0.01 (0.09)	0.00 (0.13)
Lt. FL ↔ Lt. TL	4.76 (0.56)	4.42 (0.48)	0.01 (0.15)	0.01 (0.12)
Lt. FL ↔ Rt. VT	5.66 (0.87)	5.20 (0.57)	-0.07 (0.07)	-0.06 (0.09)
Rt. FL+BG ↔ Lt. OFC plus BG	4.56 (0.63)	4.32 (0.56)	0.16 (0.08)	0.17 (0.09)
Rt. FL+BG ↔ Lt. VC <sup>b</sup>	5.00 (0.93)	4.75 (0.56)	-0.06 (0.07)	-0.11 (0.07)
Rt. FL+BG ↔ Lt. TL	6.05 (0.88)	5.65 (0.59)	-0.04 (0.09)	-0.06 (0.07)
Rt. FL+BG ↔ Rt. VT	4.61 (0.67)	4.39 (0.45)	0.00 (0.06)	0.00 (0.05)
Lt. OFC plus BG ↔ Lt. VC	4.68 (0.83)	4.45 (0.66)	-0.01 (0.09)	-0.05 (0.11)
Lt. OFC plus BG ↔ Lt. TL	4.35 (0.69)	4.20 (0.57)	0.04 (0.11)	0.08 (0.13)
Lt. OFC plus BG ↔ Rt. VT	5.66 (0.81)	5.43 (0.66)	-0.09 (0.10)	-0.12 (0.10)
Lt. VC ↔ Lt. TL	4.09 (0.70)	3.86 (0.46)	-0.05 (0.09)	-0.03 (0.10)
Lt. VC ↔ Rt. VT	4.49 (0.95)	4.22 (0.48)	-0.04 (0.07)	-0.02 (0.10)
Lt. TL ↔ Rt. VT	5.86 (0.94)	5.52 (0.58)	-0.01 (0.10)	-0.02 (0.07)

The numbers represent mean (standard deviation) value.

Abbreviations: BG, basal ganglia; FL, frontal lobe; Lt, left; OFC, orbitofrontal cortex; Rt, right.

<sup>a</sup>Significantly different structural path length density (FA weighted) between groups (corrected  $P < 0.05$ ).

<sup>b</sup>Significantly different functional connectivity density between groups (corrected  $P < 0.05$ ).

Table 10. Correlations between the clinical variables and the characteristic path length of the preoperative structural network

Variable	HAS ( <i>n</i> = 56)	HRSD ( <i>n</i> = 58)	IQCODE ( <i>n</i> = 55)	MMSE ( <i>n</i> = 58)
<b>NOS-ROI weighted structural network</b>				
Characteristic Path Length	-0.06 (0.671)	-0.13 (0.345)	0.23 (0.090)	-0.01 (0.949)
SPLD (Med. FP ↔ Rt. VT)	-0.07 (0.590)	-0.22 (0.101)	0.16 (0.235)	0.08 (0.546)
SPLD (Med. FP ↔ Lt. L+BG)	-0.11 (0.439)	-0.13 (0.330)	0.50 (<0.001)	-0.15 (0.251)
FCD (OFC plus BG ↔ Lt. VT)	0.31 (0.022)	0.10 (0.478)	0.10 (0.464)	-0.15 (0.271)
<b>FA weighted structural network</b>				
Characteristic Path Length	-0.06 (0.654)	-0.08 (0.572)	0.42 (0.002)	-0.28 (0.035)
SPLD (Lt. FL ↔ Rt. FL+BG)	-0.15 (0.268)	-0.20 (0.140)	0.36 (0.007)	-0.15 (0.275)
FCD (Rt. FL+BG ↔ Lt. VC)	0.08 (0.551)	-0.06 (0.678)	0.18 (0.193)	-0.10 (0.460)

The numbers represent Spearman's correlation coefficients (*P* value).

Abbreviations: FCD, functional connectivity density; FL, frontal lobe; FP, frontal-parietal; HAS, Hamilton anxiety scale; HRSD, Hamilton rating scale for depression; IQCODE, informant questionnaire on cognitive decline in the elderly; L, limbic areas; Lt, left; Med, medial; MMSE, mini mental state examination; OFC, orbitofrontal cortex; Rt, right; SPLD, structural path length density; VC, visual cortex; VT, visuotemporal areas.

## E. Relationships with Clinical Variables

Among the graph metrics, the path length of both NOS-ROI and FA weighted structural networks showed the significant differences between preoperative delirium and comparison patients (Table 10). Thus, the correlation analysis between the clinical variables and path length was conducted for each group. In the FA weighted structural network, the IQCODE was significantly correlated with the characteristic path length within the preoperative delirium ( $r = 0.43$  and  $P = 0.038$ ). There were no significant correlations observed between the graph metrics and a duration of delirium as well as K-DRS score.

Table 11. Preoperative risk factors for postoperative delirium using logistic regression

Variable Name	Abbreviation	Odds Ratio (95 % CI)	P-value
<b>Demographic and Clinical Variables</b>			
Age		1.07 (0.98, 1.17)	0.097
Sex		0.36 (0.09, 1.39)	0.136
Mini mental state examination	MMSE	0.92 (0.84, 1.00)	0.052
Major mental disorder history	MMDH	3.41 (0.89, 13.05)	0.073
Hamilton anxiety scale	HAS	1.07 (0.99, 1.15)	0.071
<b>Connectivity Density (in NOS-ROI weighted Structural Module)</b>			
Med. Frontal-parietal ↔ Rt. Visuotemporal	SPLD1	4.2E+12 (651.7, 2.6E+22)	0.012
Med. Frontal-parietal ↔ Lt. L+BG	SPLD2	1.5E+12 (282, 8.1E+21)	0.014
OFC plus BG ↔ Lt. Visuotemporal	FCD1	167.9 (1, 2.7E+04)	0.048
<b>Connectivity Density (in FA weighted Structural Module)</b>			
Lt. Frontal Lobe ↔ Rt. FL+BG	SPLD3	3.7 (1.3, 10.3)	0.013
Rt. FL+BG ↔ Lt. Visual Cortex	FCD2	1.4E+05 (12.1, 1.6E+09)	0.013

Abbreviations: FCD, functional connectivity density; FL+BG, frontal lobe plus basal ganglia; Lt, left; L+BG, limbic areas plus basal ganglia; Med, medial; OFC, orbitofrontal cortex; Rt, right; SPLD, structural path length density.

### 3. Prediction Model for Preoperative Delirium

Modeling the preoperative delirium was performed using the graph metrics that showed significant group differences in connectivity density (Tables 8-9). A total of three (two) connectivity density values from FA (NOS-ROI) weighted structural modular partitions were considered in the bivariate logistic regression. For the comparison purpose, delirium prediction models using clinical and demographic variables were considered. For the multivariate logistic regression analysis, various combinations of variables were considered including one variable from structural path length density, the other from functional connectivity density, and another from their interaction term.

## **A. Bivariate Logistic Regression**

Table 11 shows the summary of bivariate logistic regression analysis to see delirium prediction power of each variable. Among the demographic and clinical variables, MMSE score was played a crucial role in predicting postoperative delirium ( $P = 0.052$ ). Also, age, Hamilton anxiety scale, and history of major mental disorder were marginally associated with postoperative delirium ( $P < 0.1$ ).

In the neuroimaging-based delirium prediction analysis, postoperative delirium was found to be significantly associated with altered structural and functional connectivity density. For NOS-ROI weighted modular organization, the increased inter-module structural path length densities connecting the medial frontal-parietal to the right visuotemporal and left limbic areas plus basal ganglia regions were found to be associated with postoperative delirium ( $P < 0.05$ ). Also, the increased functional connectivity density between the orbitofrontal cortex plus basal ganglia and left visuotemporal region was found to be associated with postoperative delirium ( $P = 0.048$ ).

For FA weighted modular organization, the increased inter-module structural path length density connecting the frontal region to right frontal lobe plus basal ganglia was found to be associated with postoperative delirium ( $P = 0.013$ ). Also, the increased functional connectivity density between the right frontal lobe plus basal ganglia and left visual cortex was found to be a neural risk factor for postoperative delirium ( $P = 0.013$ ).

## **B. Model Selection**

Based on the bivariate logistic regression, we created a prediction model using preoperative (1) demographic and clinical variables and (2) neuroimaging data. Each pre-

Table 12. Delirium prediction models using multivariate logistic regression

Prediction model	Sensitivity (%)	Specificity (%)	Accuracy (%)	ROC (%)
<b>Model Using Demographic and Clinical Variables</b>				
MMSE + MMDH	56.0	78.8	69.0	72.2
MMSE + MMDH + HAM	52.2	81.8	69.6	72.4
MMSE + MMDH + HAM + Age	47.8	75.8	64.3	73.6
<b>Model Using Preoperative Neuroimaging Data</b>				
FCD1 + SPLD1 + FCD2 + SPLD3	64.0	84.8	75.9	83.3
FCD1 + SPLD2 + FCD2 + SPLD3	68.0	84.8	77.6	81.9
FCD1×SPLD1 + FCD2×SPLD3	40.0	87.9	67.2	64.4
FCD1×SPLD2 + FCD2×SPLD3	40.0	87.9	67.2	63.8
FCD1 + FCD1×SPLD1 + FCD2 + FCD2×SPLD3	72.0	84.8	79.3	83.5
FCD1 + FCD1×SPLD2 + FCD2 + FCD2×SPLD3*	84.0	84.8	84.5	85.7
SPLD1 + FCD1×SPLD1 + SPLD3 + FCD2×SPLD3	52.0	84.8	70.7	82.7
SPLD2 + FCD1×SPLD2 + SPLD3 + FCD2×SPLD3	68.0	84.8	77.6	81.2

Full name of FCDs and SPLDs are listed in Table 11.

Abbreviations: HAS, Hamilton anxiety scale; MMDH, major mental disorder history; MMSE, mini mental state examination; ROC, receiver operating characteristic.

\*The best prediction model for postoperative delirium with the highest average of the classification accuracy and area under ROC curve.

diction model was validated regarding sensitivity, specificity, accuracy, and area under ROC curve (Table 11). In neuroimaging-based delirium prediction model, four types of variable combinations were considered as following. First, a total of four variables was considered in the model: One functional connectivity density (FCD) and one structural path length density (SPLD) from NOS-ROI weighted module, and one FCD and one SPLD from FA weighted module. Second, two interaction variables were included in the model: one interaction variable between FCD and SPLD from NOS-ROI weighted module, and another interaction variable of FCD and SPLD from FA weighted modules. Third, two FCDs and two interactions were modeled: One inter-module FCD from

NOS-ROI weighted module, and another inter-module FCD from FA weighted module, and one interaction between FCD and SPLD from NOS-ROI weighted module, and another interaction between FCD and SPLD from FA weighted module. Last, two SPLDs and two interactions were modeled: One inter-module SPLD from NOS-ROI weighted module, and another inter-module SPLD from FA weighted module, and one interaction between FCD and SPLD from NOS-ROI weighted module, and another interaction between FCD and SPLD from FA weighted module. A total of eight models was tested to find the most significant delirium prediction model (Table 12).

The best prediction model for postoperative delirium was selected with the highest average of the overall accuracy and area under ROC curve. The combination of functional connectivity density and interaction of functional connectivity and structural path length density from NOS-ROI and FA weighted modules showed the best performance delirium prediction. Structural path length density between the left frontal lobe and left temporal lobe, and functional connectivity density between right frontal lobe plus basal ganglia and left visual cortex were the most important predictors of delirium. The combination of these structural and functional factors allows us to predict delirium with a sensitivity of 84.0 % and a specificity of 84.8 %. The area under a ROC curve was 85.7 %. The neuroimaging-based delirium prediction model was 28 %p higher sensitivity and 3 %p higher specificity compared to any prediction models that used demographic and clinical variables (Table 12).



#### 4. Brain Network and Motor Subtypes of Delirium

Within delirium patients, statistical comparisons of brain network properties among three motor subtypes of delirium using one-way ANOVA.

Structural network properties were not significantly different from motor subtypes of delirium (Table 13). However, in a functional network, several graph metric showed a significant difference among motor subtypes of delirium. Figure 11 shows post-hoc analysis of the functional graph metric. Global efficiency was significantly increased in mixed type compared to hypoactive type ( $P = 0.037$ ). Also, characteristic path length and modularity of a functional network were significantly decreased in mixed type compared to hypoactive type ( $P < 0.05$ ). Global efficiency, path length, and modularity in a functional network of hyperactive type delirium were in the middle of a hypoactive and mixed type of delirium.

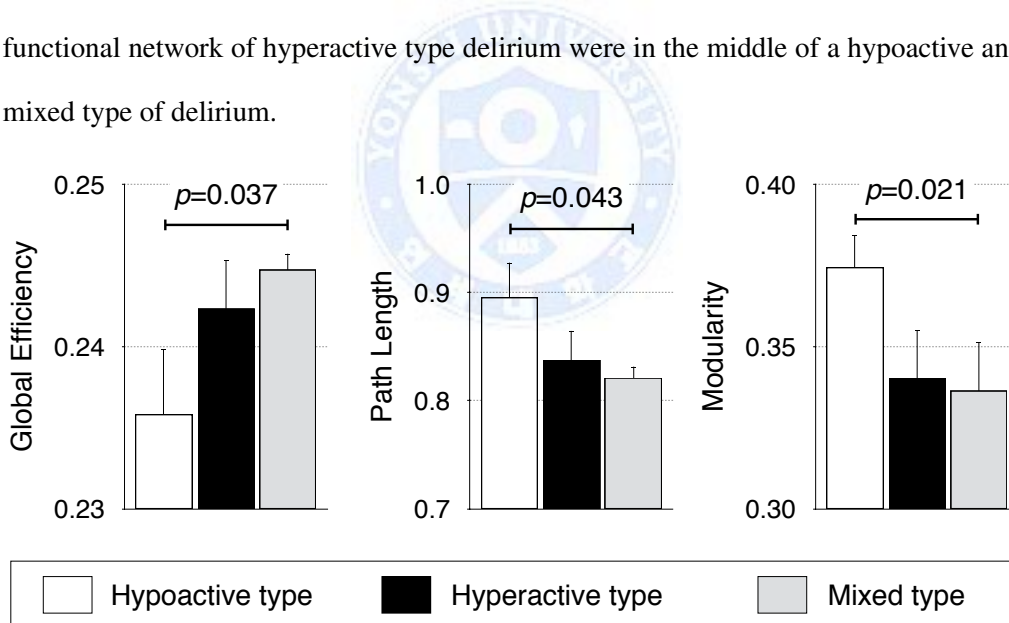


Figure 11. Comparisons of functional network properties among three motor subtypes of delirium. The mean value and corresponding standard error were plotted on a graph. Bonferroni corrected  $P$  values were presented in the graph.

Table 13. Differences of preoperative structural and functional network properties as a function of motor subtypes

	Hypoactive ( <i>n</i> = 9)	Hyperactive ( <i>n</i> = 3)	Mixed ( <i>n</i> = 13)	<i>F</i> <sub>2,22</sub>	<i>P</i> value
<b>Structural Network (NOS-ROI weighted)</b>					
Global Efficiency	7.174 (1.523)	7.807 (0.832)	6.879 (0.662)	0.95	0.401
Local Efficiency	11.794 (2.068)	12.510 (1.080)	11.351 (0.980)	0.82	0.455
Path Length	0.233 (0.120)	0.170 (0.017)	0.200 (0.025)	0.98	0.391
Clustering Coefficient	2.000 (0.335)	2.137 (0.076)	1.994 (0.141)	0.50	0.613
$\lambda$	1.629 (0.476)	1.350 (0.010)	1.429 (0.120)	1.56	0.232
$\gamma$	4.503 (0.294)	4.410 (0.406)	4.542 (0.323)	0.21	0.811
Modularity, <i>Q</i>	0.573 (0.032)	0.577 (0.012)	0.581 (0.020)	0.25	0.782
<b>Structural Network (FA weighted)</b>					
Global Efficiency	0.240 (0.046)	0.267 (0.064)	0.259 (0.032)	0.73	0.495
Local Efficiency	0.342 (0.055)	0.370 (0.069)	0.355 (0.033)	0.46	0.635
Path Length	4.786 (0.592)	4.427 (0.908)	4.530 (0.564)	0.61	0.551
Clustering Coefficient	0.116 (0.016)	0.123 (0.023)	0.115 (0.011)	0.39	0.681
$\lambda$	1.173 (0.048)	1.171 (0.015)	1.153 (0.024)	1.08	0.358
$\gamma$	3.461 (0.327)	3.275 (0.307)	3.455 (0.272)	0.51	0.610
Modularity, <i>Q</i>	0.426 (0.030)	0.420 (0.030)	0.430 (0.032)	0.14	0.867
<b>Functional Network</b>					
Global Efficiency*	0.236 (0.011)	0.242 (0.006)	0.245 (0.004)	3.74	0.040
Local Efficiency	0.320 (0.013)	0.316 (0.009)	0.311 (0.008)	1.96	0.165
Path Length*	0.895 (0.095)	0.837 (0.046)	0.821 (0.035)	3.60	0.044
Clustering Coefficient	0.252 (0.027)	0.240 (0.019)	0.230 (0.015)	3.17	0.062
$\lambda$	0.497 (0.051)	0.470 (0.026)	0.460 (0.020)	2.96	0.073
$\gamma$	1.094 (0.109)	1.047 (0.076)	1.005 (0.066)	2.92	0.075
Modularity, <i>Q</i> *	0.374 (0.030)	0.340 (0.026)	0.336 (0.030)	4.65	0.021

The numbers represent mean (standard deviation) value.

In ANOVA, network properties were included as dependent variables and a categorical variable for motor subtypes (hypoactive, hyper, and mixed type) was considered as a independent variable

Abbreviations:  $\lambda$ , normalized path length;  $\gamma$ , normalized clustering coefficient.

\*Values show the significant differences among three motor subtypes of delirium (*P* < 0.05).

## 5. Delirium with Hallucination

For the preoperative delirium, patients with- and without hallucinations were divided into two groups to investigate any differences in brain network properties. Among preoperative delirium, thirteen patients reported hallucination during an episode of delirium, *i.e.*, patients who have a non-zero perception and hallucination item score of K-DRS (item score  $\geq 1$ ), and ten patients were categorized into delirium without hallucination.

Table 14 showed the summary of statistical comparison. In NOS-ROI weighted structural network, global efficiency was significantly increased in delirium with hallucination compared to delirium without hallucination ( $P = 0.049$ ). Whereas, normalized clustering coefficient ( $\gamma$ ) was significantly decreased in delirium with hallucination then delirium without hallucination ( $P = 0.002$ ). In FA weighted structural network, global efficiency, local efficiency, clustering coefficient were significantly increased in delirium with hallucination compared to delirium without hallucination ( $P < 0.05$ ). Whereas, path length and modularity were significantly decreased in delirium with hallucination then delirium without hallucination ( $P < 0.05$ ). However, no group differences were found in the functional network properties.

The connectivity density variables that included in the final delirium prediction model (Tables 11–12) were compared to identify the neural correlate of hallucination in delirium. The inter-module structural path length density between the left frontal and left temporal lobe was significantly decreased in patients with hallucination compared to patients without hallucination ( $P = 0.004$ ). However, the inter-module functional connectivity density connecting the right frontal plus basal ganglia to right visual cortex was not significantly different between hallucination groups ( $P = 0.274$ ).

Table 14. Statistical comparison of network properties between hallucination and non-hallucination groups within preoperative delirium

	With hallucination ( <i>n</i> = 13)	Without hallucination ( <i>n</i> = 10)	<i>T</i> statistic	<i>P</i> value
<b>Structural Network (NOS-ROI weighted)</b>				
Global Efficiency*	7.481 (0.995)	6.568 (1.091)	2.09	0.049
Local Efficiency	11.962 (1.485)	11.147 (1.518)	1.29	0.211
Path Length	0.180 (0.024)	0.236 (0.103)	-1.90	0.071
Clustering Coefficient	2.053 (0.210)	1.985 (0.257)	0.70	0.492
$\lambda$	1.367 (0.045)	1.567 (0.352)	-2.04	0.054
$\gamma^\dagger$	4.370 (0.297)	4.745 (0.193)	-3.46	0.002
Modularity, <i>Q</i>	0.576 (0.019)	0.584 (0.028)	-0.80	0.435
<b>Structural Network (FA weighted)</b>				
Global Efficiency $^\dagger$	0.275 (0.039)	0.227 (0.029)	3.27	0.004
Local Efficiency $^\dagger$	0.378 (0.042)	0.325 (0.033)	3.24	0.004
Path Length $^\dagger$	4.255 (0.557)	5.010 (0.415)	-3.58	0.002
Clustering Coefficient*	0.124 (0.014)	0.108 (0.009)	3.02	0.007
$\lambda$	1.162 (0.026)	1.161 (0.047)	0.08	0.940
$\gamma^*$	3.311 (0.256)	3.633 (0.254)	-3.00	0.007
Modularity, <i>Q</i> *	0.421 (0.029)	0.443 (0.026)	-1.91	0.070
<b>Functional Network</b>				
Global Efficiency	0.243 (0.007)	0.239 (0.010)	1.18	0.251
Local Efficiency	0.311 (0.009)	0.320 (0.011)	-2.03	0.055
Path Length	0.838 (0.065)	0.868 (0.083)	-0.97	0.344
Clustering Coefficient	0.233 (0.019)	0.247 (0.025)	-1.58	0.128
$\lambda$	0.469 (0.033)	0.484 (0.045)	-0.96	0.349
$\gamma$	1.015 (0.082)	1.077 (0.098)	-1.65	0.114
Modularity, <i>Q</i>	0.345 (0.034)	0.354 (0.035)	-0.66	0.520

The numbers represent mean (standard deviation) value.

Abbreviations:  $\lambda$ , normalized path length;  $\gamma$ , normalized clustering coefficient.

\*Values show the significant differences between two groups ( $P < 0.05$ ).

$^\dagger$ Values show the significant differences between two groups ( $P < 0.005$ ).

Table 15. A repeated-measures analysis of variance to test for group and time effects and group by time interactions in functional network properties

Graph Metric	Group		Time		Group $\times$ Time	
	$F_{1,30}$	$P$ value	$F_{1,30}$	$P$ value	$F_{1,30}$	$P$ value
Global Efficiency	0.00	0.987	0.22	0.643	0.01	0.932
Local Efficiency	0.01	0.929	3.75	0.062	0.21	0.650
Path Length	0.00	0.966	0.63	0.435	0.63	0.434
Clustering Coefficient	0.01	0.925	1.65	0.209	0.03	0.862
$\lambda$	0.00	0.979	0.61	0.441	0.63	0.434
$\gamma$	0.00	0.949	2.16	0.152	0.06	0.805
Modularity, $Q$	0.02	0.898	0.19	0.667	0.45	0.509

Where group variable indicates between-subjects effect (delirium and non-delirium), and time variable indicates within-subject effect (preoperative and postoperative).

## 6. Brain Network Alteration during an Episode of Delirium

Results from the mixed design ANOVA will be presented in this section. Various graph metrics and functional connectivity densities will be tested by mixed design ANOVA.

### A. Preserved Graph Measures during an Episode of Delirium

The mixed design ANOVA revealed that hip fracture surgery would not change functional network properties compared to that of preoperative characteristics. Also, functional network properties in delirium were not found to be different from the non-delirium group. Finally, no significant group by time interactions were found in functional graph metrics. In short, the functional network properties were preserved regardless of hip fracture surgery (Table 15).

Table 16. A repeated-measures analysis of variance to test for group, time, and group by time interaction effects in functional connectivity density for structural modular organization

Module Name	Group		Time		Group × Time	
	$F_{1,30}$	<i>P</i> value	$F_{1,30}$	<i>P</i> value	$F_{1,30}$	<i>P</i> value
<b>NOS-ROI Weighted Structural Modules</b>						
Orbitofrontal cortex + BG ↔ Left visuotemporal	0.01	0.916	1.41	0.244	2.74	0.108
<b>FA Weighted Structural Modules</b>						
Right frontal lobe + BG ↔ Left visual cortex	0.61	0.443	0.04	0.845	5.71	0.023

Where group indicator represents between-subjects effect (delirium and non-delirium), and time indicator represents within-subject effect (preoperative and postoperative).

Abbreviations: BG, basal-ganglia.

## B. Altered Functional Connectivity during an Episode of Delirium

In this section, statistical comparisons to investigate whether or not hip fracture surgery would change functional connectivity density. The intra- and inter-module functional connectivity densities were entered in the mixed design ANOVA as dependent variables. For this study, the inter-module functional connectivity densities, which were significantly increased in preoperative delirium compared to preoperative non-delirium (Tables 8–9), were considered.

**Functional connectivity density for NOS-ROI weighted structural modular organizations:** The inter-module functional connectivity density connecting the orbitofrontal cortex plus basal ganglia to left visuotemporal area showed no significant group, time, and group by time interaction effects (Table 16).

**Functional connectivity density for FA weighted structural modular organizations:** The inter-module functional connectivity density connecting the right frontal lobe plus

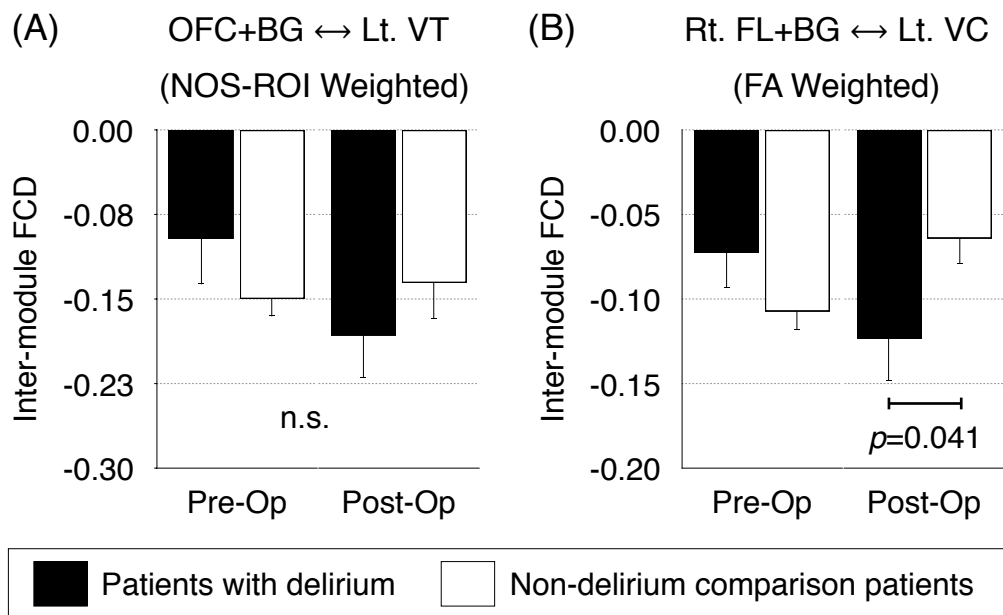


Figure 12. Significant group by time interactions for functional connectivity density. Connectivity density was obtained from FA weighted structural modular partitions. Abbreviations: Lt, left; Rt, right; FL, frontal lobe; BG, basal ganglia; Pre-Op, preoperative; Post-Op, postoperative; VC, visual cortex.

basal ganglia to left visual cortex showed no significant group and time effects (Table 16). However, a significant group by time interaction effect was observed in the inter-module functional connectivity density (Table 16). In a post-hoc analysis, the inter-module functional connectivity density between the right frontal plus basal ganglia and left visual cortex was found to be significantly suppressed in postoperative delirium compared to that of postoperative non-delirium (Figure 12).

Table 17. A repeated-measures analysis of variance to test for group and time effects and group by time interactions in the SN–FN coupling strength

Coupling Method	Group		Time		Group $\times$ Time	
	$F_{1,30}$	$P$ value	$F_{1,30}$	$P$ value	$F_{1,30}$	$P$ value
<b>Proposed method using <math>\mathcal{F}</math>(FN) and the distance matrix from SN</b>						
$\mathcal{F}$ (FN) <sup>a</sup> - $\mathcal{D}$ (SN) (NOS-ROI) <sup>c,*</sup>	0.02	0.898	4.63	0.040	4.83	0.036
$\mathcal{F}$ (FN) <sup>a</sup> - $\mathcal{D}$ (SN) (FA) <sup>d</sup>	2.87	0.101	3.83	0.060	2.12	0.156
<b>Old method using <math>\mathcal{S}</math>(FN) and SN</b>						
$\mathcal{S}$ (FN) <sup>b</sup> - SN (NOS-ROI weighted)	2.52	0.123	1.52	0.227	0.59	0.449
$\mathcal{S}$ (FN) <sup>b</sup> - SN (FA weighted)	1.04	0.316	0.01	0.929	1.17	0.287

Where group indicator represents between-subjects effect (delirium and non-delirium), and time indicator represents within-subject effect (preoperative and postoperative).

<sup>a</sup> $\mathcal{F}$ (FN), Full adjacency matrix of functional network.

<sup>b</sup> $\mathcal{S}$ (FN), Sparse adjacency matrix of functional network, which are the counterparts of the corresponding structural network.

<sup>c</sup> $\mathcal{D}$ (SN) (NOS-ROI), a distance matrix obtained from NOS-ROI weighted structural network.

<sup>d</sup> $\mathcal{D}$ (SN) (FA), a distance matrix obtained from FA weighted structural network.

\*Significant group (delirium and non-delirium) by time (preoperative and postoperative) interaction effects with  $P$  value less than 0.05.

### C. Altered SN-FN Coupling Strength during an Episode of Delirium

The mixed design ANOVA revealed that SN–FN coupling strength was changed after hip fracture surgery. Also, significant group (delirium and non-delirium) by time (preoperative and postoperative) interactions were found in the new SN–FN coupling methods as summarized in Table 17.

For the SN–FN coupling strength that showed significant group by time interactions, post-hoc analysis was performed to investigate interaction effects (Figure 13). Within delirium patients, there showed a significantly decreased SN-FN coupling strength. Whereas, the alteration of SN–FN coupling after hip fracture surgery was not observed in non-delirium patients.



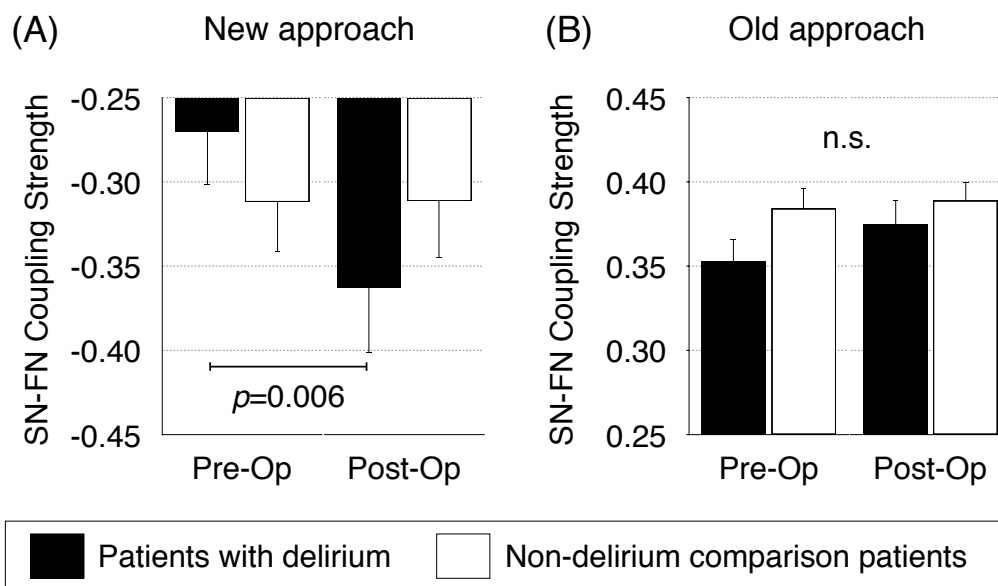


Figure 13. Significant group by time interactions for the coupling strength. The coupling strengths between NOS-ROI weighted structural network and functional network were evaluated by two different methods: (A) new approach and (B) old approach.

#### D. Multi-sliced Functional Modular Organization

Multi-sliced modularity optimization algorithm found functional modular organizations using pre- and postoperative functional network data. Figure 14 shows multi-sliced functional network modular organizations. The multi-sliced modularity algorithm optimized the modularity for the interdependent networks such as pre- and postoperative functional networks. The overall patterns of the multi-sliced functional modular architectures were symmetrically organized and almost similar across two groups (NMI=0.95).

Among them, the modular organizations of the frontal lobe, sensorimotor area, and visual cortex were identical ( $J = 1$ ). However, the right middle temporal gyrus and right inferior temporal gyrus were clustered into the visual module in delirium group. Whereas,

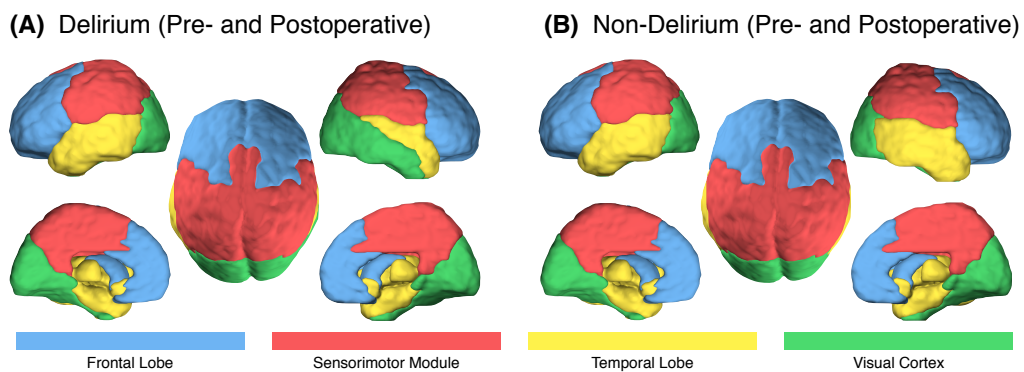


Figure 14. Multi-layered modularity optimization for (A) delirium and (B) non-delirium using pre- and postoperative functional network data. See Table A3 for a detailed description of brain areas for each module.

those regions were clustered into a single temporal module in non-delirium group. In short, the right temporal regions were partitioned into two parts in delirium group. The superior temporal gyrus, superior temporal pole, and middle temporal pole were clustered into the right temporal lobe 1 (superior part). Also, the middle temporal gyrus and inferior temporal gyrus were clustered into the right temporal lobe 2 (inferior part).

Since the major differences in functional associations in the right temporal lobe and visual cortex were observed, a post-hoc analysis to revealed the alterations of functional connectivity densities was conducted. As described in Table 18, the mixed design ANOVA of the intra- and inter-module functional connectivity density found no significant main effects in group (delirium and non-delirium). However, significant main effects in time (preoperative and postoperative) were observed in the inter-module functional connectivity density within the left temporal lobe ( $P = 0.051$ ), and in the inter-module functional connectivity density between the right temporal lobe 1 and right temporal lobe 2 ( $P = 0.038$ ). In the cross groups paired sample  $T$ -test analysis, the

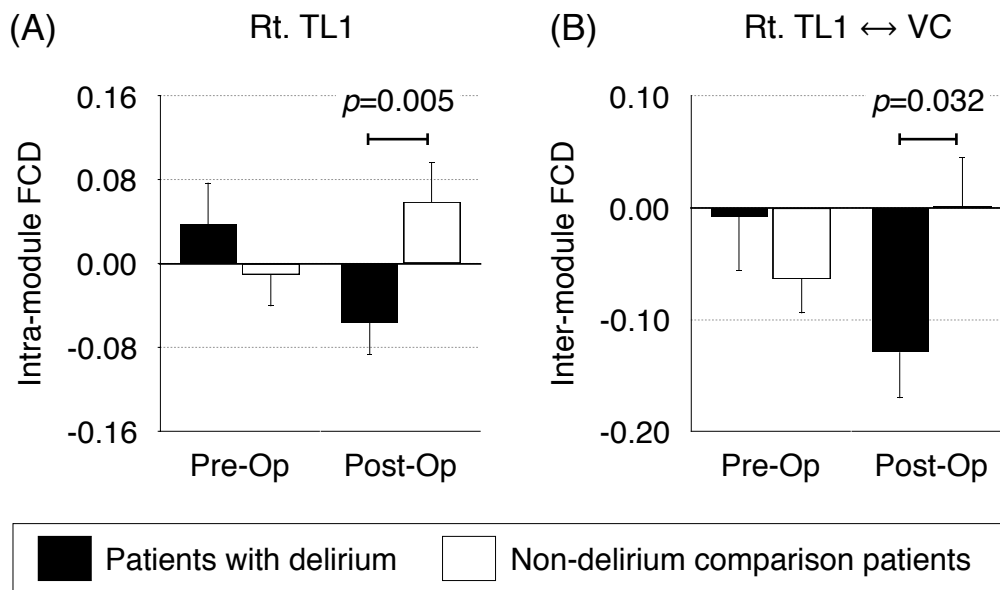


Figure 15. Significant group by time interactions for functional connectivity density (FCD) of the multi-layered modular organizations. (A) Intra-module FCD within right temporal lobe 1 (Rt. TL1). (B) inter-module FCD between the left visual cortex (Lt. VC) and right temporal lobe 1 (Rt. TL1). (C) inter-module FCD between the right visual cortex (Rt. VC) and right temporal lobe 1 (Rt TL1). Bonferroni corrected statistical significance values were presented.

marginally increased functional connectivity density within the left temporal lobe was observed ( $T = 2.02$  and  $P = 0.053$ ). Also, the inter-module functional connectivity density between the temporal lobe 1 and 2 was significantly increased after a hip fracture surgery ( $T = 2.08$  and  $P = 0.046$ ).

Interestingly, the mixed design ANOVA was revealed the significant group by time interactions in the intra-module functional connectivity density within the right temporal lobe 1 ( $P = 0.019$ ). Also, the significant group by time interactions were found in the inter-module functional connectivity densities connecting the right temporal lobe 1 to the

Table 18. A repeated-measures analysis of variance to test for group and time effects and group by time interactions in functional connectivity for multi-sliced functional modules

Graph Metric	Group		Time		Group $\times$ Time	
	$F_{1,30}$	$P$ value	$F_{1,30}$	$P$ value	$F_{1,30}$	$P$ value
<b>Intra-Module Functional Connectivity Density</b>						
Visual Cortex	0.00	0.961	0.56	0.459	1.789	0.191
Right Temporal Lobe 1 (Rt. TL1) <sup>a</sup>	3.19	0.084	0.03	0.867	6.109	0.019
Right Temporal Lobe 2 (Rt. TL2)	0.44	0.515	0.06	0.815	0.407	0.528
<b>inter-module Functional Connectivity Density</b>						
Visual Cortex $\leftrightarrow$ Rt. TL1 <sup>a</sup>	0.74	0.397	0.14	0.707	6.496	0.016
Visual Cortex $\leftrightarrow$ Rt. TL2 <sup>b</sup>	0.73	0.398	3.97	0.055	0.575	0.454
Rt. TL1 $\leftrightarrow$ Rt. TL2 <sup>b</sup>	0.17	0.685	4.72	0.038	0.858	0.362

Where group indicator represents between-subjects effect (delirium and non-delirium), and time indicator represents within-subject effect (preoperative and postoperative).

<sup>a</sup>Significant group (delirium and non-delirium) by time (preoperative and postoperative) interaction effects with  $P$  value less than 0.05.

<sup>b</sup>Significant within-subject effects (preoperative vs postoperative) with  $P$  value less than 0.05.

left visual cortex ( $P = 0.02$ ) and right visual cortex ( $P = 0.036$ ). The post-hoc analysis of those interactions was found the significant increase of intra-module functional connectivity within the right temporal lobe 1 in postoperative delirium compared to that of postoperative non-delirium ( $P < 0.005$ ). However, the inter-module functional connectivity densities connecting the right temporal lobe 1 to the bilateral visual areas were significantly decreased in postoperative delirium compared to postoperative non-delirium ( $P < 0.05$ ).

## 7. Topology-based Subgroups Identification in Delirium

In this subsection, the results of topological data analysis will be presented. Input variable selection procedures, distribution for the image of filter function, and graphical illustration of the resulting topology will be described.

### A. Variable Selection

The purpose of topological data analysis is to identify hidden structures in the large size data. Therefore, if the number of rows in a dataset is large enough, the inclusion of all possible continuous variable would produce an insightful result. However, if the number of rows in a dataset, the variable selection should be conducted before feeding data into topological data analysis. The variables that associated with delirium were selected based on the literature review. In general, age is a risk factor for postoperative delirium. However, age was not included in topological data analysis because most of the patients in our data were elderly enough ( $\sim 80$ ). To discriminate patients with delirium from non-delirium, K-DRS score was included with inserting zero values for non-delirium patients. Also, the severity of cognitive impairment measured by IQCODE and dementia scale measured by MMSE were included in the topological data analysis. Although a strong negative correlation between IQCODE and MMSE ( $r = -0.55$  and  $P < 0.001$ ) was observed in the current dataset, both variables were included to extract more significant first principal component from the data. Lastly, personality factors were considered because personality has reported to be associated with an outcome of delirium. Among various personality dimensions, the association between neuroticism and delirium was reported.<sup>74</sup> Furthermore, stress is associated with the development of post-

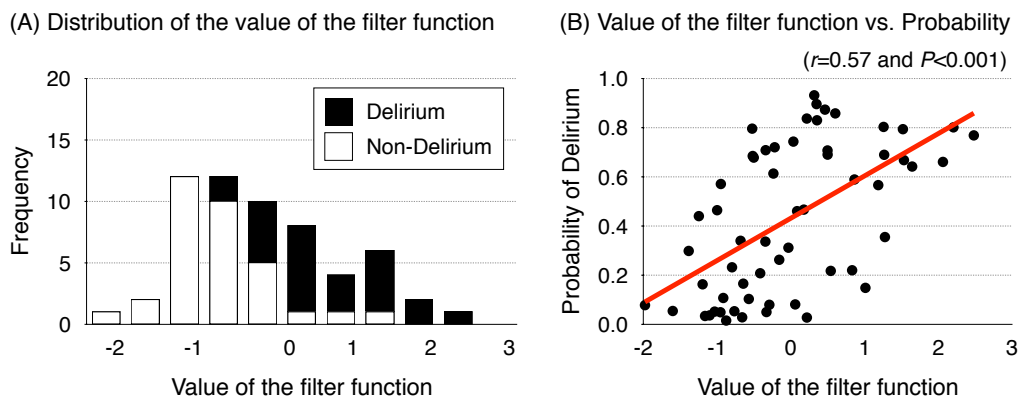


Figure 16. Filter function. (A) Distribution of the filter function and (B) its correlation with the prediction probability for postoperative delirium, where the prediction probability was obtained from preoperative structural and functional neuroimaging data.

operative delirium.<sup>75–78</sup> Interestingly, a coping strategy for stress is closely related to a conscientiousness.<sup>79,80</sup> Other personality dimensions have not reported to be associated with outcomes of delirium to the best of my knowledge. In general, older age is a risk factor for delirium. However, this study included mostly elderly patients (> 70 years old) and logistic regression analysis was revealed that age does not play a central role in predicting delirium (Tables 11–12). Finally, a total of five variables, such as K-DRS, IQCODE, MMSE, neuroticism, and conscientiousness were included in the topological data analysis.

## B. Distribution for Image of Filter Function

The filter function was successfully measured the deviation from non-delirious state, and it showed Y-shape distribution as shown in Figure 16A. Also, the value of filter function showed significant positive correlation with the prediction probability for preoperative delirium ( $r = 0.57$  and  $P < 0.001$ ), where the prediction probability was obtained from

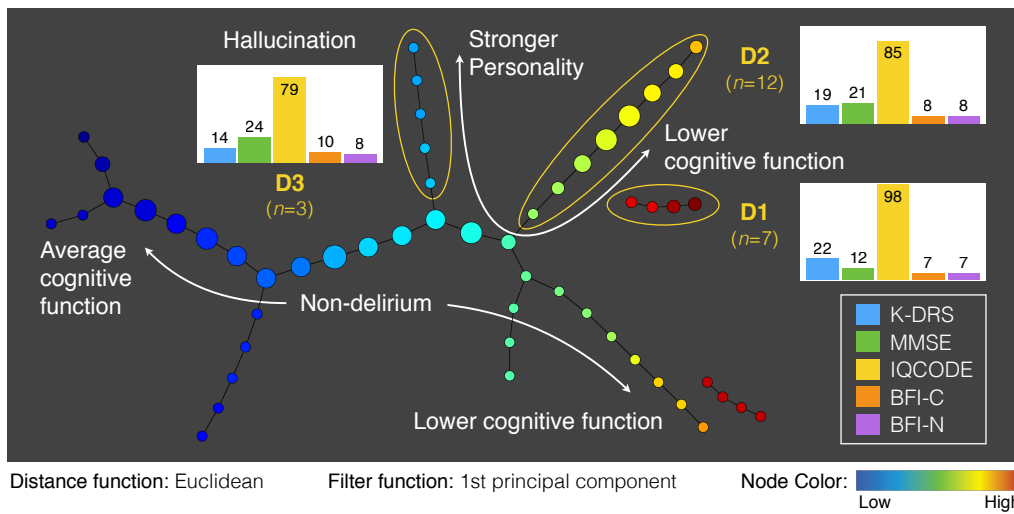


Figure 17. Output of topological data analysis. An illustration of the relationships among fifty-eight hip fracture patients, with labels and ellipses added to indicate the subgroups. The patients in D1 subgroup have a lowered cognitive function and mild personality. Whereas, the patients in D3 subgroup have an average cognitive function and a stronger personality. The image of filter function was subdivided into ten intervals with 80 % overlap. Several bins are disconnected from the main graph. The subgroup D3 contained three delirium patients who experienced a hallucination during an episode of delirium. Abbreviation: BFI, Big Five Inventory; BFI-C, consciousness in BFI; BFI-N, neuroticism in BFI; IQCODE, Informant Questionnaire on Cognitive Decline in the Elderly; K-DRS, Korean version of delirium rating scale; MMSE, Mini-Mental State Examination.

preoperative structural and functional network data.

### C. Graphical Illustration of the Output Topology

Using the filter and distance functions, topological data analysis was applied to get new insight from the clinical variables. Abnormal subgroups among the non-delirious patients were identified. Figure 17 shows a graphical illustration of TDA output. Topology-based data analysis revealed three distinct subgroups of delirium. Seven patients with delirium were clustered into delirium subgroups 1 (D1) and they showed a low cogni-

tive function (*i.e.*, high MMSE) and low neuroticism score. Three patients with delirium were grouped into delirium subgroup 3 (D3) and they showed a high cognitive function and strong personality (*i.e.*, high neuroticism). Delirium subgroup D1 and D3 showed the contrasting psychological and cognitive characteristics.

#### **D. Post-hoc Analysis among Subgroups of Delirium**

The one-way ANOVA were conducted to test the differences of graph metrics among three subgroups of delirium. Table 19 shows a summary of one-way ANOVA. The normalized clustering coefficient of NOS-ROI weighted structural network showed a significant difference among three subgroups of delirium ( $F_{2,19} = 5.42$  and  $P = 0.014$ ). The significant differences among three subgroups of delirium were found in the global efficiency ( $F_{2,19} = 3.59$  and  $P = 0.048$ ) and characteristic path length ( $F_{2,19} = 4.05$  and  $P = 0.034$ ) of the FA weighted structural network. The significant differences of the functional network properties among subgroups of delirium were found in the global efficiency ( $F_{2,19} = 3.86$  and  $P = 0.039$ ), local efficiency ( $F_{2,19} = 3.69$  and  $P = 0.044$ ), characteristic path length ( $F_{2,19} = 3.54$  and  $P = 0.049$ ), clustering coefficient ( $F_{2,19} = 4.03$  and  $P = 0.035$ ), and normalized characteristic path length ( $F_{2,19} = 3.93$  and  $P = 0.037$ ).



Table 19. Statistical comparisons of graph metrics among three phenotypic subgroups of delirium

Graph measures	D1 ( <i>n</i> = 7)	D2 ( <i>n</i> = 12)	D3 ( <i>n</i> = 3)	<i>F</i> <sub>2,19</sub>	<i>P</i> value
<b>Structural network (NOS-ROI weighted)</b>					
Global Efficiency	7.35 (0.74)	6.82 (1.34)	7.72 (0.85)	0.98	0.394
Local Efficiency	11.99 (1.10)	11.38 (1.87)	12.00 (1.35)	0.40	0.677
Path Length	0.18 (0.02)	0.24 (0.10)	0.17 (0.02)	1.32	0.290
Clustering Coefficient	2.06 (0.15)	1.96 (0.29)	2.01 (0.13)	0.47	0.632
$\lambda$	1.39 (0.04)	1.60 (0.42)	1.36 (0.01)	1.28	0.301
$\gamma$	4.50 (0.29)	4.57 (0.25)	4.03 (0.17)	5.42	0.014
Modularity, <i>Q</i>	0.59 (0.01)	0.57 (0.03)	0.57 (0.01)	0.99	0.390
<b>Structural network (FA weighted)</b>					
Global Efficiency	0.25 (0.03)	0.25 (0.04)	0.31 (0.04)	3.59	0.048
Local Efficiency	0.35 (0.03)	0.34 (0.05)	0.41 (0.04)	2.94	0.077
Path Length	4.66 (0.52)	4.68 (0.53)	3.74 (0.47)	4.05	0.034
Clustering Coefficient	0.12 (0.01)	0.11 (0.01)	0.13 (0.02)	2.69	0.094
$\lambda$	1.18 (0.04)	1.15 (0.04)	1.15 (0.01)	1.75	0.201
$\gamma$	3.44 (0.27)	3.47 (0.27)	3.06 (0.25)	2.91	0.079
Modularity, <i>Q</i>	0.43 (0.03)	0.43 (0.02)	0.39 (0.04)	1.92	0.174
<b>Functional network</b>					
Global Efficiency	0.234 (0.010)	0.244 (0.007)	0.247 (0.001)	3.86	0.039
Local Efficiency	0.323 (0.015)	0.311 (0.007)	0.311 (0.001)	3.69	0.044
Path Length	0.906 (0.084)	0.832 (0.062)	0.805 (0.012)	3.54	0.049
Clustering Coefficient	0.257 (0.029)	0.232 (0.016)	0.227 (0.003)	4.03	0.035
$\lambda$	0.506 (0.045)	0.463 (0.032)	0.453 (0.006)	3.93	0.037
$\gamma$	1.113 (0.126)	1.012 (0.066)	1.010 (0.026)	3.23	0.062
Modularity, <i>Q</i>	0.366 (0.048)	0.346 (0.023)	0.363 (0.031)	0.89	0.427

The subgroups of delirium, which are D1, D2, and D3, were identified by topological data analysis.

The numbers represents mean (standard deviation) value.

Abbreviations:  $\lambda$ , normalized path length;  $\gamma$ , normalized clustering coefficient.

\*Values show the significant differences among three motor subgroups of delirium ( $P < 0.05$ ).

## **IV. DISCUSSION**

This dissertation investigated structural and functional neural risk factors of delirium, and proposed the delirium prediction model using preoperative neuroimaging data. The strength of this study is an inclusion of homogeneous delirium patients while many other published studies dealt with heterogeneous delirium. The question about whether or not there exists a preoperative neural substrate for delirium was somehow answered throughout this dissertation. This study analyzed the multimodal neuroimaging data and tried to combine the structural and functional network data.

Throughout this study, a new approach to computing the coupling strength between structural and functional network were developed as a measure of brain network alteration during an episode of delirium. Also, multi-sliced brain network analysis methods were applied in the neuroimaging society for the first time to the best of my knowledge. Figure 18 shows analysis methods and key results for three research topics. The comments and discussion for these research topics will be described. First is about the study of neural substrates in delirium. Second is about the investigation of functional connectivity alterations during an episode of delirium. The last discussion point is about identifying the subgroups of delirium using topological data analysis.

### **1. Neural Substrates of Preoperative Delirium**

The increased characteristic path length in preoperative delirium suggests that the reduced number of streamlines and FA values in the structural network may be the potential sources of delirium. In the network science point of view, the increased path length could be interpreted as following. Paths are known to be sequences of distinct nodes

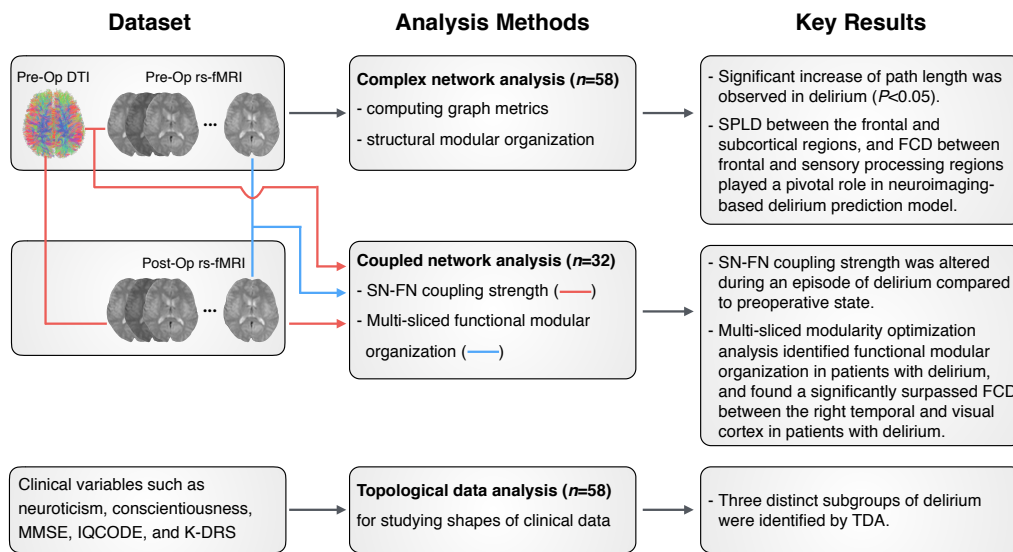


Figure 18. Summary of analysis methods and key results. Abbreviations: DTI, diffusion tensor imaging; FCD, functional connectivity density; IQCODE, informant questionnaire on cognitive decline in the elderly; K-DRS, korean version of delirium rating scale; MMSE, mini mental state examination; Pre-Op, preoperative; Post-Op, postoperative; rs-fMRI, resting state fMRI; SPLD, structural path length density; SN-FN, structural network and functional network; TDA, topological data analysis.

and links, and in anatomical networks represent potential routes of information flow between pairs of brain regions. Path lengths estimate the potential for information flow between brain regions, with shorter paths implying stronger potential for information integration.<sup>26</sup>

Significant positive correlation between IQCODE and the characteristic path length of FA weighted structural network indicates reduced FA values in the structural network may be related to the cognitive impairment in preoperative delirium. Although any relationships among graph metrics and delirium severity or duration were found in this study, there is a comparable study that revealed the relationship between white matter

integrity, delirium duration, and cognitive impairments in intensive care unit survivors.<sup>19</sup> In short, hip fracture patients of postoperative delirium have a cognitive deficit<sup>6</sup> and it is related to the altered path length of the structural network. However, functional information processing in the segregated subregions and information transferring among remote regions are somehow appropriately working in preoperative delirium (Table 6).

### **A. Structural Modular Organization**

The modularity optimization analyses of the structural network were revealed striking differences of the whole-brain neural network organizations between preoperative delirium and non-delirium (Figure 9). In the modularity optimization analysis, both FA and NOS-ROI weighted structural networks were considered because those two connection weights have different physiological meaning. For example, a higher FA value between two regions indicates a good myelination, and a higher NOS-ROI between two regions represents an existence of multiple streamlines indicating a possibility of parallel information processing. Interestingly, the striking differences in a modular organization were observed depending on the nature of connection weights regardless of group differences. In FA weighted structural network, the major differences in module compositions were observed in the left visual cortex and left temporal lobe regions. The left visual cortex and left temporal lobe comprised a single module in preoperative non-delirium group. However, in preoperative delirium, the left visual cortex and left temporal lobe were separated into two modules.

### **B. Neuroimaging-based Delirium Prediction Model**

Multivariate logistic regression showed the predictive factors for postoperative delirium

using the preoperative structural and functional networks. Most existing studies used the various clinical information for predicting postoperative delirium. No studies focused on neuroimaging-based risk factors for postoperative delirium. A total of three factors were considered in the multivariate delirium prediction model (Tables 11–12). One variable was from the functional connectivity density, and another was from the interaction between the functional connectivity density and structural path length density.

The best model predicts postoperative delirium with 80.4 % sensitivity and 84.8 % specificity. According to the best prediction model for postoperative delirium, structural path length density connecting the frontal to subcortical regions and functional connectivity density connecting prefrontal cortex plus subcortical regions to visuotemporal regions were played a pivotal role in predicting delirium.

The structural path length density between the frontal and audio-visual sensory areas was significantly increased in preoperative delirium. In the study of schizophrenia with an auditory hallucination, alterations of the gray matter volume were observed in the temporal and frontal regions.<sup>81,82</sup> Particularly, the inverse correlation between volume reduction of the superior temporal gyrus and hallucination severity was observed.<sup>81,83,84</sup> In short, the increased shortcut pathway in the pathways between the auditory-sensory regions and frontal areas is associated with the disruption of the myelination of fiber tracts in preoperative delirium. This suggests that the altered structural pathway connecting the audio-visual sensory regions and frontal regions might be neural substrates of hallucination in delirium.

Previously, the relationship between abnormality of visual cortex and the visual hallucination were reported in Parkinson's patients.<sup>85</sup> Also, the visual cortex has activated

during a rapid eye movement sleep or visual imagery.<sup>86,87</sup> Also, the frontal area activation were observed during the episode of hallucination.<sup>88,89</sup> The cortical infarctions and brain stimulation to the visual association cortex were reported to be a trigger for visual hallucination.<sup>85</sup> However, the increased functional connectivity density between the frontal plus basal ganglia and visual cortex showed no relationships with hallucination in delirium.

In short, the connectivity patterns observed in the frontal, auditory, and visual regions played the important role in characterizing postoperative delirium at the preoperative stage. Also, the information underflow in the auditory processing and information overflow in the visual processing are the most important indicators for predicting delirium.

### **C. Brain Network and Motor Subtypes of Delirium**

The one-way ANOVA evaluated statistical differences of brain network properties. Interestingly, neural correlates of motor subtypes of delirium were observed in the functional network properties while the structural network properties were not different among three motor subtypes. In the post-hoc comparison of the functional network properties, hypoactive delirium showed the decreased global efficiency and increased characteristic path length of the network. Why are decreased efficiency and increased path length associated with the development of hypoactive delirium? The answer is likely that two network properties are both markers of functional information integration. In general, decreased global efficiency is known to be associated with a declined cognitive performance<sup>90</sup> and older age.<sup>91</sup> The previous study reported that patients with hypoactive delirium are more likely to have older age and anemia.<sup>92</sup>

In short, this suggests that motor subtypes of delirium are independent of the structural network backbone. However, decreased abilities of information integration in the preoperative functional network could be a neural predictor for the development of hypoactive delirium.

#### **D. Delirium and Hallucination**

According to a review on hallucinating brain,<sup>81</sup> structural and functional neuroimaging studies have revealed neural substrates of auditory hallucination in patients with schizophrenia. However, only a few studies have reported a visual hallucination in elderly patients with Alzheimer's disease. Also, a hallucination in other psychiatric diseases and multimodal neuroimaging studies for hallucinating brain have rarely been investigated so far. In this study, the comparison of graph metrics between delirium with hallucination and delirium without hallucination revealed the increased global efficiency and decreased path length of the structural network in delirium with hallucination compared to delirium without hallucination. The increased global efficiency and decreased path length in the brain network provides fast information transfer in the network.<sup>26,27</sup> However, another study has reported occipital periventricular white matter hyperintensities<sup>93</sup> and overall cerebral atrophy in Alzheimer's disease patients with hallucination.<sup>94</sup> In schizophrenia studies, gray matter volume reduction in temporal regions has observed.<sup>95-97</sup>

Taken together, these findings suggest that altered backbone network of the brain might allow information overflow during a confusion state or an episode of delirium. Yet, efficiency for information processing in preoperative resting state functional network was

not different between two delirium groups of patients with and without hallucinations.

## **2. Brain Network Alteration during an Episode of Delirium**

The reduced functional connectivity between the dorsolateral prefrontal cortex and posterior cingulate cortex was the only neural substrates for describing patients during an episode of delirium<sup>23</sup>. However, the comparison of the preoperative structural and functional neuroimaging data have not been included in Choi.<sup>23</sup> To the best of my knowledge, the alteration of functional network properties during an episode of delirium compared to that of preoperative has never investigated. The importance of this study is the examination of functional connectivity re-organizations during an episode of delirium.

### **A. Alteration of Functional Network Properties**

The mixed ANOVA of functional network properties revealed that no significant main effects in group (delirium and non-delirium) and time (before and after a hip fracture surgery), and group by time interaction. However, in the mixed ANOVA for functional connectivity densities, the significant group by time interactions were observed. The intra-module functional connectivity densities in the right frontal plus basal ganglia and left visual cortex regions were significantly increased during an episode of delirium compared to that of preoperative delirium. Interestingly, the inter-module functional connectivity density between those two modules was significantly decreased in delirium compared to non-delirium after a hip fracture surgery. These functional connectivity density was significantly higher in preoperative delirium compared to that of non-delirium with full preoperative dataset (Table 9 and Figure 10B). This suggests that the increased functional connectivity density between the visual and frontal regions and its alteration



during an episode of delirium might be associated with visual hallucination in delirium. Among the postoperative delirium patients, visual hallucinations are the most common type of hallucination.<sup>98</sup>

Although the strong suppression of inter-module functional connectivity density connecting the frontal lobe plus basal ganglia and visual regions during an episode of delirium was observed, the whole-brain functional network properties were preserved. This suggests that the functional connectivity was reorganized to preserve the complexity of the brain network before and after a hip fracture surgery. Nonetheless, this interpretation is tentative since many aspects of connectivity alterations in a delirious brain have not been investigated and remain poorly understood.

### **B. Altered Structural-Functional Coupling Strength**

A new approach for SN-FN coupling methods was revealed the decreased synchronization of the structural network and functional network during an episode of delirium. By the way, a new approach SN-FN coupling method used a distance matrix rather than a structural connection matrix itself. The significantly decreased SN-FN coupling strength during an episode of delirium implies that the functional connectivity connecting two regions become stronger if two areas have a short path length in the structural network backbone. Where, a physical meaning of a short path length in the NOS-ROI weighted structural network is a larger number of streamlines. Whereas, the path length of the NOS-ROI weighted structural network in preoperative delirium was significantly increased in preoperative delirium (Table 5).

Taken together, the decreased SN-FN coupling strength in delirium suggests the increase

of the functional connectivity as a function of the number of fiber tracts during an episode of delirium. The fast flowing of functional information during an episode of delirium might change the brain as a confusion state.

### **C. Multi-sliced Functional Modular Organization**

Multi-sliced functional modular organization analysis is independent of a structural network modular organization. The importance of multi-sliced modularity optimization is the inclusion of a coupling term in the modularity equation to estimate the best partitions from the inter-dependent networks. Resting-state functional connectivity reflects the dynamics of low-frequency fluctuations,<sup>24</sup> and thus the altered brain state could produce different patterns of functional connectivity (*i.e.*, different modular organizations). According to the statistical comparisons of the intra- and inter-module functional connectivity densities (Table 18 and Figure 15), a hip fracture surgery is enough to change the normal brain into a different brain state like a chaotic or confusion state. After a hip fracture surgery, the functional connectivity densities in the bilateral auditory cortices have significantly increased regardless of delirium. The hyperconnectivity in the auditory cortex associated with exposure to various sounds such as drilling or hammering during surgery. Unwanted annoying noisy sounds cause stress, and psychological stress was reported to associate with the auditory activation.<sup>99</sup> In the animal study, the morphometric changes in chronically stressed animals have found to be related to dysfunctions in auditory attention.<sup>100</sup>

A significantly decreased functional connectivity densities between the right temporal lobe and visual regions was found in postoperative delirium (Figure 12). This suggests

that a re-allocation of auditory-visual sensory resources was occurred during an episode of delirium.

### **3. Topology-based Subgroups Identification in Delirium**

Topological data analysis is a powerful tool to find hidden patterns or identify subgroups in the complex dataset. It was widely used in a various research field and applied to identify the subgroups of breast cancer,<sup>39</sup> basketball player subtypes,<sup>101</sup> and imaging based phenotypic subgroups.<sup>41,42</sup>

Using topological data analysis, subgroups of preoperative hip fracture patients were identified. Patients with abnormal clinical characteristics classified as a separate subgroup. Among patients with delirium, one subgroup includes patients with a stronger personality and another subgroup includes patients with lower cognitive function. Personality dependent subgroups were observed in the normal population and their functional connectivity patterns were also altered.<sup>33</sup> Similarly, different patterns of functional network among subgroups of delirium in dimensions of personality and cognitive function was found in this study. Importantly, one subgroup was clustered delirium patients who were experienced a hallucination. However, motor subtypes of delirium were not identified by topological data analysis. Topological data analysis suggests that neural substrates of delirium could be different for phenotypic subgroups of delirium even though the important pathophysiology of 'delirium' might be explained by the same neural substrates.

### **4. Limitations**

This study has several limitations. First, diffusion tensor imaging data used in this study

were the relatively low number of diffusion gradients ( $n = 15$ ) due to minimizing the total MRI scanning time. In principle, tracking fibers from the fifteen directional diffusion images is possible because the minimum number of diffusion images to evaluate a direction of a fiber tract at each voxel is six. However, more accurate tractography might be possible with more diffusion images. Also, a high-angular resolution diffusion imaging protocol would enhance tractography for crossing-fibers.<sup>102,103</sup> Second, this dissertation would not give direct evidence for the sleep-wake cycle disturbance of delirium. The more comprehensive understanding of delirium would be established by taking into account for diurnal variation related biosignals such as the heart rate variability<sup>104</sup> or melatonin hormone concentration.<sup>105</sup> Third, applications of topological data analysis to clinical data would be a powerful tool in the search for demographical and clinical phenotypes of neuropsychiatric disorders.<sup>41</sup> However, this study with the small sample size, a few distinct phenotypic patterns among motor subtypes were identified. Perhaps, detecting more phenotypic subgroups, which have different characteristics of personality or symptoms, would be possible with a larger number of datasets (*e.g.*,  $n \sim 100$  or more).

## V. CONCLUSION

This dissertation included comprehensive analyses to find the neural substrates of preoperative delirium using the various methodological considerations. The increased path length of structural network in preoperative delirium implies that there existed disruptions of the connection weights such a fractional anisotropy and the number of streamlines in the backbone network. At the same time, there existed functional connectivity re-organization to preserve a cognitive function as a normal-like because no significant differences in functional network measures have observed between preoperative delirium and non-delirium.

The human brain is the most important example of multi-layer networks. The brain network consisted of two interdependent networks. One is a structural network that is a backbone of the large-scale brain network, another is a functional network that reflects the dynamic properties of the brain function. In general, the coupled network has high potential to catastrophic failures when the brain is at a critical point such as an acute confusion state. Multi-sliced functional modular optimization analysis revealed the modular re-organizations in sensory areas during an episode of delirium. Especially, the inter-module functional connectivity density between the right temporal lobe and visual cortex has shown the significant group by time interaction. This interaction suggests that a re-allocation of auditory-visual sensory resources after hip fracture surgery plays a central role in characterizing the delirious phenomena such as dysfunction in perception, unconsciousness, and hallucination.

Topology-based data analysis identified phenotypic subgroups of delirium, and provided

the fact that the patterns of brain networks in delirium have associated with cognitive impairment and personality. Topological data analysis suggests that neural substrates of delirium could be different for phenotypic subgroups of delirium even though the important pathophysiology of 'delirium' might be explained by the same neural substrates.



## REFERENCES

1. American Psychiatric Association. *Diagnostic and Statistical Manual of Mental Disorders, 5th Edition*. Arlington, VA; 2013.
2. Morrison RS, Chassin MR, Siu AL. The medical consultant's role in caring for patients with hip fracture. *Ann Intern Med*. 1998;128(1):1010–20.
3. Schuurmans MJ, Duursma SA, Shortridge-Baggett LM, Clevers GJ, Pel-Littel R. Elderly patients with a hip fracture: the risk for delirium. *Appl Nurs Res*. 2003;16(2):75–84.
4. Galanakis P, Bickel H, Gradinger R, Von Gumpfenberg S, Förstl H. Acute confusional state in the elderly following hip surgery: incidence, risk factors and complications. *Int J Geriatr Psychiatry*. 2001;16(4):349–55.
5. Duppils GS, Wikblad K. Acute Confusional States in Patients Undergoing Hip Surgery. *Gerontology*. 2000;46:36–43.
6. Juliebø V, Bjørø K, Krogseth M, Skovlund E, Ranhoff AH, Wyller TB. Risk factors for preoperative and postoperative delirium in elderly patients with hip fracture. *J Am Geriatr Soc*. 2009;57(8):1354–61.
7. Saxena S, Lawley D. Delirium in the elderly: a clinical review. *Postgrad Med J*. 2009;85(1006):405–13.
8. Newman MF, Kirchner JL, Phillips-Bute B, Gaver V, Grocott H, Jones RH, et al. Longitudinal assessment of neurocognitive function after coronary-artery bypass surgery. *N Engl J Med*. 2001;344(6):395–402.
9. Shehabi Y, Grant P, Wolfenden H, Hammond N, Bass F, Campbell M, et al. Prevalence of delirium with dexmedetomidine compared with morphine based therapy after cardiac surgery: a randomized controlled trial (DEXmedetomidine Compared to Morphine-DEXCOM Study). *Anesthesiology*. 2009;111(5):1075–84.
10. Rudolph JL, Jones RN, Levkoff SE, Rockett C, Inouye SK, Sellke FW, et al. Derivation and Validation of a Preoperative Prediction Rule for Delirium After Cardiac Surgery. *Circulation*. 2009;119(2):229–36.
11. Dasgupta M, Dumbrell AC. Preoperative risk assessment for delirium after non-cardiac surgery: a systematic review. *J Am Geriatr Soc*. 2006;54(10):1578–89.
12. Pol RA, van Leeuwen BL, Reijnen MMPJ, Zeebregts CJ. The relation between atherosclerosis and the occurrence of postoperative delirium in vascular surgery patients. *Vasc Med*. 2012;17(2):116–22.

13. Schneider F, Böhner H, Habel U, Salloum JB, Stierstorfer A, Hummel TC, et al. Risk factors for postoperative delirium in vascular surgery. *Gen Hosp Psychiatry*. 2002;24(1):28–34.
14. Böhner H, Hummel TC, Habel U, Miller C, Reinbott S, Yang Q, et al. Predicting delirium after vascular surgery: a model based on pre- and intraoperative data. *Ann Surg*. 2003;238(1):149–56.
15. Benoit AG, Campbell BI, Tanner JR, Staley JD, Wallbridge HR, Biehl DR, et al. Risk factors and prevalence of perioperative cognitive dysfunction in abdominal aneurysm patients. *J Vasc Surg*. 2005;42(5):884–90.
16. Etzioni DA, Liu JH, Maggard MA, Ko CY. The aging population and its impact on the surgery workforce. *Ann Surg*. 2003;238(2):170–7.
17. Soiza RL, Sharma V, Ferguson K, Shenkin SD, Seymour DG, MacLulich AMJ. Neuroimaging studies of delirium: a systematic review. *J Psychosom Res*. 2008;65(3):239–48.
18. Grueter BE, Schulz UG. Age-related cerebral white matter disease (leukoaraiosis): a review. *Postgrad Med J*. 2012;88(1036):79–87.
19. Morandi A, Rogers BP, Gunther ML, Merkle K, Pandharipande P, Girard TD, et al. The relationship between delirium duration, white matter integrity, and cognitive impairment in intensive care unit survivors as determined by diffusion tensor imaging: the VISIONS prospective cohort magnetic resonance imaging study. *Crit Care Med*. 2012;40(7):2182–9.
20. Gunther ML, Morandi A, Krauskopf E, Pandharipande P, Girard TD, Jackson JC, et al. The association between brain volumes, delirium duration, and cognitive outcomes in intensive care unit survivors: the VISIONS cohort magnetic resonance imaging study. *Crit Care Med*. 2012;40(7):2022–32.
21. Hatano Y, Narumoto J, Shibata K, Matsuoka T, Taniguchi S, Hata Y, et al. White-matter hyperintensities predict delirium after cardiac surgery. *Am J Geriatr Psychiatry*. 2013;21(10):938–45.
22. Shioiri A, Kurumaji A, Takeuchi T, Matsuda H, Arai H, Nishikawa T. White matter abnormalities as a risk factor for postoperative delirium revealed by diffusion tensor imaging. *Am J Geriatr Psychiatry*. 2010;18(8):743–53.
23. Choi SH, Lee H, Chung TS, Park KM, Jung YC, Kim SI, et al. Neural network functional connectivity during and after an episode of delirium. *Am J Psychiatry*. 2012;169(5):498–507.
24. Biswal B, Yetkin FZ, Haughton VM, Hyde JS. Functional connectivity in the motor cortex of resting human brain using echo-planar MRI. *Magn Reson Med*. 1995;34(4):537–41.



25. Calhoun VD, Adali T, Pearlson GD, Pekar JJ. A Method for Making Group Inferences from Functional MRI Data Using Independent Component Analysis. *Hum Brain Mapping*. 2001;14:140–51.
26. Rubinov M, Sporns O. Complex network measures of brain connectivity: Uses and interpretations. *Neuroimage*. 2010;52(3):1059–69.
27. Bullmore E, Sporns O. Complex brain networks: graph theoretical analysis of structural and functional systems. *Nat Rev Neurosci*. 2009;10(3):186–98.
28. Fortunato S. Community detection in graphs. *Phys Rep*. 2010;486(3-5):75–174.
29. Guimera R, Nunes Amaral LA. Functional cartography of complex metabolic networks. *Nature*. 2005;433(7028):895–900.
30. Kim EY, Hwang DU, Ko TW. Multiscale ensemble clustering for finding modules in complex networks. *Phys Rev E*. 2012;85:026119.
31. Davis FC, Knodt AR, Sporns O, Lahey BB, Zald DH, Brigidi BD, et al. Impulsivity and the Modular Organization of Resting-State Neural Networks. *Cereb Cortex*. 2013;23(6):1444–52.
32. Meunier D, Achard S, Morcom A, Bullmore E. Age-related changes in modular organization of human brain functional networks. *Neuroimage*. 2009;44(3):715–23.
33. Kyeong S, Kim E, Park HJ, Hwang DU. Functional network organizations of two contrasting temperament groups in dimensions of novelty seeking and harm avoidance. *Brain Res*. 2014;1575:33–44.
34. van den Heuvel MP, Sporns O. Rich-club organization of the human connectome. *J Neurosci*. 2011;31(44):15775–86.
35. He Y, Wang J, Wang L, Chen ZJ, Yan C, Yang H, et al. Uncovering intrinsic modular organization of spontaneous brain activity in humans. *PLoS ONE*. 2009;4(4):e5226.
36. Chen ZJ, He Y, Rosa-Neto P, Germann J, Evans AC. Revealing modular architecture of human brain structural networks by using cortical thickness from MRI. *Cereb Cortex*. 2008;18(10):2374–81.
37. Chen ZJ, He Y, Rosa-Neto P, Gong G, Evans AC. Age-related alterations in the modular organization of structural cortical network by using cortical thickness from MRI. *Neuroimage*. 2011;56(1):235–45.
38. Reis SDS, Hu Y, Babino A, Andrade Jr JS, Canals S, Sigman M, et al. Avoiding catastrophic failure in correlated networks of networks. *Nat Phys*. 2014;10(10):762–7.

39. Nicolau M, Levine AJ. Topology based data analysis identifies a subgroup of breast cancers with a unique mutational profile and excellent survival. *PNAS*. 2011;108(17):7265–70.
40. Singh G, Memoli F, Carlsson G. Topological Methods for the Analysis of High Dimensional Data Sets and 3D Object Recognition. *Eurographics Symposium on PBG*. 2007;p. 1–11.
41. Romano D, Nicolau M, Quintin EM, Mazaika PK, Lightbody AA, Cody Hazlett H, et al. Topological methods reveal high and low functioning neuro-phenotypes within fragile X syndrome. *Hum Brain Mapping*. 2014;35(9):4904–15.
42. Kyeong S, Park S, Cheon KA, Kim JJ, Song DH, Kim E. A New Approach to Investigate the Association between Brain Functional Connectivity and Disease Characteristics of Attention-Deficit/Hyperactivity Disorder: Topological Neuroimaging Data Analysis. *PLoS ONE*. 2015;10(9):e0137296.
43. Neurology AAo. Practice parameter for diagnosis and evaluation of dementia. Report of the Quality Standards Subcommittee of the American Academy of Neurology. *Neurology*. 1994;44(11):2203–6.
44. Trzepacz PT, Mittal D, Torres R, Kanary K, Norton J, Jimerson N. Validation of the Delirium Rating Scale-revised-98: comparison with the delirium rating scale and the cognitive test for delirium. *J Neuropsychiatry Clin Neurosci*. 2001;13(2):229–42.
45. Andersson JLR, Skare S. A model-based method for retrospective correction of geometric distortions in diffusion-weighted EPI. *Neuroimage*. 2002;16(1):177–99.
46. Mori S, van Zijl PCM. Fiber tracking: principles and strategies - a technical review. *NMR Biomed*. 2002;15(7-8):468–80.
47. Tzourio-Mazoyer N, Landeau B, Papathanassiou D, Crivello F, Etard O, Delcroix N, et al. Automated anatomical labeling of activations in SPM using a macroscopic anatomical parcellation of the MNI MRI single-subject brain. *Neuroimage*. 2002;15(1):273–89.
48. Iturria-Medina Y, Sotero RC, Canales-Rodríguez EJ, Alemán-Gómez Y, Melie-García L. Studying the human brain anatomical network via diffusion-weighted MRI and Graph Theory. *Neuroimage*. 2008;40(3):1064–76.
49. van den Heuvel MP, Sporns O, Collin G, Scheewe T, Mandl RCW, Cahn W, et al. Abnormal Rich Club Organization and Functional Brain Dynamics in Schizophrenia. *JAMA Psychiatry*. 2013;70(8):783–10.
50. Kim DJ, Davis EP, Sandman CA, Sporns O, O'Donnell BF, Buss C, et al. Longer gestation is associated with more efficient brain networks in preadolescent children. *Neuroimage*. 2014;100:619–27.

51. Lo CY, Wang PN, Chou KH, Wang J, He Y, Lin CP. Diffusion Tensor Tractography Reveals Abnormal Topological Organization in Structural Cortical Networks in Alzheimer's Disease. *J Neurosci.* 2010;30(50):16876–85.
52. Newman MEJ. Finding community structure in networks using the eigenvectors of matrices. *Phys Rev E.* 2006;74:036104.
53. Watts DJ, Strogatz SH. Collective dynamics of 'small-world' networks. *Nature.* 1998;393(6684):440–2.
54. Sporns O, Chialvo DR, Kaiser M, Hilgetag CC. Organization, development and function of complex brain networks. *Trends Cogn Sci.* 2004;8(9):418–25.
55. van den Heuvel MP, Stam CJ, Kahn RS, Hulshoff Pol HE. Efficiency of functional brain networks and intellectual performance. *J Neurosci.* 2009;29(23):7619–24.
56. Shin DJ, Jung WH, He Y, Wang J, Shim G, Byun MS, et al. The effects of pharmacological treatment on functional brain connectome in obsessive-compulsive disorder. *Biol Psychiatry.* 2014;75(8):606–14.
57. Kyeong S, Kim E, Park HJ, Hwang DU. Functional network organizations of two contrasting temperament groups in dimensions of novelty seeking and harm avoidance. *Brain Res.* 2014;1575:33–44.
58. Subelj L, Bajec M. Unfolding communities in large complex networks: combining defensive and offensive label propagation for core extraction. *Phys Rev E.* 2011;83:036103.
59. Blondel VD, Guillaume JL, Lambiotte R, Lefebvre E. Fast unfolding of communities in large networks. *J Stat Mech.* 2008;2008(10):P10008.
60. Davis FC, Knodt AR, Sporns O, Lahey BB, Zald DH, Brigidi BD, et al. Impulsivity and the Modular Organization of Resting-State Neural Networks. *Cereb Cortex.* 2013;23(6):1444–52.
61. Lundström M, Edlund A, Karlsson S, Brännström B, Bucht G, Gustafson Y. A multifactorial intervention program reduces the duration of delirium, length of hospitalization, and mortality in delirious patients. *J Am Geriatr Soc.* 2005;53(4):622–8.
62. Kennedy M, Enander RA, Tadiri SP, Wolfe RE, Shapiro NI, Marcantonio ER. Delirium risk prediction, healthcare use and mortality of elderly adults in the emergency department. *J Am Geriatr Soc.* 2014;62(3):462–9.
63. Han JH, Eden S, Shintani A, Morandi A, Schnelle J, Dittus RS, et al. Delirium in older emergency department patients is an independent predictor of hospital length of stay. *Acad Emerg Med.* 2011;18(5):451–7.
64. Inouye SK. Delirium in older persons. *N Engl J Med.* 2006;354(11):1157–65.

65. Fong TG, Tulebaev SR, Inouye SK. Delirium in elderly adults: diagnosis, prevention and treatment. *Nat Rev Neurol*. 2009;5(4):210–20.
66. Zhang Z, Liao W, Chen H, Mantini D, Ding JR, Xu Q, et al. Altered functional-structural coupling of large-scale brain networks in idiopathic generalized epilepsy. *Brain*. 2011;134(10):2912–28.
67. Mucha PJ, Richardson T, Macon K, Porter MA. Community structure in time-dependent, multiscale, and multiplex networks. *Science*. 2010;328(5980):876–8.
68. Carlsson G. Topology and Data. *Bull Amer Math Soc*. 2009;46(2):255–308.
69. Yao Y, Sun J, Huang X, Bowman GR, Singh G, Lesnick M, et al. Topological methods for exploring low-density states in biomolecular folding pathways. *J Chem Phys*. 2009;130(14):144115.
70. Wang L, Zhu C, He Y, Zang Y, Cao Q, Zhang H, et al. Altered small-world brain functional networks in children with attention-deficit/hyperactivity disorder. *Hum Brain Mapping*. 2008;30(2):638–49.
71. Yu Q, Sui J, Rachakonda S, He H, Gruner W, Pearlson G, et al. Altered Topological Properties of Functional Network Connectivity in Schizophrenia during Resting State: A Small-World Brain Network Study. *PLoS ONE*. 2011;6(9):e25423.
72. Liu Y, Liang M, Zhou Y, He Y, Hao Y, Song M, et al. Disrupted small-world networks in schizophrenia. *Brain*. 2008;131(4):945–61.
73. Zalesky A, Fornito A, Bullmore ET. Network-based statistic: Identifying differences in brain networks. *Neuroimage*. 2010;53(4):1197–207.
74. Novakovic M, Dejanovic SD, Maric-Burmazevic J, Dakic Z, Dimitrijevic I. Alcoholic and postoperative delirium: a case-control study. *Psychiatr Danub*. 2015;27(1):90–6.
75. Kain ZN, Caldwell-Andrews AA, Maranets I, McClain B, Gaal D, Mayes LC, et al. Preoperative Anxiety and Emergence Delirium and Postoperative Maladaptive Behaviors. *Anesth Analg*. 2004;99:1648–54.
76. Cerejeira J, Batista P, Nogueira V, Vaz-Serra A, Mukaetova-Ladinska EB. The Stress Response to Surgery and Postoperative Delirium: Evidence of Hypothalamic-Pituitary-Adrenal Axis Hyperresponsiveness and Decreased Suppression of the GH/IGF-1 Axis. *J Geriatr Psychiatry Neurol*. 2013;26(3):185–94.
77. Mast RC, Broek WW, Fekkes D, Peplinkhuizen L, Habbema JDF. Incidence of and preoperative predictors for delirium after cardiac surgery. *J Psychosom Res*. 1999;46(5):479–83.
78. Mcintosh TK, Bush HL, Yeston NS, Grasberger R, Palter M, Aun F, et al. Beta-endorphin, cortisol and postoperative delirium: a preliminary report. *Psychoneuroendocrinology*. 1985;10(3):303–13.

79. Bartley CE, Roesch SC. Coping with daily stress: The role of conscientiousness. *Pers Individ Dif.* 2011;50(1):79–83.
80. Bogg T, Slatcher RB. Activity Mediates Conscientiousness' Relationship to Diurnal Cortisol Slope in a National Sample. *Health Psychol.* 2015;p. 1–5.
81. Allen P, Larøi F, McGuire PK, Aleman A. The hallucinating brain: A review of structural and functional neuroimaging studies of hallucinations. *Neurosci Biobehav Rev.* 2008;32(1):175–91.
82. Turetsky B. Frontal and Temporal Lobe Brain Volumes in Schizophrenia. *Arch Gen Psychiatry.* 1995;52(12):1061–70.
83. Cowell PE, Kostianovsky DJ, Gur RC, Turetsky BI, Gur RE. Sex differences in neuroanatomical and clinical correlations in schizophrenia. *Am J Psychiatry.* 1996;153(6):799–805.
84. Flaum M, O'Leary DS, Swayze VW, Miller DD, Arndt S, Andreasen NC. Symptom dimensions and brain morphology in schizophrenia and related psychotic disorders. *J Psychiatr Res.* 1995;29(4):261–76.
85. Holroyd S, Wooten GF. Preliminary fMRI Evidence of Visual System Dysfunction in Parkinson's Disease Patients With Visual Hallucinations. *J Neuropsychiatry Clin Neurosci.* 2006;18:402–4.
86. Kosslyn SM, Thompson WL. When is early visual cortex activated during visual mental imagery? *Psychol Bull.* 2003;129(5):723–46.
87. Tong F. Cognitive neuroscience: Primary visual cortex and visual awareness. *Nat Rev Neurosci.* 2003 Mar;4(3):219–29.
88. Lennox BR, Park SBG, Medley I, Morris PG, Jones PB. The functional anatomy of auditory hallucinations in schizophrenia. *Psychiatry Res Neuroimaging.* 2000;100:13–20.
89. Sommer IEC, Diederer KMJ, Blom JD, Willems A, Kushan L, Slotema K, et al. Auditory verbal hallucinations predominantly activate the right inferior frontal area. *Brain.* 2008;131(12):3169–77.
90. Vlooswijk MCG, Vaessen MJ, Jansen JFA, de Krom MCFTM, Majoie HJM, Hofman PAM, et al. Loss of network efficiency associated with cognitive decline in chronic epilepsy. *Neurology.* 2011;77(10):938–44.
91. Achard S, Bullmore E. Efficiency and Cost of Economical Brain Functional Networks. *PLoS Comput Biol.* 2007;3(2):e17.
92. Robinson TN, Raeburn CD, Tran ZV, Brenner LA, Moss M. Motor subtypes of postoperative delirium in older adults. *Arch Surg.* 2011;146(3):295–300.

93. Lin JH, Kwan SY, Wu D. Postictal Aphasia with Transient Sulcal Hyperintensity on MRI. *J Chin Med Assoc.* 2006;69(10):499–502.
94. Howanitz E, Bajulaiye R, Losonczy M. Magnetic Resonance Imaging Correlates of Psychosis in Alzheimer's Disease. *J Nerv Ment Dis.* 1995;183(8):548–9.
95. Levitan C, Ward PB, Catts SV. Superior Temporal Gyrus Volumes and Laterality Correlates of Auditory Hallucinations in Schizophrenia. *Biol Psychiatry.* 1999;46:955–62.
96. Neckelmann G, Specht K, Lund A, Ersland L, Smievoll AI, Neckelmann D, et al. MR Morphometry Analysis of Grey Matter Volume Reduction in Schizophrenia: Association with Hallucinations. *Int J Neurosci.* 2006;116(1):9–23.
97. Onitsuka T, Shenton ME, Salisbury DF, Dickey CC, Kasai K, Toner SK, et al. Middle and Inferior Temporal Gyrus Gray Matter Volume Abnormalities in Chronic Schizophrenia: An MRI Study. *Am J Psychiatry.* 2004;161:1603–11.
98. Webster R, Holroyd S. Prevalence of psychotic symptoms in delirium. *Psychosomatics.* 2000;41(6):519–22.
99. Tucker DM, Roth RS, Arneson BA, Buckingham V. Right hemisphere activation during stress. *Neuropsychologia.* 1977;15:697–700.
100. Dagnino-Subiabre A. Effects of chronic stress on the auditory system and fear learning: an evolutionary approach. *Rev Neurosci.* 2013;24(2):227–37.
101. Lum PY, Singh G, Lehman A, Ishkanov T, Vejdemo-Johansson M, Alagappan M, et al. Extracting insights from the shape of complex data using topology. *Sci Rep.* 2013;3:1236.
102. Tuch DS, Reese TG, Wiegell MR, Makris N, Belliveau JW, Wedeen VJ. High angular resolution diffusion imaging reveals intravoxel white matter fiber heterogeneity. *Magn Reson Med.* 2002;48(4):577–82.
103. Zalesky A, Fornito A, Harding IH, Cocchi L, Yücel M, Pantelis C, et al. Whole-brain anatomical networks: Does the choice of nodes matter? *Neuroimage.* 2010;50(3):970–83.
104. Rechlin T, Weis M, Kaschka WP. Is diurnal variation of mood associated with parasympathetic activity? *J Affect Disord.* 1995;34:249–55.
105. Piotrowicz K, Klich-Raczka A, Pac A, Zdzienicka A, Grodzicki T. The diurnal profile of melatonin during delirium in elderly patients—preliminary results. *Exp Gerontol.* 2015;72:45–9.

## APPENDICES

Appendices included detailed descriptions for structural and functional modular organizations. For obtaining structural modular organizations, NOS-ROI and FA weighted structural network data were used. Modularity optimization of NOS-ROI weighted structural network produced seven distinct community partitions (Table A1). Also, modularity optimization of FA weighted structural network produced six distinct community partitions (Table A2).

In multi-sliced functional modularity optimization analysis, preoperative and postoperative functional network were used and four distinct functional communities were observed as described in Table A3.





**Table A1. NOS-ROI weighted structural modular organizations using preoperative structural network data of patients with delirium**

Module	Brain regions within a module
Frontal-Parietal (Left)	Precentral gyrus (L), Orbitofrontal cortex (middle) (L), Inferior frontal gyrus (opercular) (L), Inferior frontal gyrus (triangular) (L), Orbitofrontal cortex (inferior) (L), Rolandic operculum (L), Insula (L), Postcentral gyrus (L), Superior parietal lobule (L), Inferior parietal lobule (L), Supramarginal gyrus (L), Angular gyrus (L), Heschl gyrus (L), Superior temporal gyrus (L), Temporal pole (superior) (L)
Frontal-Parietal (Right)	Precentral gyrus (R), Inferior frontal gyrus (opercular) (R), Inferior frontal gyrus (triangular) (R), Orbitofrontal cortex (inferior) (R), Rolandic operculum (R), Insula (R), Postcentral gyrus (R), Superior parietal lobule (R), Inferior parietal lobule (R), Supramarginal gyrus (R), Angular gyrus (R), Heschl gyrus (R), Superior temporal gyrus (R), Temporal pole (superior) (R)
Frontal-Parietal (Medial)	Superior frontal gyrus (dorsal) (L/R), Middle frontal gyrus (L/R), Supplementary motor area (L/R), Superior frontal gyrus (medial) (L/R), Anterior cingulate cortex (L/R), Middle cingulate gyrus (L/R), Posterior cingulate cortex (L/R), Precuneus (L/R), PCL (L/R),
OFC plus BG	Orbitofrontal cortex (superior) (L/R), Orbitofrontal cortex (middle) (R), Olfactory (L/R), Orbitofrontal cortex (medial) (L/R), Rectus gyrus (L/R), Caudate (R), Putamen (R), Pallidum (R), Thalamus (R)
Limbic (Left)	Hippocampus (L), Parahippocampal gyrus (L), Amygdala (L), Caudate (L), Putamen (L), Pallidum (L), Thalamus (L)
Visual-Temporal (Left)	Calcarine cortex (L), Cuneus (L), Lingual gyrus (L), Superior occipital gyrus (L), Middle occipital gyrus (L), Inferior occipital gyrus (L), Fusiform gyrus (L), Middle temporal gyrus (L), Temporal pole (middle) (L), Inferior temporal gyrus (L)
Visual-Temporal (Right)	Hippocampus (R), Parahippocampal gyrus (R), Amygdala (R), Calcarine cortex (R), Cuneus (R), Lingual gyrus (R), Superior occipital gyrus (R), Middle occipital gyrus (R), Inferior occipital gyrus (R), Fusiform gyrus (R), Middle temporal gyrus (R), Temporal pole (middle) (R), Inferior temporal gyrus (R)

Abbreviations: BG, basal ganglia; L, left; OFC, orbitofrontal cortex; R, right.



**Table A2. FA weighted structural modular organizations using preoperative structural network data of patients with delirium**

Module	Brain regions within a module
Frontal (Left)	Precentral gyrus (L), Superior frontal gyrus (dorsal) (L), Middle frontal gyrus (L), Orbitofrontal cortex (middle) (L), Inferior frontal gyrus (opercular) (L), Inferior frontal gyrus (triangular) (L), Rolandic operculum (L), Supplementary motor area (L), Superior frontal gyrus (medial) (L), Insula (L), Anterior cingulate cortex (L), Middle cingulate cortex (L), Postcentral gyrus (L), Supramarginal gyrus (L), Paracentral lobule (L), Heschl gyrus (L), Superior temporal gyrus (L)
OFC plus BG (Left)	Orbitofrontal cortex (superior) (L), Orbitofrontal cortex (inferior) (L), Olfactory (L), Orbitofrontal cortex (medial) (L), Rectus gyrus (L), Caudate (L), Putamen (L), Pallidum (L), Thalamus (L)
Frontal plus BG (Right)	Precentral gyrus (R), Superior frontal gyrus (dorsal) (R), Orbitofrontal cortex (superior) (R), Middle frontal gyrus (R), Orbitofrontal cortex (middle) (R), Inferior frontal gyrus (opercular) (R), Inferior frontal gyrus (triangular) (R), Orbitofrontal cortex (inferior) (R), Rolandic operculum (R), Supplementary motor area (R), Olfactory (R), Superior frontal gyrus (medial) (R), Orbitofrontal cortex (medial) (R), Rectus gyrus (R), Insula (R), Anterior cingulate cortex (R), Middle cingulate cortex (R), Superior parietal lobule (R), Heschl gyrus (R), Caudate (R), Putamen (R), Pallidum (R), Thalamus (R)
Temporal (Left)	Hippocampus (L), Parahippocampal gyrus (L), Amygdala (L), Lingual gyrus (L), Fusiform gyrus (L), Temporal pole (superior) (L), Middle temporal gyrus (L), Temporal pole (middle) (L), Inferior temporal gyrus (L)
Visual (Left)	Posterior cingulate cortex (L), Hippocampus (R), Calcarine cortex (L), Cuneus (L), Superior occipital gyrus (L), Middle occipital gyrus (L), Superior parietal lobule (L), Inferior parietal lobule (L), Angular gyrus (L), Precuneus (L)
Visuo-Temporal (Right)	Parahippocampal gyrus (R), Amygdala (R), Calcarine cortex (R), Cuneus (R), Lingual gyrus (R), Superior occipital gyrus (R), Middle occipital gyrus (R), Inferior occipital gyrus (R), Fusiform gyrus (R), Postcentral gyrus (R), Precuneus (R), Inferior parietal lobule (R), Supramarginal gyrus (R), Angular gyrus (R), Paracentral lobule (R), Superior temporal gyrus (R), Temporal pole (superior) (R), Middle temporal gyrus (R), Temporal pole (middle) (R), Inferior temporal gyrus (R)

Abbreviations: BG, basal ganglia; L, left; OFC, orbitofrontal cortex; R, right.

**Table A3. Multi-sliced functional modular organizations using pre- and postoperative functional network data of patients with delirium**

Module	Brain regions within a module
Frontal (bilateral)	Superior frontal gyrus (dorsal) (L/R), Orbitofrontal cortex (superior) (L/R), Middle frontal gyrus (L/R), Orbitofrontal cortex (middle) (L/R), Inferior frontal gyrus (opercular) (L/R), Inferior frontal gyrus (triangular) (L/R), Orbitofrontal cortex (inferior) (L/R), Olfactory (L/R), Superior frontal gyrus (medial) (L/R), Orbitofrontal cortex (medial) (L/R), Rectus gyrus (L/R), Anterior cingulate cortex (L/R), Caudate (L/R)
Parietal (bilateral)	Precentral gyrus (L/R), Supplementary motor area (L/R), Middlelingulate cortex (L/R), Posterior cingulate cortex (L/R), Postcentral gyrus (L/R), Superior parietal lobule (L/R), Inferior parietal lobule (L/R), Supramarginal gyrus (L/R), Angular gyrus (L/R), Precuneus (L/R), Paracentral lobule (L/R)
Temporal (bilateral)	Rolandic operculum (L/R), Insula (L/R), Hippocampus (L/R), Parahippocampal gyrus (L/R), Amygdala (L/R), Putamen (L/R), Pallidum (L/R), Thalamus (L/R), Heschl gyrus (L/R), Superior temporal gyrus (L/R), Temporal pole (superior) (L/R), Temporal pole (middle) (L/R), Middle temporal gyrus (L), Inferior temporal gyrus (L)
Visual (bilateral)	Calcarine cortex (L/R), Cuneus (L/R), Lingual gyrus (L/R), Superior occipital gyrus (L/R), Middle occipital gyrus (L/R), Inferior occipital gyrus (L/R), Fusiform gyrus (L/R), Middle temporal gyrus (R), Inferior temporal gyrus (R)

Abbreviations: L, left; R, right.

## ABSTRACT (IN KOREAN)

복잡계 네트워크 분석과 위상수학 기반의 데이터 분석을 이용한  
섬망의 위험인자 규명

〈지도교수 김 재 진〉

연세대학교 대학원 의과학과

경 성 현

**연구 배경:** 인간의 뇌는 여러 영역들이 서로 긴밀하게 연결되어 있는 복잡계 네트워크로 볼 수 있으며, 구조 네트워크와 역동적 기능 네트워크로 구성되어 있다. 많은 연구에서 밝혀졌듯이 비정상적 뇌네트워크는 뇌질환의 발현과 긴밀하게 연관되어 있다. 섬망이 신경인지 장애로 분류되고 있지만, 섬망의 신경학적 병인 규명 연구는 많이 보고되지 않았다. 본 연구에서는 섬망의 위험인자 발견을 위해서, 복잡계 네트워크 분석을 이용하여 섬망의 신경기전을 규명하고, 위상수학 기반의 데이터 분석을 활용하여 성격과 인지 기능 정도에 따른 섬망의 하위 그룹을 찾고 그 특성을 규명하고자 한다.

**재료 및 방법:** 본 연구에는 총 58명의 고관절 골절 환자가 참여했다. 모든 고관절 골절 환자의 수술 전 구조 및 기능 뇌영상 데이터를 획득했다. 전체 수술 환자 중에서 32명은 수술 후 기능 뇌영상 데이터 측정에도 참여했다. 복잡계 네트워크 분석 기법을 통해서 뇌영상 기반의 수술 전 섬망 예측인자를 찾고, 섬망 중 환자에게서 보여지는 기능적 연결성의 재조직화에 대한 신경 기전을 연구했다. 위상수학적 데이터 분석에서는 인지 기능 정도, 성격의 신경증과 성실성 요소, 섬망 점수를 고려하여 섬망의 하위그룹 범주화 연구를 진행했다.

**결과:** 전체 58명 중에서 고관절 골절 수술 이후에 섬망 증상이 나타난 환자는 25명이었다. 수술 전 환자의 구조 네트워크의 특성 연구에서는 노드간 평균 연결 경로 길이가 섬망군에서 유의미하게 증가되어 있음이 관찰됐다( $P < 0.05$ ). 또한, 전두엽과 피질하영역 그리고 전두엽과 시각 감각 영역간의 연결 경로 증가가 수술 전에 섬망 환자를 예측하는데 중요한 역할을 함을 발견했다 (corrected  $P < 0.05$ ). 더욱이 수술 전 섬망 환자는 전두엽과 시각 및 청각 감각 영역간의 기능적 연결성이 대조군에 비해서 증가되어 있음이 발견 되었다 (corrected  $P < 0.05$ ). 흥미롭게도 수술 전 섬망 환자에서 증가되어 있던 전두엽과 시각 및 청각 감각 영역과의 연결성과 시각 영역과 청각 감각 영역과의 연결성이 수술 후 섬망 환자에게서 유의미하게 감소되었다( $P < 0.05$ ). 마지막으로 위상수학 기반의 데이터 분석은 인지 기능과 성격 유형에 따라서 섬망군을 세 개의 하위 그룹으로 범주화 했다.

**결론:** 본 연구에서는 고관절 골절 환자의 수술 전 뇌영상 데이터로부터 섬망의 신경학적 예측인자를 밝혀냈다. 수술 전 섬망 환자의 구조 네트워크 특성 연구에서 밝혀진 노드간 평균 연결 경로 길이의 증가는 구조 네트워크의 기반이 되는 백질 섬유질의 비등방도나 신경다발 개수가 감소해 있음을 시사한다. 섬망 중에 발견된 시각 영역과 청각 영역 간의 기능적 연결성 감소는 감각 기관 간의 정보처리에 문제가 있음을 의미하고 이는 섬망 환자에게서 보이는 인지 장애, 의식 장애, 환각 등의 증상의 신경 기전이 될 수 있음을 시사한다. 위상수학적 데이터 분석 결과는 섬망의 신경 기전이 섬망 환자의 형질에 따라서 다르게 나타날 수 있음을 시사한다.

---

**핵심되는 말:** 복잡계 네트워크 분석, 위상수학 기반의 데이터 분석, 연결체학, 섬망, 고관절 골절 수술

## PUBLICATION LIST

(†: first or equally contributed author, \*: corresponding author)

1. **Kyeong S**<sup>†</sup>, Park S, Cheon KA, Kim JJ, Song DH, and Kim E. A New Approach to Investigate the Association between Brain Functional Connectivity and Disease Characteristics of Attention-Deficit / Hyperactivity Disorder: Topological Neuroimaging Data Analysis. PLoS one. 2015;10(9):e0137296.
2. **Kyeong S**<sup>†</sup>, Kim E, Park HJ, Hwang DU. Functional network organizations of two contrasting temperament groups in dimensions of novelty seeking and harm avoidance. Brain Research. 2014;1575:33–44.
3. Kim HG, Lee S, **Kyeong S**<sup>\*</sup>. Discovering Hot Topics using Twitter Streaming Data: social topic detection and geographic clustering. Proceedings of the 2013 IEEE/ACM International Conference on Advances in Social Networks Analysis and Mining; 2013 Aug 25–28; Niagara, Canada. New York:ACM; 2014.
4. Park S, Park HJ, **Kyeong S**, Moon IS, Kim M, Kim HN, Choi JY. Combined rTMS to the auditory cortex and prefrontal cortex for tinnitus control in patients with depression: a pilot study. Acta Oto-Laryngologia. 2013;113:600–6.
5. Kim JC, **Kyeong S**, Lee JD, and Park HJ. A System for Concurrent TMS-fMRI and Evaluation of Imaging Effects. Journal of the Korean Society of Magnetic Resonance in Medicine. 2013;17(3):169–80.
6. **Kyeong S**<sup>†</sup> *et al.* (Belle Collaboration). Measurements of charmless hadronic  $b \rightarrow s$  penguin decays in the  $\pi^+ \pi^- K^+ \pi^-$  final state and first observation of  $B^0 \rightarrow \rho^0 K^+ \pi^-$ . Physical Review D. 2009;80:051103.